

Seismic Performance of Glazed Curtain Walls Connections: Experimental Testing and Finite Element Modelling

D.A. Nuñez Enriquez

 **TU Delft**



DELFT UNIVERSITY OF TECHNOLOGY

Author: Daniel Alejandro Nuñez Enriquez

Student Number: 5244935

SEISMIC PERFORMANCE OF GLAZED CURTAIN WALLS. CONNECTIONS: EXPERIMENTAL TESTING AND FINITE ELEMENT MODELLING

MASTER THESIS

Master of Science Civil Engineering

Master track: Building Engineering – Structural Design

Thesis Committee:

Prof.dr.ir. Christian Louter (Chair)	TU Delft Civil Engineering & Geosciences
Dr. Simona Bianchi (Supervisor)	TU Delft Architecture & the Built Environment
Dr.ir. Roel Schipper	TU Delft Civil Engineering & Geosciences
Dr. Francesco Messali	TU Delft Civil Engineering & Geosciences
Dr. Guido Lori	Permasteelisa Group S.p.A

Date of public defence: December 20th, 2022

Faculty of Civil Engineering and Geosciences

Stevinweg 1, Delft

Preface

This document is the result of months of research on seismic performance of glazed curtain walls, understanding the behaviour of its connections with experimental testing and using finite element models. This project was a key to proposing a numerical model to estimate the structural behaviour of the connections within a glazed curtain wall façade system and basically to introduce a general guideline for the elaboration of FEM capable of replicate the behaviour of the connections within a CW unit.

I would like to extend my gratitude to Delft University of Technology for giving me the opportunity to follow this MSc. in Civil Engineering. I enjoyed the journey this challenging Master represented to me, which increased my understanding and passion for civil engineering. Moreover, I would like to thank Permasteelisa Group for its collaboration in this research project with the experimental tests that were necessary to validate the models I elaborated. Specially I would specially like to thank Guido Lori for being prone to discuss results and answer the questions that arose during the testing sequence of the connections.

In addition, I want to say that I am very happy to have completed this stage of my life successfully, because it helped me grow not only professionally, but also personally. I can say that the experience of studying abroad was one of the most important and beautiful of my life, which allowed me to have a much fresher and more open perspective and vision of things and life.

It was a long and a hard way to get where I am now, with ups and downs, and today after two years, I feel blessed by this achievement, for having persisted until the end, of course, this would not have been possible without God and my wonderful mom, dad, and brothers who have been the fundamental support so that I can fulfil this dream of culminating another phase of my life. Also, I would like to thank the friends I found during this journey, and specially to Karol who with her constant support helped me during the hard moments.

Finally, I would like to express my sincere gratitude to the members of my graduation committee: Simona Bianchi, Roel Schipper, Christian Louter and Francesco Messali for their predisposition to help in the realisation of this research with their comments, inputs and questions that arose during the thesis meeting.,

Daniel Alejandro Núñez Enriquez

Delft, December 20th, 2022

Abstract

Seismic events have shown the hazardous and expensive consequences resulting from seismic damage of non-structural elements. For this reason, the concern regarding the seismic performance of glazed curtain walls has acquired more relevance in the building industry; however, there is still a gap of information in the literature about this topic. To contribute with a broader panorama about the seismic performance of CW, this thesis project is focused on the seismic of the connections within a curtain wall.

This thesis intends to evaluate the performance of the connections that contribute to the seismic response of a glazed curtain wall with finite element models and experimental tests. To achieve this objective, several important points were taken into account. First, a literature study to understand what is a CW, and which are the components that may have influence in seismic design. Second, the two case-studies considered in this research are presented; in this section information about the specimens tested and types of tests performed is provided. Third, elaborate finite element models of the connections corresponding to each case study describing the criteria used. Finally, a comparison between the experimental and numerical results is elaborated to determine if the modelling approach is correct.

The experimental tests were carried out with the collaboration of Permasteelisa Group, and the numerical models were elaborated with DIANA FEA software. Five connections were analysed in this research: mullion to mullion, transom to starter sill, top aluminium bracket and hook, starter sill- bottom steel bracket, and silicone by a non-linear analysis with incremental displacements. At the end of this analysis it was observed a good agreement in the behaviour of the frame to frame connections with a minimal over estimation of the stiffness of certain frame to frame connections. Regarding the connections involving brackets, it was observed that the behaviour in the in-plane horizontal direction can be affected by the rotation of this elements because bolted connections shall be modelled as rotational springs. Finally about silicone it was observed that there exists a good match between the experimental results and the numerical models.

In conclusion, the modelling procedure was validated with experimental tests with relatively optimal results. Nonetheless, there are still limitations in the development of this topic that will be described in the recommendations but much more openness is expected in the future in terms of research on this topic.

List of Contents

1	Introduction	1
1.1	Background	1
1.2	Problem Statement	5
1.3	Research Question and objectives.....	6
1.4	Research Methodology.....	7
1.5	Report Outline	7
2	Literature Review	8
2.1	Curtain Wall	8
2.1.1	Components	9
2.1.2	Types of glazed curtain walls	14
2.2	Design considerations	16
2.2.1	Structural integrity	16
2.2.2	Seismic damage states	18
2.3	Seismic regulations	21
2.3.1	Eurocodes	22
2.3.2	FEMA 450	23
2.3.3	JASS 14	26
2.3.4	Summary.....	27
3	Case Study	29
3.1	Case study 1 (2011).....	29
3.1.1	Introduction	29
3.1.2	Specimen details	31
3.2	Case study 2 (2022).....	32
3.2.1	Introduction	32
3.2.2	Specimen details	34
3.2.3	Experimental sequence and experimental tests	36
3.2.4	Monitoring system.....	39
4	Finite Element Model	42
4.1	FEM software and considerations	42
4.1.1	Geometric Non-linearity	43
4.1.2	Contact elements.....	43
4.1.3	Structural interface elements	45
4.1.4	Finite elements.....	47

4.2 Finite Element Models	52
4.2.1 General material properties	52
4.2.2 Transom - starter sill.....	55
4.2.3 Mullion - Mullion	62
4.2.4 Top and Bottom brackets.....	69
4.2.5 Silicone	74
5 Numerical and Experimental Results	78
5.1 Discussion and results	78
5.1.1 Transom – starter sill	79
5.1.2 Mullion-mullion.....	83
5.1.3 Top aluminium bracket and hook	86
5.1.4 Bottom steel bracket	89
5.1.5 Silicone	91
5.1.6 Potential causes of discrepancy	93
6 Conclusions and Recommendations.....	95
6.1 Conclusions	95
6.2 Recommendations	97
References.....	99
Annex A: Boundary conditions Case Study 2	105
Annex B: Results Case Study 2.....	111
Annex C: Connections Case Study 1.....	114
Annex D: Connection tests photographs	120

List of Figures

Figure 1.1 Major tectonic plates. Red arrows show the direction of the plate motion [2].....	1
Figure 1.2 Left: Sketch of the Earth’s crust and fault plane. Right: Earthquake waves [2].....	2
Figure 1.3 World map of zones with seismic activity areas and the most populated cities in 2005 [9].	3
Figure 1.4 a) Glazing system damage (Chile-2010) [15] b) Cladding system damage (Italy-2016) [14]. c) Ceiling collapse (Northridge-1994) [13]. d) Exterior masonry walls collapse (Italy-1996) [14].	4
Figure 1.5 Enel Headquarters [23].....	5
Figure 2.1 Unitized CW assembly [44].	9
Figure 2.2 Float glass process. When molten glass enters the tin bath, gently cooled, and passed to the annealing lehr for a final gradual cooling before being cut [36].....	10
Figure 2.3 Glass failure pattern. From left to right: annealed, heat-strengthened, thermally toughened [37].....	10
Figure 2.4 Laminated glass. Left: laminated glass assembly. Right: Short- and long-term bending stresses [36,61].....	11
Figure 2.5 Double and triple IGU glazed IGU [62].....	12
Figure 2.6 Example of anchorage system. Top: anchorage system photography. Bottom: vertical section	14
Figure 2.7 Left: stick system. Right: unitized system [60]	15
Figure 2.8 Scheme of the expected behaviour of a CW facade during seismic action [14].....	17
Figure 2.9 Glass crushing, cracking, and fallout developed at the glass edge [67].	18
Figure 2.10 In plane drift CW [24,48]	19
Figure 2.11 Left: Gasket distortion. Right: Gasket pull-out [67].....	20
Figure 2.12 Left: Transom deformations after testing. Right: Mullion with deformation damage [67].	21
Figure 2.13 Typical multi-storey mock-up (AAMA 501.04) [56].....	25
Figure 2.14 Example of a dynamic crescendo test. Starting with 0,8 Hz [57].....	26
Figure 3.1 Manchester Metropolitan University [14]	30
Figure 3.2 Displacement transducers. a) Over external glass b) Over the framing c) Upper anchorage SG550 d) Upper anchorage SG500.....	30
Figure 3.3 Specimen overall view and connection's location	31
Figure 3.4 Connections cross-sections. a) Mullion, bracket, and hooks (top view) b) Transom, starter sill, bracket (lateral view) c) Bracket and hook (lateral view).....	31
Figure 3.5 Facade type 1. Specimens T1.2 and T1.3	32
Figure 3.6 Enel's headquarters [23]	33
Figure 3.7 Sketch and photograph of specimen T1.3 [69].....	34
Figure 3.8 Frame cross-sections and connections. a) Large - small transom (top view) b) Small - small transom (top view) c) Bottom transom - starter sill (lateral view).....	35
Figure 3.9 Starter sill and bottom bracket.....	35
Figure 3.10 Anchorage system top and lateral view	36
Figure 3.11 Connection test. Left: Transom-transom in-plane. Right: Top aluminium bracket and hook	38
Figure 3.12 Water penetration resistance – static pressure test.....	39
Figure 3.13 Sensor location. Left: Over aluminium frame (internal view) Right: Over glass panels (external view) [69].....	40
Figure 3.14 Monitoring system for specimen T1.3 a) Draw wires at the bottom-left corner b) Pixel pattern located at bottom-right corner for DIC c) Laser and accelerometer sensors located at the top- right upper bracket d) displacement sensors located on small and large frame	41
Figure 4.1 Large displacements [75].....	43

Figure 4.2 Contact behaviour [75]	44
Figure 4.3 2D line interface configuration [75]	45
Figure 4.4 Variables of a two-dimensional line interface [75].	46
Figure 4.5 Variables of the a three-dimensional surface interface [75].	47
Figure 4.6 Plane strain elements [75].	48
Figure 4.7 Nodal displacements of plane strain elements [75].	48
Figure 4.8 Deformations of plane strain elements [75].	48
Figure 4.9 Positive direction of Cauchy stresses for a plane stress element on a unit cube [75].	49
Figure 4.10 Characteristics of solid elements [75].	50
Figure 4.11 Deformation of solid elements [75].	50
Figure 4.12 Positive direction of Cauchy stresses for a solid element on a unit cube [75].	51
Figure 4.13 Bi-linear model diagram from Eurocode 9 [77].	53
Figure 4.14 Strain-hardening model of steel elements [66].	54
Figure 4.15 Transom-Starter sill displacement direction.	55
Figure 4.16 Drawing simplification for DIANA. Left: original geometry. Right: simplified geometry	56
Figure 4.17 Interface elements location.	56
Figure 4.18 Bi-linear model diagram calculated.....	57
Figure 4.19 Transom- starter sill restraints and load application in-plane. Left: FEM. Right: test.	58
Figure 4.20 Transom-Starter sill in-plane. Final deformed shape and plastic strains.	59
Figure 4.21 Location of contact elements. Transom-starter sill out-of-plane outwards.	60
Figure 4.22 Transom-starter sill restraints and load application out-of-plane outwards. Left: FEM. Right: picture.	61
Figure 4.23 Transom-starter sill out-of-plane outwards. Final deformed shape and plastic strains.	62
Figure 4.24 Mullion-Mullion displacement directions.	63
Figure 4.25 Mullion-mullion (large-small units) simplified geometry	63
Figure 4.26 Structural interface non-linearity due to an opening. Left: before contact. Right: after contact.....	64
Figure 4.27 Open non-linear elastic interface diagram to reach contact.....	64
Figure 4.28 Mullion-mullion restraints and load application in-plane. Left: FEM. Right: Test picture.	65
Figure 4.29 Mullion-mullion in-plane. Interface and contact elements location.	66
Figure 4.30 Mullion-mullion in-plane. Final deformed shape and plastic strains.	67
Figure 4.31 Mullion-mullion restraints and load application out-of-plane outwards. Left: FEM. Right: picture.	68
Figure 4.32 Mullion-mullion out-of-plane outwards. Contact elements.....	69
Figure 4.33 Mullion-mullion out-of-plane outwards. Final deformed shape and plastic strains	69
Figure 4.34 Brackets displacement directions. a) Bottom bracket b) Top bracket and hook.	69
Figure 4.35 3D model top bracket + hook	70
Figure 4.36 Bi-linear model aluminium alloys AW 6005-T6 and AW	71
Figure 4.37 Top bracket-hook horizontal. Restraints and load application	71
Figure 4.38 Aluminium bracket horizontal. Final deformed shape and plastic strains.....	72
Figure 4.39 Top bracket-hook vertical. Restraints and load application.	73
Figure 4.40 Aluminium bracket vertical. Final deformed shape and plastic strains.....	74
Figure 4.41 Silicone shear. a) Vertical b) Horizontal	74
Figure 4.42 Silicone and aluminium boundary conditions	75
Figure 4.43 Silicone extension. Final deformed shape.	76
Figure 4.44 Silicone and aluminium vertical shear boundary conditions.....	77
Figure 4.45 Silicone vertical shear. Deformed shape at 10 mm of displacement. front view.....	77
Figure 5.1 Transom-starter sill. In-plane. Force vs. Displacement.....	80
Figure 5.2 Transom-starter sill in-plane first plastic stain formed.....	80

Figure 5.3 Transom-starter sill. Out-of-plane inward. Force vs. Displacement.....	81
Figure 5.4 Out-of-plane inwards. Left: First plastic strains. Right: Stress diagram.	81
Figure 5.5 Transom-starter sill. Out-of-plane outward. Force vs. Displacement.....	82
Figure 5.6 Out-of-plane outwards. First plastic strains.....	83
Figure 5.7 Mullion-Mullion. Out-of-plane inwards. Force vs. Displacement	84
Figure 5.8 Out-of-plane inwards. Plastic strain formations. Left: L-S Right: S-S.....	85
Figure 5.9 Mullion-Mullion connections. a) Tested b) L-S c) S-S	85
Figure 5.10 Mullion-Mullion out-of-plane inwards with reduced stiffness. Force vs. Displacement ..	86
Figure 5.11 Top bracket and hook. In-plane horizontal (load on bracket). Force vs. Displacement. ...	86
Figure 5.12 Top bracket and hook. In-plane horizontal. Initial Plastic strains	87
Figure 5.13 Top bracket and hook. In-plane vertical (down). Force vs. Displacement.....	88
Figure 5.14 Top bracket and hook. In-plane vertical. Initial Plastic strains	88
Figure 5.15 Bottom bracket. In-plane horizontal. Force vs. Displacement.	89
Figure 5.16 Bottom bracket. In-plane horizontal. Initial Plastic strains	90
Figure 5.17 Bottom bracket. In-plane vertical (down). Force vs. Displacement	90
Figure 5.18 Silicone. Shear (vertical). Force vs. Displacement.....	91
Figure 5.19 Load vs. Displacement Shear. Left: Silvestru V., et all results [78]. Right: research result	92
Figure 5.20 Silicone. Tension. Force vs. Displacement.....	92
Figure 5.21 Load vs. Displacement Tension. Left: Silvestru V., et all results [78]. Right: research result.....	93
Figure 5.22 Transom-starter sill. Boundary conditions model vs. real	94

List of Tables

Table 1.1 Most populated cities 2022 [8]	3
Table 2.1 Framing maximum deflection perpendicular to the plane [31].....	9
Table 2.2 Characteristic values of bending strength for float glass [39].....	11
Table 2.3 Most common Infill attachments [40,20,42].....	13
Table 2.4 JASS 14 provisions for inter-storey displacements [59].....	27
Table 3.1 Displacement applied to the specimens according to JASS 14.....	34
Table 3.2 Testing sequence specimen T1.3 (7 th of July 2022).....	37
Table 3.3 Connections testing sequence.	37
Table 3.4 Sensor's part of the monitoring system	40
Table 4.1 Aluminium AW 6063-T6 summary of properties.....	57
Table 4.2 Interface linear properties. Transom – starter sill in-plane	57
Table 4.3 Finite element types and details.	58
Table 4.4 Target material definitions transom - starter sill out-of-plane outward	60
Table 4.5 Finite element types and details.	61
Table 4.6 Mullion-mullion in-plane structural interface linear properties.....	64
Table 4.7 Target material definitions mullion-mullion in-plane.....	65
Table 4.8 Finite element types and details.	65
Table 4.9 Target material definitions mullion-mullion out-of-plane outward	67
Table 4.10 Finite element types and details.	68
Table 4.11 Aluminium alloys AL 6005-AT6 and AL 6082-T6 summary of properties.....	70
Table 4.12 Top bracket- hook interface linear properties.	70
Table 4.13 Finite element types and details.	72
Table 4.14 Aluminium linear elastic properties.	75
Table 4.15 Silicone-aluminium interface properties.	75
Table 4.16 Mooney-Rivlin constants Dow Corning 993 [78].....	75
Table 4.17 Finite element types and details.	75

Symbols and abbreviations

Abbreviations

AAMA:	Architectural Manufacturers Association.
CW:	Curtain wall
FEM:	Finite element model
FEMA:	Federal Emergency Management Agency
IGU:	Insulated glass unit
JASS:	Japanese Architectural Standard Specification
NEHRP:	National Earthquake Hazard Reduction Program
NSE:	Non-structural element
PVB:	Poly vinyl butyral
SSG:	Structural silicone glazing
2SSG:	2-sided structural silicone glazing
DIC:	Digital Image Correlation
4SSG:	4-sided structural silicone glazing
EN 13830:	Eurocode 8 - Curtain Walling Product Standard
EN 1998-1:	Eurocode 8 – Design of structures for earthquake resistance – Part 1:1
EN 1999-1-1	Eurocode 9: Design of aluminium structures: General structural rules

Symbols

A_p :	Component amplification factor
bn:	Billion
b_p :	Width of the rectangular glazing unit
c_1 :	Vertical clearance between glazing unit and curtain wall frame
c_2 :	Horizontal clearance between glazing unit and curtain wall frame
d_{CW} :	Total lateral deformation capacity of a CW
D_p :	Design inter-storey drift FEMA 450
D_{sx} :	Elastic shear interface stiffness
D_{ny} :	Elastic normal interface stiffness
D_{Clear} :	Relative horizontal displacement, which causes initial glass-frame contact. For rectangular glazing units within a curtain wall frame
d_r :	Design inter-storey drift from Eurocode 8 (section 4.4.2.2-2)
ϵ_u :	Nominal value of ultimate strain.
F:	Force applied
F_a :	Horizontal seismic force at the mass centre of the element in the most unfavourable direction
f_o :	Characteristic value of 0.2% proof strength
F_p :	Horizontal seismic design force FEMA 450
$F_{p,V}$:	Vertical seismic force acting at the mass centre of the element, JASS 14
$F_{p,H}$:	Horizontal seismic force acting at the mass centre of the element, JASS 14
f_u :	Characteristic value of ultimate tensile strength

H:	Building height measured from the foundation or from the top of a rigid basement
h:	Storey height
h _p :	Height of the rectangular glazing unit
h _{sx} :	Story height used in the definition of the allowable story drift (Δ_a)
I _p :	Component importance factor
I _p :	Component importance factor, FEMA 45
L:	Span
m:	Million
M _L :	Richter scale
q _a :	Behaviour factor of the element
R _p :	Component response modification factor
S:	Soil Factor
S _a :	Seismic coefficient applicable to the non-structural element
S _{DS} :	Spectral response acceleration at short period
S _p :	Seismic coefficient in vertical direction, JASS 14
S _S :	Seismic coefficient in horizontal direction, JASS 14
T _a :	Fundamental vibration period of the NSE
t _{sx} :	Shear traction tangential to the interface
T ₁ :	fundamental vibration period of the building in the relevant direction
U _e :	displacement of the node
U _x :	displacement in the local x direction
U _y :	displacement in the local y direction
U _z :	displacement in the local z direction
v:	Reduction factor which considers the lower return period of the seismic action associated with the damage limitation requirement
W:	Weight of the element
W _a :	Weight of the element
W _p :	Component weight
X:	Height above the base of the upper support attachment (at level x), FEMA 450
Y:	Height above the base of the lower support attachment (at level y), FEMA 450
Y _a :	Importance factor of the element, Eurocode 8
z:	Height of the NSE above the level of application of the seismic action (foundation or top of a rigid basement), FEMA 450
ε:	Green-Lagrange strain
ε _{xx} :	Green-Lagrange strain in the local x direction
ε _{yy} :	Green-Lagrange strain in the local y direction
ε _{zz} :	Green-Lagrange strain in the local z direction
δ _{cant.max} :	Maximum deflection at length L of a cantilever beam
δ _{xA} :	Deflection at level x of structure A, FEMA 450
δ _{yA} :	Deflection at level y of structure A, FEMA 450
Δ _{aA} :	Allowable story drift for structure A, FEMA 450
Δ _{fallout} :	Relative displacement (drift) at which glass fallout from a curtain wall, FEMA 450
Δ _{Uny} :	Normal relative displacement Y direction (opening)

ΔU_{sx} : Shear relative displacement X direction (slip)
 σ_{xx} : Cauchy stresses in the local x axis
 σ_{yy} : Cauchy stresses in the local y axis
 σ_{zz} : Cauchy stresses in the local z axis
 σ_{xy} : Cauchy shear stress perpendicular to the x axis in y direction
 σ_{yz} : Cauchy shear stress perpendicular to the y axis in z direction
 σ_{zx} : Cauchy shear stress perpendicular to the z axis in x direction

1

Introduction

1.1 Background

Earthquakes are natural events which can lead to damage or collapse of structures causing, as a consequence, human casualties, economic loss, and secondary risks such as landslides, tsunamis, and fires [10]. Nevertheless, these events can also be the result of human activity over the years; for example, the seismic activity in Groningen, The Netherlands has its origins in the gas extraction that occurred in the past. Nonetheless, 90% of the seismic activity occurs naturally and is concentrated at the boundaries of the tectonic plates (Figure 1.1) [2]. To reduce the danger this geological hazard represents, several research studies to analyse and reduce damages caused by earthquakes have been carried out with important outcomes to improve structural design according to the different seismic regions.

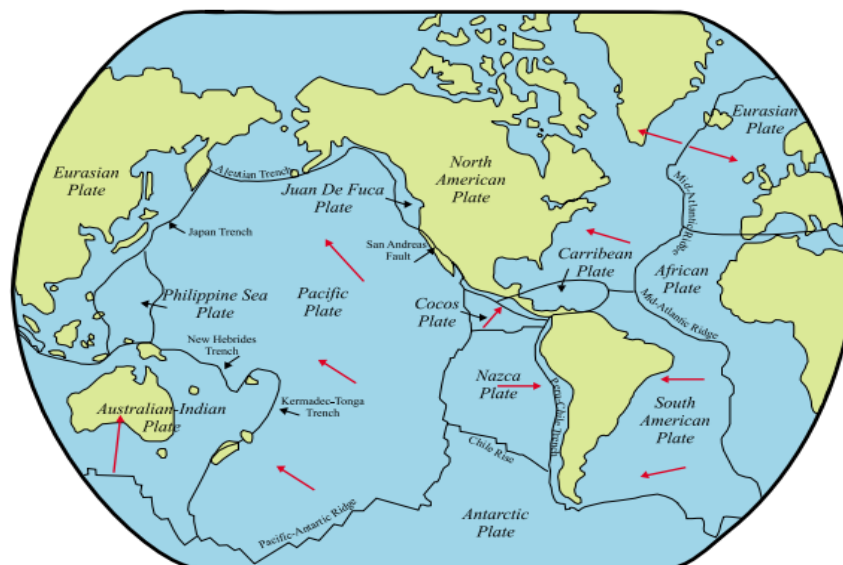


Figure 1.1 Major tectonic plates. Red arrows show the direction of the plate motion [2]

As aforementioned, an earthquake is a dangerous natural disaster that may lead to catastrophic consequences. Therefore, it is important first to understand what an earthquake is, and how it propagates. An earthquake is the result of released energy caused by the slipping movement between two parts of the Earth's crust over a fault plane (Figure 1.2) [3]. When the stress accumulated in the Earth's crust reaches its peak value, it is released in the form of elastic energy into heat and elastic waves, which are responsible of the shaking movement of the earth. [10]. The released elastic waves are divided into surface waves and body waves; moreover, body waves are split into primary and secondary waves (Figure 1.2). Primary waves (P waves)

are the fastest and have a back-and-forth motion along the direction of the wave [2], and the secondary waves (S waves) travel through solid materials with a lower speed (when compared to a P wave) with a wavy movement perpendicular to the propagation direction [2].

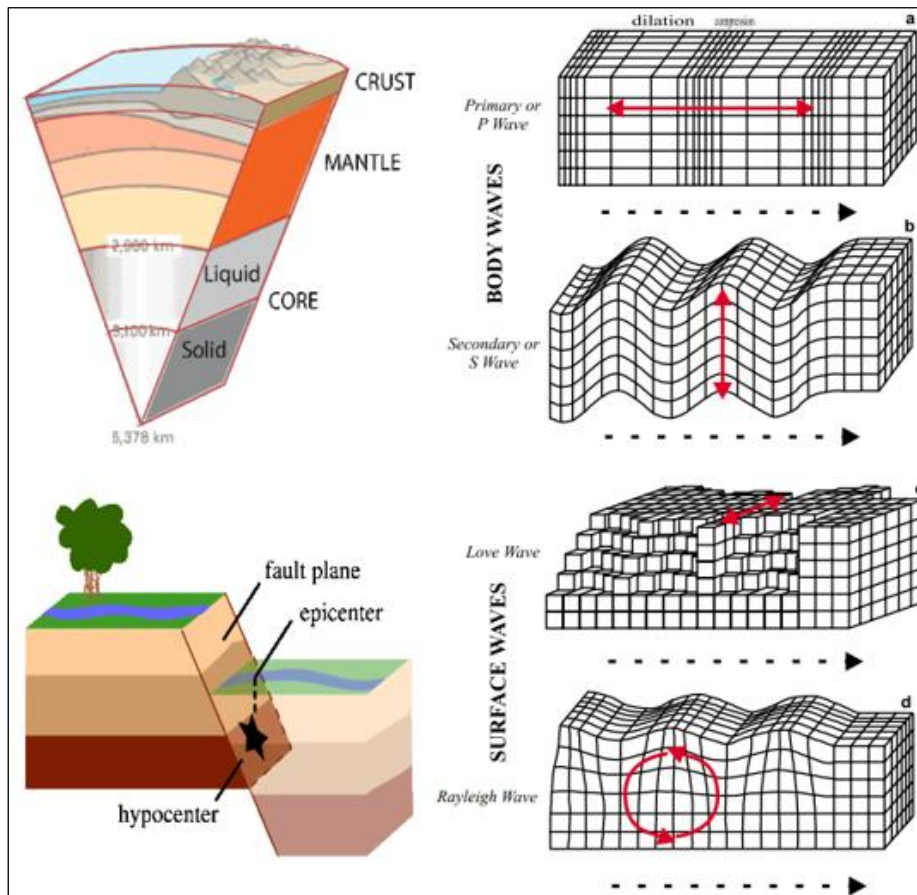


Figure 1.2 Left: Sketch of the Earth's crust and fault plane. Right: Earthquake waves [2].

Surface waves have lower speed compared to body waves but are the ones that affect the most to building structures causing considerable damage. Surface waves are divided into Love and Rayleigh waves (Figure 1.2). Love waves propagate with a shear motion perpendicular to the spread direction, and Rayleigh waves are the combination of longitudinal compression and dilatation that results in an elliptical motion along the Earth's surface [2].

To counter the seismic hazardous effect, people in zones with high seismic activity have tried to live among the risk adopting new rules and routines. For example, Japanese traditional architecture started to adopt lightweight and flexible materials around the 1700s to counter seismic effects on the structures [1, 11]. In the past century, the substantial improvement of the seismic considerations in the design of structural elements was triggered by three high-magnitude earthquakes [9]. First, a seism (M_L 8,0) which occurred in the Chinese city of Tangshan (1976) with 242.000 deceased and 176.000 wounded [4]. In 1994, a quake with 6,7 Richter magnitude shacked Northridge, Los Angeles, where 60 people died [5], and in Japan, one year later (1995), another movement affected Kobe (M_L 6,9), killing 5.600 [6, 11].

Despite the high amount of human victims in these catastrophic events, the main reason to reconsider changes in seismic design of structures was not only the number of casualties, but

also the monetary costs [9] [12]. As a result of the seismic in 1976 more than 95% of the building structures collapsed in Tangshan [4]. Moreover, approximately 15.000 buildings were demolished in Northridge with economic losses around \$15bn to \$40bn [5]. In Kobe, around 180.00 buildings had severe structural damages or collapsed with a cost for the city ranging from \$90bn to \$150bn [6].

In addition, it was considered the potential damage that an earthquake of moderate magnitude could cause in densely populated areas to human lives and the economy. By 2030, urban areas are expected to accommodate more than 60 percent of the human population [7,12]; thus, the population in cities located at seismic risk zones will also increase. According to Giouncu V. and Mazzonlani F. [9], four out of the five cities with more than 20 millions of inhabitants in the world were located in areas with seismic activity in the year 2005.

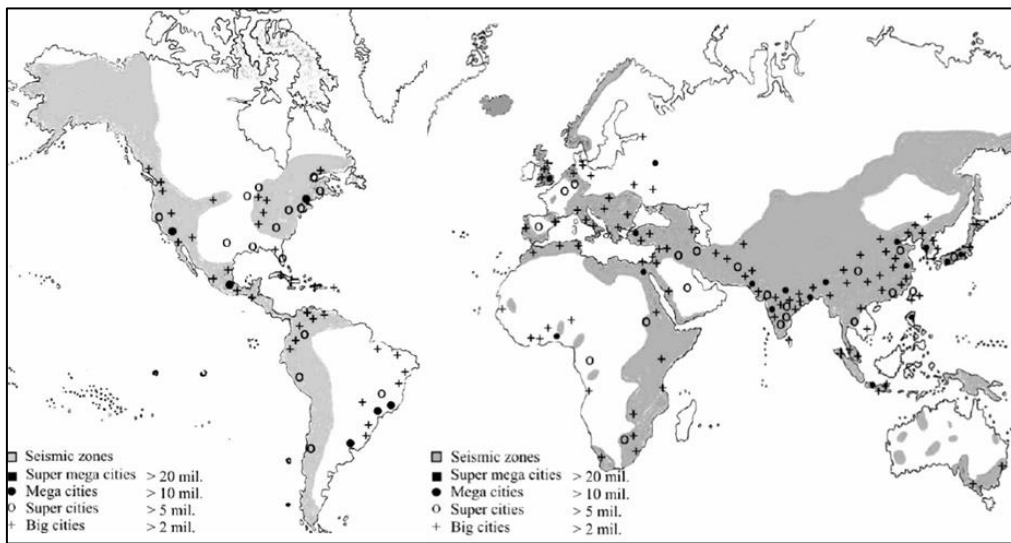


Figure 1.3 World map of zones with seismic activity areas and the most populated cities in 2005 [9].

Comparing this information with data from 2022 (Table 1.1) by considering the same seismic activity areas shown in Figure 1.3, it can be noticed that the number of cities with more than 20 million residents increased, and it is possible to see that now 11 out of 12 cities are situated in a zone with seismic activity.

Table 1.1 Most populated cities 2022 [8]

City	Country	Population million
Tokyo*	Japan	37,7
Jakarta*	Indonesia	33,7
Delhi*	India	32,2
Guangzhou*	China	30,0
Mumbai*	India	25,0
Manila*	Philippines	24,9
Shanghai*	China	24,0
Sao Paulo	Brazil	23,0
Seoul*	South Korea	23,0
México DF*	México	21,8

* City with seismic activity

As a result of the disasters occurred in the 20th century, different and more specific rules were adopted to reduce the damage costs of buildings. Therefore, non-structural, and structural elements started to be designed considering an acceptable damage level according to the importance of the element, starting the principles of performance based seismic design [1].

In a typical building, a major part of the construction costs relies in the non-structural elements (NSE) [17]; during an earthquake, the damage cost of NSE can even outpace the structural losses [13]. Even though NSE are subjected to equal dynamic conditions like the structural elements during a seismic event, these elements are not designed with the same principles of the main load-bearing systems. Moreover, even if the performance of the main structural system allows immediate occupancy after a seism, the failure of NSE such as, cladding facades, ceilings, partitions, masonry, and curtain walls can be a truly menace for people's safety and can affect the post-earthquake functionality of a building (Figure 1.5) [14,18]. This will imply costs not only for rehabilitation, but also for the non-use of the building during the repairment period. However, only basic and limited requirements are stated in the European code for seismic design of NSE in comparison to the requirements for structural components [16,13].

Generally, non-structural elements are attached to the main load-bearing structure [14], so displacements and stresses can be transferred from the main structure to the NSE leading to possible failure damages [19]. An example of the previously stated happens during an earthquake, where the structural system is subjected to high displacements and stresses caused by the ground motion; once the displacements and stresses are transferred to the NSE, these seismic effects may not be resisted due the restriction of movement of the NSE when attached to the load-bearing elements. Hence, it becomes fundamental to assess this movement restriction in seismic designing of NSEs.

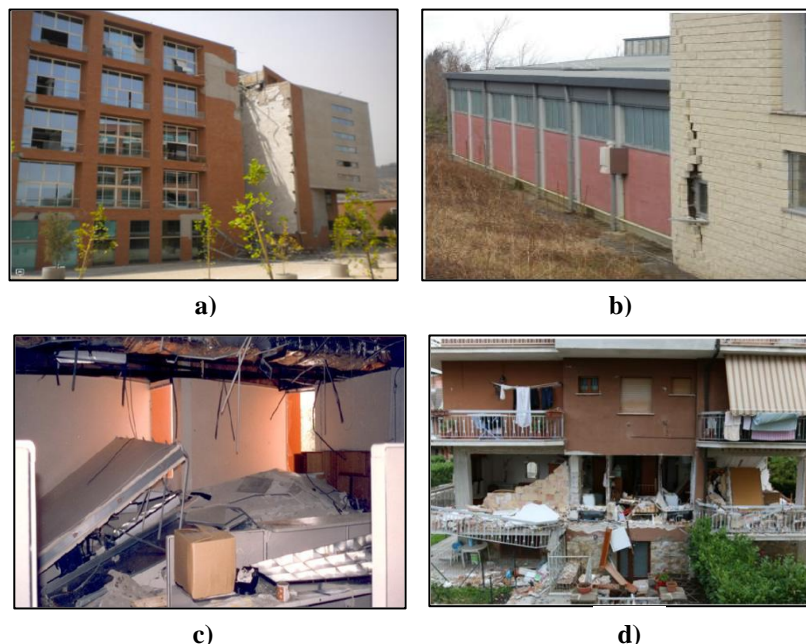


Figure 1.4 a) Glazing system damage (Chile-2010) [15] b) Cladding system damage (Italy-2016) [14].
c) Ceiling collapse (Northridge-1994) [13]. d) Exterior masonry walls collapse (Italy-1996) [14].

The shortage of available information and specific instructions on the seismic design of NSE for different multi-performance levels, and the excessive cost of the tests required to check

their performance made manufacturers the main responsible of the seismic performance design of NSE. This is the case of the curtain wall cladding system which requires full-size mock-up tests to study its seismic performance. A glazed curtain wall (CW) is a lightweight building enclosure, which commonly consists of glass sheets fixed to a metal frame assuming the function of an external wall [20]. From a structural perspective, CWs are submitted to wind, snow, ice, temperature, and earthquake loadings, and must be able to dissipate and transmit loads to the primary structural systems (e.g.: columns, beams, or slabs) or to other supporting systems and to sustain displacements and stresses imposed by the main structure [21].

Permasteelisa Group is a leading global company specialized in the delivery of architectural envelopes with expertise in design, engineering, fabrication, installation, and post-sales service processes [22]. As a manufacturer, Permasteelisa is also responsible of testing their products. In the case of CWs, several types of tests are executed to control their performance under different circumstances, including seismic performance. In June 2022, Permasteelisa started a series of full-size tests for different CW units, designed to renovate the Enel Headquarters façade in Rome (Fig. 1.5) [25]. During this testing sequence, the seismic performance of the units was tested by imposing displacements to the CW units through a seismic beam. The objective of this sequence of tests was to analyse the behaviour of the units and obtain valuable data for the elaboration of a finite element model, considering global and local behaviour.



Figure 1.5 Enel Headquarters [23]

1.2 Problem Statement

The concern of engineers related with the behaviour of CWs under seismic actions has increased because past events have shown the hazardous consequences resulting from the seismic damage of NSE [26]. However, it is difficult to find in the literature recent studies about the seismic performance of CW systems when compared to the information available about main structural elements and other façade systems such as infill walls. The main cause of this situation is the need of expensive and time-consuming tests required to simulate seismic loads acting over this type of elements [24]. Moreover, the information available does not provide clear indications about CW modelling, including its connections. Therefore, there is a need to increase substantial research regarding the seismic performance of CW by analysing

samples experimentally and by creating a finite element model (FEM) to replicate the behaviour of a tested sample [27].

For better understanding of the seismic behaviour of a CW, it is necessary to collect and process relevant data from experimental tests and FEMs capable of replicate the behaviour observed during the tests. The outcome of both phases can be used to determine critical aspects causing a negative effect in the CW integrity, so they can be considered during the design of the cladding unit. A CW model should start with a proper analysis of its connections, and a connection analysis shall be done by considering the next aspects: element geometries, material properties, load application, boundary conditions and interface conditions. The evaluation of the accuracy of the model must be done by following a validation protocol. The validation protocol can be established as a comparison between experimental and the FEM result and could finish with a calibration of the numerical model based on the experimental results.

This thesis intends to contribute with a broader panorama of the seismic behaviour of CWs by establishing a model capable of analysing the performance of the connections that can be found within a CW façade unit. The approach of this research is focused on the individual evaluation of each connection for their further implementation in a model simulating a full-size CW submitted to seismic displacements. To find outcomes, 2D and 3D models of the connections are analysed by applying an imposed displacement and considering material and geometrical non-linearities. It is worth mentioning that the results are sustained by their comparison with experimental results. Two full-size mock-up tests, and several connections experimental assessments were completed by Permasteelisa Group, simulating in- and out-of-plane seismic displacements. The validated outcome is expected to be implemented in the modelling of a full-size CW façade specimen (global model) to increase the accuracy of the numerical calculations and to determine the influence of the connections in seismic action.

1.3 Research Question and objectives

From the problem statement the main research question can be defined as:

How to evaluate the performance of the connections that contribute to the seismic response of a glazed curtain wall by considering finite element models and experimental results?

To support the answer to this question, 6 sub-questions are answered in this report

1. How to determine which connections influence the seismic performance of a glazed Curtain Wall.
2. How to establish a Finite Element Model simulating the in- and out-of-plane displacement behaviour of the following connections: mullion-mullion, transom-starter sill, seismic beam-top bracket and hook, and starter sill-floor bracket by a non-linear analysis with incremental displacements.
3. How to elaborate a Finite Element Model to determine the deformation performance of the different structural silicones and gaskets within a tested glazed curtain wall establishing their influence as an interface connection between glass and frame.

4. How to determine special boundary conditions and assumptions adopted to calibrate the model based on the full-scale laboratory test and connection tests.
5. How to translate the results obtained from the Finite Element Models into spring models which represent the deformation capacity of the connections in order to be implemented in a global model of a glazed curtain wall unit.
6. How to compare numerical and experimental results by means of displacement data obtained from a global model or force-displacement diagrams obtained from the analysis of the connections within a glazed Curtain Wall.

1.4 Research Methodology

The process to answer the research questions follow the next steps. The first step is to clearly understand what a CW is, its main characteristics, and which are its components to recognize their function, influence in seismic design and damage states. Additionally, a study is required about the different design regulations available for seismic assessment of CWs to identify the scope and limitations of the requirements established for these NSE. The second step consists of presenting the two case-studies considered in this research. In this section information about the specimens tested and types of tests performed is provided. As a third step, the connections to be analysed are presented, and a description of all the criteria used to elaborate the finite element models is provided. In the next stage, results from the experimental tests and FEMs will be presented, and discussion comparing numerical and experimental results is done considering the limitations presented during this research. Finally, conclusions are elaborated to answer the sub questions and the main research questions, and recommendations will be provided for their consideration in further improvements or research.

1.5 Report Outline

This research is divided into 6 chapters. Chapter 1 describes the background, objectives and research questions which motivated the realization of this thesis. Chapter 2 defines basic aspects of curtain walls, and their performance. Additionally, it includes a description of the regulations used to assess the seismic behaviour of this façade system. Chapter 3 identifies the two case-studies analysed in this research and the experimental tests completed by Permasteelisa Group. Chapter 4 shows the approach considered to elaborate the numerical model for each connection. Chapter 5 presents the result obtained during the testing campaign and starts a discussion by comparing the experimental and numerical results. Finally, Chapter 6 includes the conclusions and recommendations of the work presented plus considerations for future studies.

2

Literature Review

2.1 Curtain Wall

A curtain wall is a lightweight cladding or building enclosure, whose main function is to be a barrier protecting the interior from external environmental conditions [43]. The vertical dimension of a CW is generally the same as one or two storey height, and it is designed to resist mainly self-weight, seismic and wind loads acting on the element [21]. A CW is a non-structural element without influence on the structural integrity of the building and incapable of resisting any load coming from the building, but able to transmit environmental loads to the structural elements with connections to beams, slabs, columns, or the rooftop [31]. The origin of the name “curtain wall” is a reference to the manner it hangs from the structural elements of the building, which is commonly connected to the slabs [31]. The design of a CW must be elaborated considering the following conditions [20,21]:

- Its own structural integrity
- Displacements originated from seismic or thermal loads, inter-storey displacements from the building
- Weathertightness
- Condensation
- Thermal insulation
- Fire safety
- Any other specific consideration depending on the type of project such as: Sound proofing, bomb-blast resistance, hurricane-borne debris resistance, etc.

A CW unit is composed by a framing, an infill, and an anchorage system. The framing is the load-bearing component of the unit, and it consists in two vertical and two horizontal components (mullions and transoms) commonly made from aluminium extrusion, but also steel [20]. The infill panel is prevalently made of glass, but it can also be made of stone, aluminium, copper, composite materials, etc. [21]. Finally, the anchorage system is the manner the unit is attached to the building, generally made with steel and aluminium materials.

CWs can be classified according to their design into standardized or customized systems. Standardized systems are constructed with standard components already tested and elaborated by the manufactures, while customized are tailored to a particular building project [32]. Moreover, a second division can be made in considering the construction method into stick and unitized systems, where the main difference is the possibility of unit assembly in-site, see Figure 2.1 [43].



Figure 2.1 Unitized CW assembly [44].

For this report purposes, when mentioning a CW, it will refer to a unit made with aluminium extrusions as framing and a glass panel as infill, unless other specification is provided before. A more substantial description of the components and classification of a curtain wall will be presented in the next sub-chapters, including an explanation regarding its design requirements in different parts of the world.

2.1.1 Components

As briefly explained before, CW can be divided in the next components: Framing, infill, infill attachment, and system anchorage.

2.1.1.1 Framing

Mullions (vertical) and transoms (horizontal) are the components of a CW framing and can be manufactured with 2 types of metal: aluminium or steel [21]. The framing design is based on the deflection of its members due to wind forces acting on the surface of the façade elements. Hence, the depth, thickness and cross-section of these elements is defined by the span (horizontal or vertical) and the tributary area among the framing pieces [33]. Typically, aluminium is the material selected due to its good strength to weight ratio and the easiness to be extruded during its manufacture to form complex shape profiles, making it easier for designer to satisfy weather protection and structural requirements [32].

Table 2.1 Framing maximum deflection perpendicular to the plane [31].

Maximum deflection	Span	
	From mm	Up to mm
L/175 or 19 mm	0	4.115
L/240 + 6 mm	4.116	12.192

*L in mm

Table 2.1 gives industry standards according to the American Architectural Manufacturers Association (AAMA) for maximum deflection perpendicular to the plane of aluminium framing profiles. Meanwhile, for vertical deflection it depends on the infill and the support conditions, but for horizontal members supporting glass it can be limited to 3mm [35].

2.1.1.2 Infill

An infill is a one piece or an assembled panel of transparent or opaque materials, installed within the frame of a CW [38]. The dimensions of the infill are determined by the ability to resist and transmit in-plane wind and lateral loads to the mullions and transoms. Typically, glass is selected as the infill material because of its translucent properties, but also it could be made of stone, aluminium, composite materials, etc. [21]. From a structural perspective, a glass infill behaves elastically until it reaches its maximum strength, causing its brittle failure. This brittle fracture can be triggered by impact, bending and thermal loads when reaching peak stresses of the material [40]. Nevertheless, there is a difference in resistance capacity depending upon the type of glass used. In accordance with the bending strength and manufacture process, glass can be classified into annealed, heat-strengthened, thermally toughened and chemically toughened [39], where only the first three are applicable for curtain walling use.

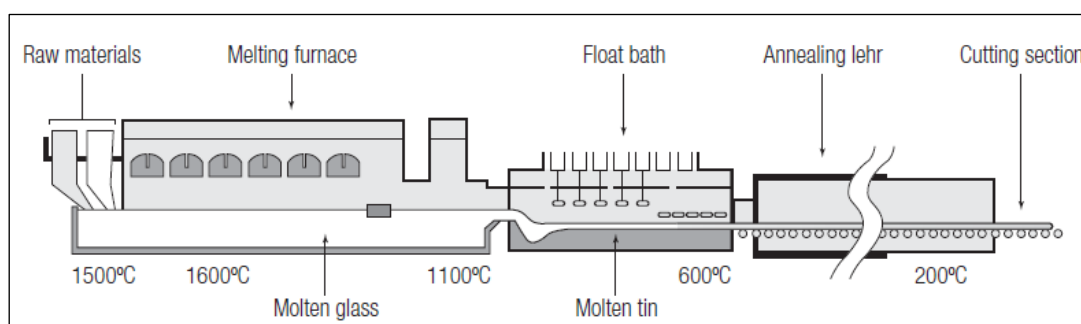


Figure 2.2 Float glass process. When molten glass enters the tin bath, gently cooled, and passed to the annealing lehr for a final gradual cooling before being cut [36].

Annealed: Also called “basic” annealed glass, is usually made with the float process shown in Figure 2.2. Bending stresses, thermal stresses and imposed strains are the failure causes of this type of glass. A characteristic result of the brittle failure in this type of glass is the formation of the large fragments of broken glass. Moreover, an important aspect to consider during design is the fact that the cut edges of annealed glass are often weaker than its surface [36].

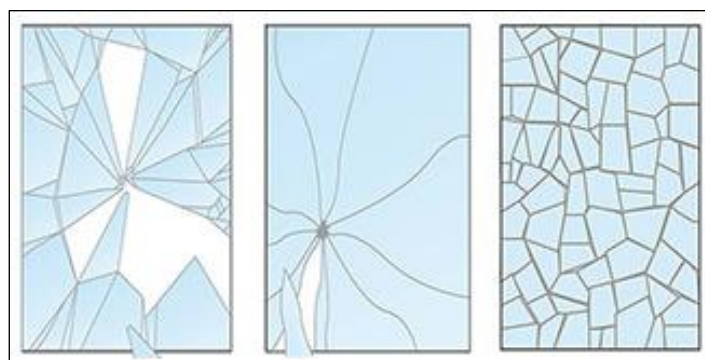


Figure 2.3 Glass failure pattern. From left to right: annealed, heat-strengthened, thermally toughened [37].

Heat-strengthened (partially toughened or semi-tempered): Follows the float process of annealed glass, with an additional heating process at 620°C and quenched by jets of cool air. This additional process generates compression stresses on the surface of the glass and tension in the inner part [36]. As a result, this glass type has almost twice the strength of basic annealed glass (Table 2.2) and is less susceptible to damages caused by thermal stresses. When brittle

failure is reached, detachment of large fragments of broken glass are expected following a similar pattern as the one from annealed glass (Figure 2.3).

Thermally toughened (fully tempered): Follows the same process of heat-strengthened glass with a faster cooling last step. As a consequence, higher compression stresses on the surface are reached, increasing its bending strength resistance (Table 2.2). Additionally, when peak stresses are reached, the cracks formed repeatedly bifurcate causing a complete fragmentation of the glass element and making it less dangerous (Figure 2.3). The number of fragments after failure depends on the compression reached on the surface during fabrication [36]. Any cutting, drilling, and grinding of this and heat-strengthened glass must be done before the toughening process because any penetration of the stressed surface will trigger fragmentation caused by the imbalance of stresses [14].

Table 2.2 Characteristic values of bending strength for float glass [39].

Glass type	Characteristic bending strength N/mm ²
Annealed	45
Heat strengthened	70
Thermally toughened	120

Additionally, an extra division of glass infills can be determined in function of their assembly into monolithic, laminated, and insulated glass unit [39]. The selection of one of the 3 systems depends on the performance requirements. A brief introduction of each of these 3 arrangements is presented in the next paragraphs.

Monolithic glass: is a glass panel composed by only one glass sheet. It can be made of any of the three types of glass discussed above.

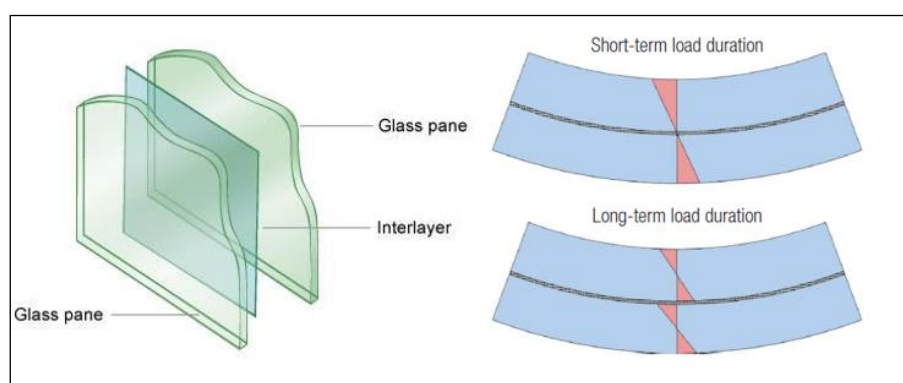


Figure 2.4 Laminated glass. Left: laminated glass assembly. Right: Short- and long-term bending stresses [36,61].

Laminated glass: combination of two or more glass plies of any type by means of a bonding material [39]. It can be done applying an interlayer gluing sheet, commonly made of poly vinyl butyral (PVB), or by the application of a resin, which can be acrylic, polyurethane and polyester [36]. With the application of PVB and resins as glue layers, the short-term out-of-plane loads can be resisted by the glass with all the plies working compositely. Oppositely, for long-term

out-of-plane loads the resistance is split by each ply according to their relative stiffness [41], see Figure 2.4. Careful considerations have to be taken regarding the temperature at which the element is exposed because it has a significant impact on the shear stiffness of the interlayer, causing a reduction of the composite behaviour if the temperature raises. Additional advantages due to the addition of the interlayer is the increased penetration resistance of the laminated glass [40], a feature used specially for design requirements such as bullet resistant laminate glass. Moreover, the lamination process provides glass panels with an extra security feature, holding broken glass fragments fixed to the interlayers [40].

Insulated glass units (IGU): is a composite unit made of two or more glass panes separated by a hermetically sealed air cavity created with the use of spacers or seals at the top and bottom of the IGU, see Figure 2.5 [34]. Double glazed (2 panes, 1 cavity) and triple glazed (3 panes, 2 cavities) units are the most common, and the panes used in its elaboration can be monolithic, laminated, or a combination of both. This type of glazing unit is used when high thermal performance and acoustic insulation is required [38].

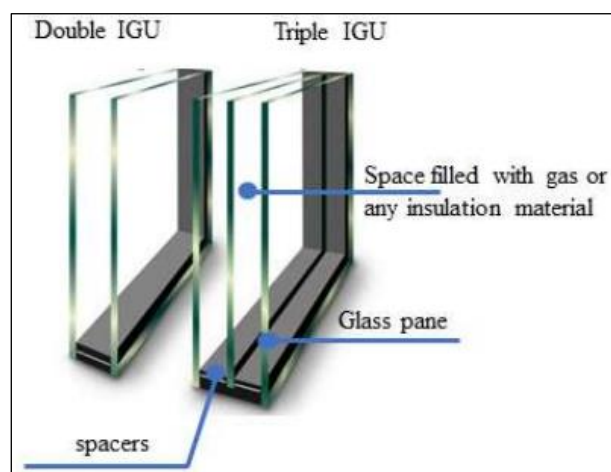


Figure 2.5 Double and triple IGU glazed IGU [62].

2.1.1.3 Infill attachment (glazing)

The infill attachment entails the method used to fix the glazing panels to the framing [32]. There are 2 different connection types applicable to glazed CW units: dry glazed and wet glazed. A dry glazed attachment refers to the mechanical fixation of the infill with the use of gaskets to attach the glass unit withing the framing by means of compression [42]. Gaskets are rubber materials, commonly made of neoprene, with high degree of cure and elasticity; the connection with gaskets relays on the elastic properties of the material to provide a compression seal [63]. However, the effectiveness of the seal can be affected during the installation process, where an inappropriate installation can cause the gasket to pullback and open the joint rather than expand and close the joint [63]. Examples of the most common infill attachments can be seen in Table 2.3.

A wet glazed connection refers to the use of structural silicone or polyurethanes to retain the glass infill within the frame. Nonetheless, structural silicone glazing (SSG) is the typical option for CW moving joints as consequence of its ability to accommodate cyclic displacements of glazing panels by elastic extension and compression [42]. To select an appropriate type of

silicone, the cohesive and adhesive strengths of the material have to be considered to ensure that failure occurs cohesively at a foreseeable degree instead of adhesively at unforeseeable degree [37]. Cohesion relies on the formulation and cure mechanisms, and adhesion is influenced by the state and type of surface where silicone is applied [58].

Table 2.3 Most common Infill attachments [40,20,42].

Glazing method	Characteristics	Legend	Sketch
Dry: Pressure plate	<ul style="list-style-type: none"> • Most common option to hold glass between frame profile and pressure plate • Pressure mechanism activated by cap screws. Compression of gaskets generate the seal • Glass installed from the exterior • Exterior gasket works as a water intrusion barrier. Interior gasket is an air barrier between frame and infill 	A Aluminium cover B Cap screw C Pressure plate D Exterior gasket E Infill unit F Interior gasket G Mullion H Thermal break I Screw chase J Glazing cavity K Glazing plane	
Dry: Stop	<ul style="list-style-type: none"> • Glass locked between a fixed and a removable aluminium section known as "stop". • Compression of the "stop" generates seal • Interior or exterior removal of the "stop". • Glass installed at the side of removable part 	A Aluminium cover B Glazing tape C Thermal break D Infill unit E "Wedge in" gasket F Interior removable section G Gasket air seal H Fixed exterior section	
Wet: Structural silicone glazed (SSG)	2-Sided Structural Silicone (2SSG) <ul style="list-style-type: none"> • 2 edges of the glass adhered to the frame with SSG and 2 edges mechanically fixed. Possible to instal on site 4-Sided Structural Silicone (4SSG) <ul style="list-style-type: none"> • 4 edges of the glass adhered to the frame with SSG. Must be installed by manufacturer 	A Silicone weather seal B Backer rod C Infill unit D Gasket/tape E Structural silicone 4SSG position F Structural silicone 2SSG position G Gasket/tape	

2.1.1.4 Anchorage system

The anchorage system defines the manner a CW is attached to the building's slab. Standard options for this type of connections are not usual because the loading cases vary according to the project, but each connection type has two main components: an embedded steel plate (bracket) within the slab, and a fixing element made of steel (hook) connecting the embedded part with the frame [40] see Figure 2.6. The system design depends on the span, temperature, and seismic or wind loading conditions; but also, the anchor has to be designed to allow tolerances during the installation process [31,14] To accommodate wind loads, out-of-plane motions have to be considered; meanwhile for seismic considerations, the anchor system must be rigid, but it shall permit a certain degree of rotation and translation in- and out-of-plane [20].

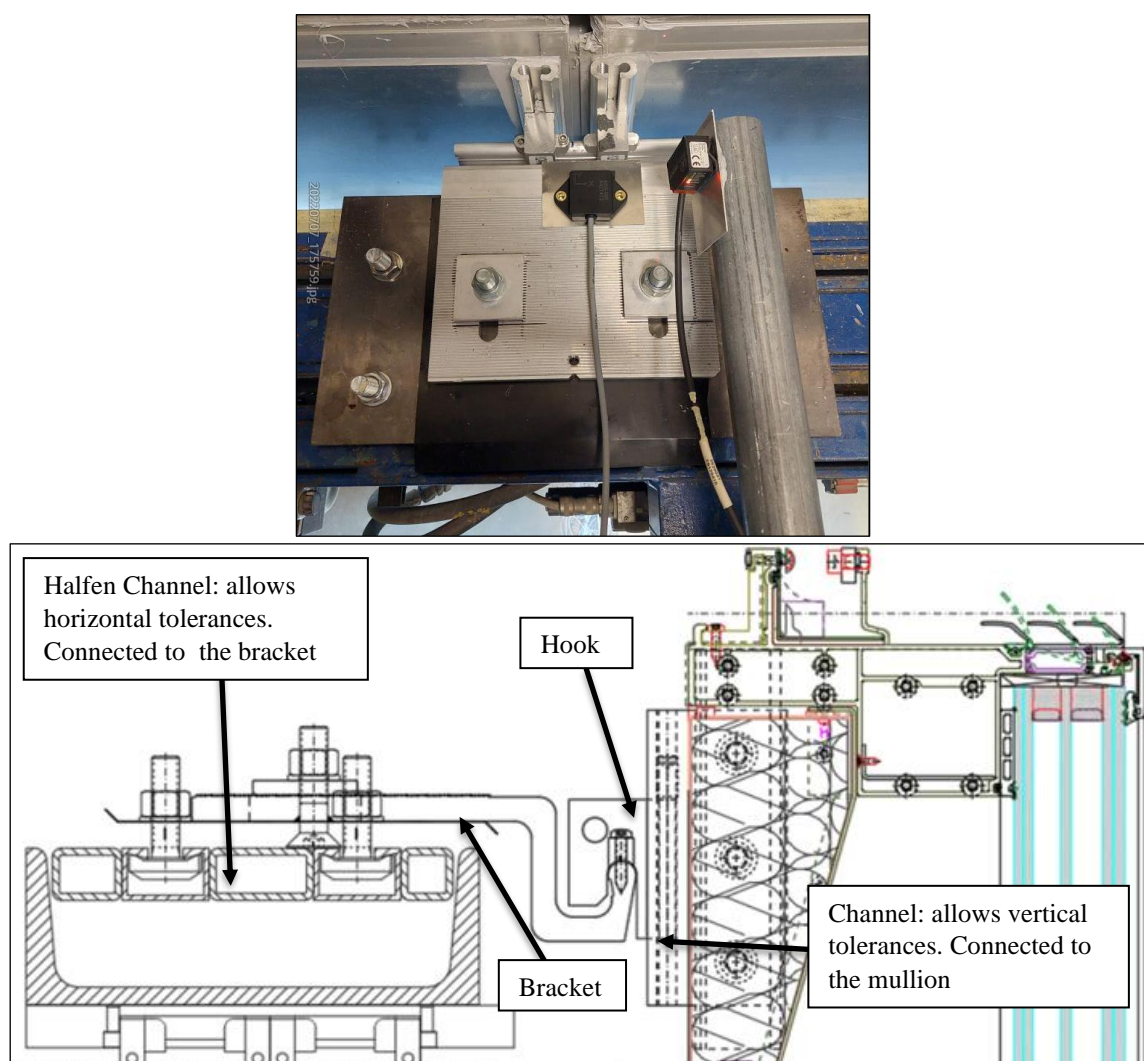


Figure 2.6 Example of anchorage system. Top: anchorage system photography. Bottom: vertical section

2.1.2 Types of glazed curtain walls

All the components mentioned before give a broader idea about the functions and design considerations of each component of a glazed CW unit, but no descriptions were made about the diverse types of CWs. A first classification can be made according to their design between standard and custom made. A standard system involves standard details and components

designed for a specific span length; however, there is certain flexibility with design and finishing enquiries [40,20]. It is possible to find information of a standard CW regarding its structural, weather, and thermal performance in catalogues [20], becoming the decision of the architects and engineers to consider if the system satisfies the building requirements. On the other hand, a custom system entails the design and detailing of components for a specific project [51]; this includes specific requirements for structural, weather, and thermal performance, but also it can include requirements to increase the occupant's comfort [20].

Finally, a second classification is made considering the installation methods into: stick and unitized. The stick system refers to the on-site assembly of CW pieces, and it is commonly used in low-rise buildings [64]. In the stick system, vertical components (mullions) are attached to the slabs, followed by the horizontal components (transoms) which are fastened to the mullions [43,20]. Once the framing is finished, the glazing unit is fixed to the mullions and transoms with pressure plates. This type of system permits a variation of the span between elements and the possibility arrange them with a staggered grid, giving freedom for façade design [64]. A drawback of this type of system is the inferior assembly quality when compared to unitized. This condition is the result of poor adhesion of sealants to joint surfaces caused by inadequate clean conditions when assembling on site [64].

A unitized CW unit is manufactured, assembled, and glazed at the shop, commonly one-story high [43], see Figure 2.7. The fabrication of unitized CWs in a controlled environment guarantees the correct assembly of each element, which means fewer human errors during the installation process. Moreover, the installation speed increases while reducing to the minimum on-site manual labour, obtaining as a result a decrease in installation costs [32]. However, this system increases the requirements for storage on-site, transportation costs, and the dependence on an external manufacturer [32]. Nevertheless, due to the building advantages and additional reliability (because of the controlled conditions), the unitized system is the most popular for high-rise and mid-rise buildings [40].

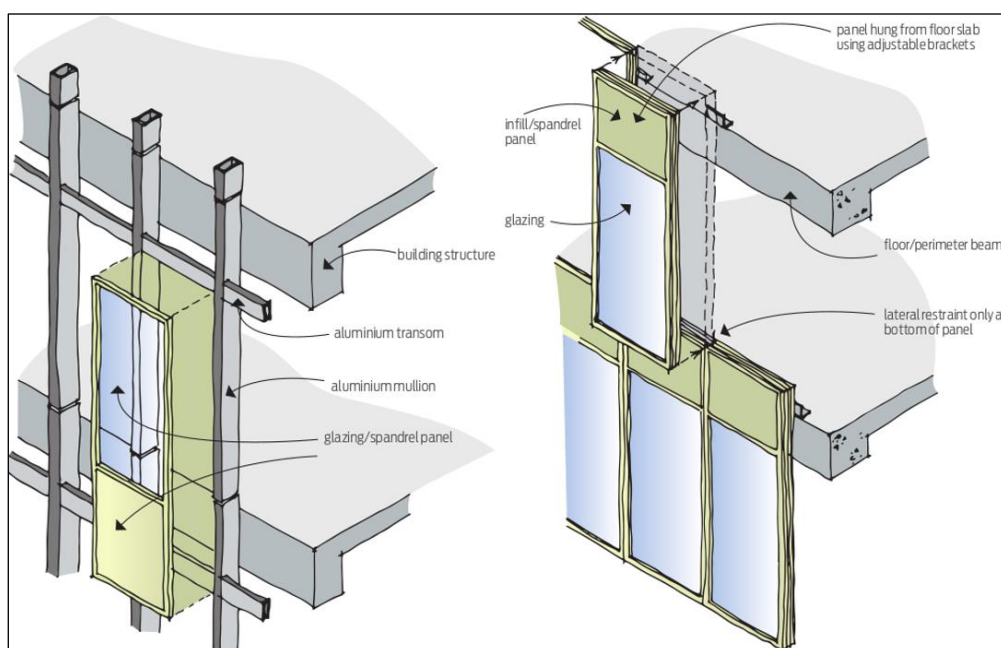


Figure 2.7 Left: stick system. Right: unitized system [60]

2.2 Design considerations

As mentioned before, a CW is the envelope of a building and a non-structural element. It is attached to the load-bearing elements of the building through an anchorage system which allows vertical and horizontal tolerances for displacement and installation. The parameters influencing its performance include watertightness, airtightness, condensation resistance, control of water vapour flow, heat flow, sound transmission, fire safety, and structural integrity [40, 45]. The importance given to a more detailed analysis of certain conditions is decided according to the project requirements.

To understand the performance parameters of a CW, it is important to start mentioning some important design features and considerations for the non-structural performance, even though it is not part of the scope of this research. To ensure watertightness and airtightness, it is important to: install waterproof seals properly, and to consider the use of internal drainage and barriers during the design [49]. The control of water vapour flow can be addressed with vapor retarding and permeable layers to reduce the risk of condensation [17]. A proper application of screen shading, coated glass, thermal breaks, and thermal insulation is necessary to control heat flow and, thus, improve the condensation resistance. Moreover, sound transmission is influenced by the distance between glass panes (in the case of IGUs), glass thickness, and glass-interlayer damping [48, 49]. At last, the control of fire can be addressed with the application of thermal resistant layers such as a firestopping layer between a CW and the edge of the slab [49].

2.2.1 Structural integrity

Structural integrity is related with life safety and repairment costs, so special attention must be given to the structural design of a CW. A well-designed CW must entail enough strength capacity to resist self-weight, wind, earthquake, blast (if required), maintenance, temperature, and environment loads [51]; nevertheless, a limited flexibility and the capacity to accommodate displacements govern the design [40].

Self-weight load is considered in the design of components within the unit and the anchorage system. However, it does not represent a design challenge due to its light weight, but wind load usually does. The selection and design of components is based on wind pressure and calculated from the wind load [50]. The loads acts over the infill, it is transmitted to the framing members, and finally to the main structure through the anchor system [45]. Therefore, the selection of the glass infill and the framing cross-sections depends on the correct calculation of the wind parameter. A proper calculation of wind pressure is necessary to determine the glass type and thickness, and the cross-section of the horizontal and vertical framing elements. The selection of the components is based on limiting their flexibility (stiffness) rather than the strength [43]. The stiffness check of the frame elements is followed by a strength check at critical points to determine an satisfactory behaviour [17].

Even if the components are properly designed with an adequate stiffness and resistance to transmit the governing wind loads, the seismic actions over the elements can compromise their performance. To address the seismic incidence in the design, inertial forces caused by the mass

of the CW, and the sway of the building must be considered [40]. With these considerations, it is clear that a CW becomes an acceleration and drift sensitive NSE [47]. The inertial forces are the result of floor accelerations originated when the seismic movement reaches the main structure [13], but these forces are not expected to govern over wind loads in the design because of the relative light weight of a CW [13, 47]. Nevertheless, the induced in- and out-of-plane displacements can have a negative effect in the façade unit, and they must be addressed; in this case in-plane displacements result in the most critical aspect to consider in the design [21]. However, despite seismic codes require CW units to accommodate drift displacements, limited instructions on how to determine drift limit states are given [46].

During an earthquake, the global behaviour of a CW unit is expected to follow two phases [14]. The first one characterized by the rigid rotation of the whole cladding unit (frame and glass) until it is locked by an adjacent unit when both units meet each other. The second phase occurs once the rigid rotation of frame is locked. In this case, the frame is deformed due to its restricted state and adopts a rhomboidal shape to accommodate the rotation; in this particular moment the integrity of the glass infill may be compromised because contact between glass and frame occurs at one or two corners of the CW, See Figure 2.8.

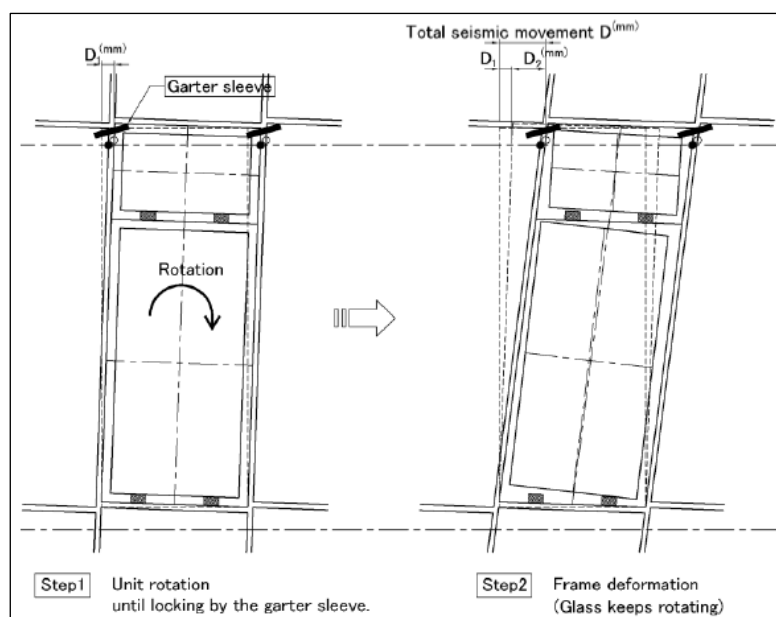


Figure 2.8 Scheme of the expected behaviour of a CW facade during seismic action [14]

It is clear that a CW system is vulnerable to displacements imposed by the main structure due to the limited movement capacity that the frame and infill have, where large space for movements reduces aesthetics and increases costs. Moreover, It was noticed after Northridge and Loma Prieta earthquakes that flexible structures experiences 3 to 4 times more glass damage compared to rigid structures [47], explaining why seismic drifts must be considered in the design phase. Even if the main structure has not suffered any considerable damage, earthquakes can lead to a significant deterioration of CW façades such as: glass cracking and fallout, gasket/seal degradation, and frame damage [65]. O'Brian W., et all. classified the CW's damages into two damage states serviceability and ultimate [67]. Glass cracking and gasket/seal degradation are considered as serviceability failures because they do not represent direct risk to human safety; on the other hand, glass fallout is considered as an ultimate limit

state failure because it represents a risk to life safety and results in an envelope unable to accomplish its main barrier function against external conditions [67, 68].

2.2.2 Seismic damage states

As aforementioned, the main damage states related to earthquakes stated in literature are glass cracking and fallout, gasket/seal degradation, and frame damage. Since the scope of this thesis is the analysis of the seismic performance of the connections within a CW unit, the understanding of the interaction and incidence in the overall performance of the façade of the components within a CW is key for the development of a numerical analysis framework.

2.2.2.1 Glass cracking

Glass cracking is a serviceability damage state that usually occurs at the edges of the glass close to the corners, see Figure 2.9 [65, 68]. It starts as glass fragmentation or cracks located at the non-vision area (area covered by frame and pressure plates) of the glass panel, and it is followed by a crack propagation to the vision area (area not covered by framing) [67, 68]. Glass crushing or fragmentation refers to the detachment of small glass fragments from the edge. Glass cracks are formed as a result of the contact between the glass panel and the frame, and this is caused when the glass infill meets the frame due to rotation and translation movements. The effect of wind and thermal stresses acting over the initial small cracks can potentially increase the cracks size and affect the thermal performance and condensation resistance of an IGU [68].

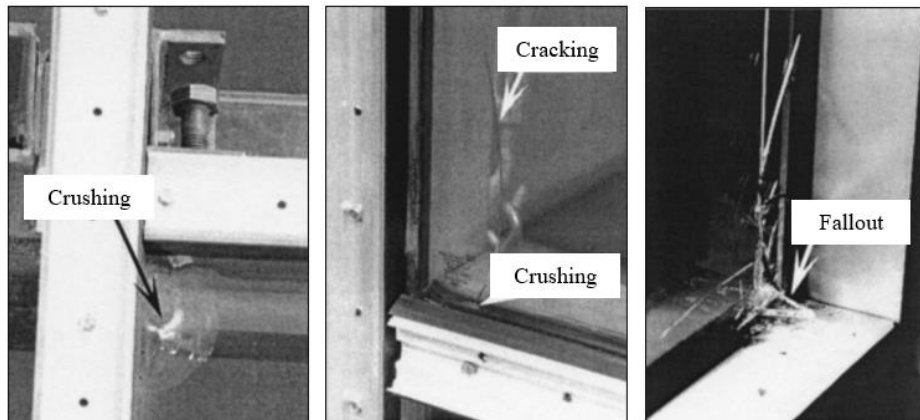


Figure 2.9 Glass crushing, cracking, and fallout developed at the glass edge [67].

2.2.2.2 Glass fallout

Glass fallout is considered an ultimate damage state due to its possible harmful effect against life safety. It corresponds to glass rupture into fragments bigger than 1 in² (645 mm²) caused by the relative moment glass-frame [55, 67]. Differential displacements between the glass infill and the frame led to glass cracking and later to glass fallout. Glass fallout cannot occur with the crack formation first even though in some cases both occur at a relative same time [67]. During experimental studies, Bouwkamp and Meehan defined a deformation sequence of windows applicable to CW, consisting in 2 phases [48]. First, the frame and the glass plate move horizontally until the frame is deformed and the first contact between both elements

occur at two opposite corners of the glass. Then, the glass infill starts rotating until the corners of both elements coincide, increasing the stresses at the glass corner until its failure, see Figure 2.10.

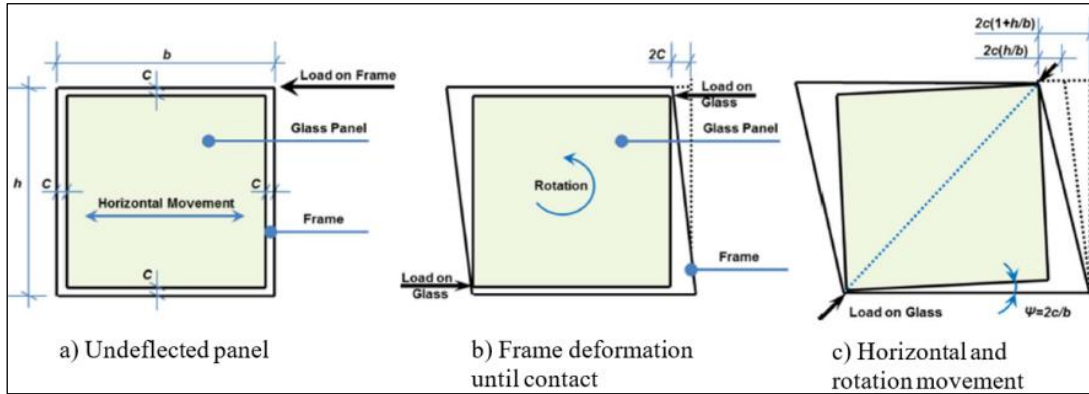


Figure 2.10 In plane drift CW [24,48]

Following the sequence proposed by Bouwkamp, a method was elaborated to determine the total lateral deformation capacity of a CW unit (D_{clear}), assuming a rigid body motion of the frame; see 2.1 equation for same values of vertical and horizontal clearance and see 2.2 equation for different clearance lengths [49]. This method is valid when a soft sealant is applied to fix the glass and frame because it allows a relative displacement of the glass with respect to the frame. Moreover, if as a result of aging the sealant hardens, the lateral drift capacity is reduced considerably [24].

$$D_{clear} = 2c \left(1 + \frac{h_p}{b_p} \right) \quad (2.1)$$

$$D_{clear} = 2c_1 \left(1 + \frac{h_p c_2}{b_p c_1} \right) \quad (2.2)$$

Where:

D_{clear} : Relative horizontal displacement, which causes initial glass-frame contact.

H_p : Height of the rectangular glazing unit.

B_p : Width of the rectangular glazing unit.

C_1 : Vertical clearance between glazing unit and curtain wall frame

C_2 : Horizontal clearance between glazing unit and curtain wall frame

Glass cracking and breakage is product of contact stresses between the framing and the infill unit. It can be noticed that the infill-framing clearance is a factor to consider when predicting possible glass damages because the larger the clearance, there is more space to accommodate displacements. However, there are other considerations ruling the potential glass damage caused by relative displacements. As mentioned in sub-chapter 2.1.1.2, the glass strength is influenced by the production method, where a heat treated element results in increased bending capacity. Additionally, the type of CW system has also an influence in the drift capacity; for example, CW unitized units are placed individually and joined together with horizontal stack joints which allow in-plane horizontal sliding, allowing each unit to move separately without causing excessive deformations [47]. An extra feature that can be

determinant to prevent glass fallout is the use of structural silicone glazing. This contributes with shear and tensile resistance capacity against displacement and provide protection against contact with the frame at the corners [47].

2.2.2.3 Gasket/seal degradation

Dynamic movements affect considerably the seal at the glazing perimeter, resulting in openings that may compromise the serviceability of the system against air and water infiltration [67]. As reported by Behr R., et al., four types of degradation were identified during dynamic racking tests: distortion, pull-out, push-in, shifting, see Figure 2.11 [68]. A racking tests is the simulation of seismic displacements acting over a CW unit.

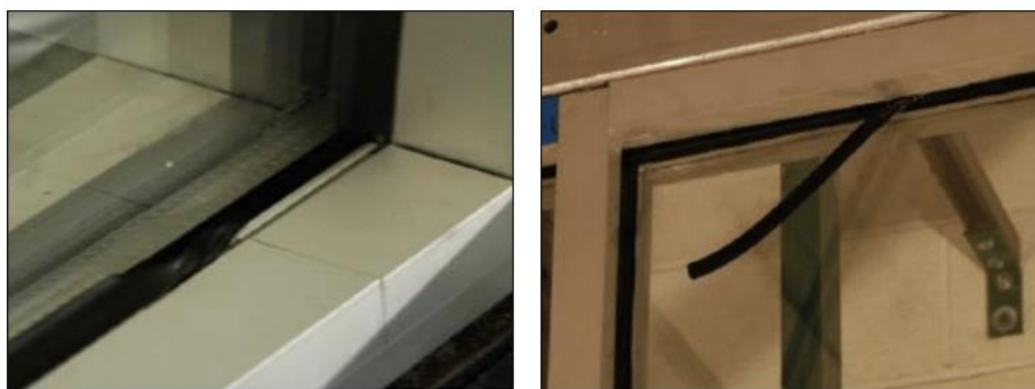


Figure 2.11 Left: Gasket distortion. Right: Gasket pull-out [67].

Gasket distortion is the result of twisting or bulging, while the gasket remains attached within the glass and the glazing pocket. Pull-out happens when a section of the gasket is withdrawn from the glazing pocket. Push-in occurs when the gasket is pushed inside the glazing pocket. Shifting is the result of a gasket section displaced along its longitudinal axis, causing an open gap between the glazing and the frame [66, 67, 68]. Moreover, degradation was also reported in SSG units; it was observed that sealant distortion, shear and cohesive/adhesive failures occurred when submitting a CW unit to racking displacements [67].

2.2.2.4 Frame damage

Frame damage has its origin when two CWs contact one to another when submitted to a racking displacement. When analysing frame to frame contact, minor damages and plastic deformations have been reported in the literature [65]. The damage is considered minor when small displacements between the elements, small decrease in framing stiffness and screws loose occurs [66, 67]. Moreover, plastic deformations were observed at the corners of the frame. It was observed during a sequence of tests elaborated by Memari A., et al. that frame damage is related to the thickness of the glazing unit. As for the causes of failure, it was observed a complete detachment of the bottom horizontal pressure plate, extreme rotation of the bottom transom, and/or failure of the bottom transom itself [67], see Figure 2.12.

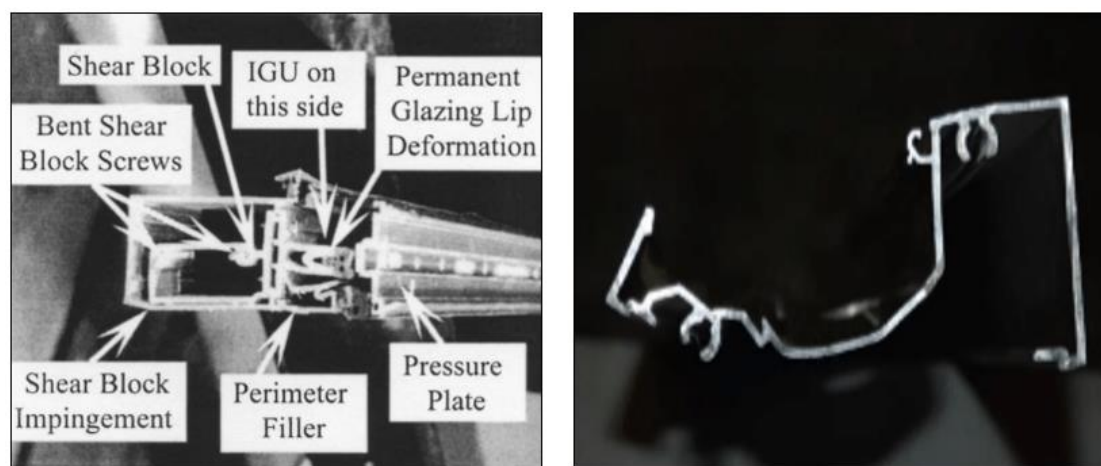


Figure 2.12 Left: Transom deformations after testing. Right: Mullion with deformation damage [67].

So far, it has been demonstrated that seismic drifts cause problems to a CW system. However, it is still important to understand how seismic drifts and inertial forces are assessed and related with the different damage states stated in the codes around the globe. This topic will be addressed when analysing and comparing European, Japanese, and American provisions.

2.3 Seismic regulations

It was already mentioned the scarcity of research concerning NSE subjected to seismic action, but no information was provided about existent seismic regulations of this elements. Therefore, in this section an explanation of how regulations address the seismic problematic of NSE is provided for three different regions, with special attention to curtain walls.

Regulations from Europe, United States and Japan are studied. The selection of these 3 regions is based on the relevance with the case studies presented in Chapter 3, the amount of information available, and the emphasis of the regulation due to high earthquake hazard.

Seismic activity affects specific zones of Europe, and it has caused building damages and human casualties. For this reason, an entire chapter of the Eurocode is dedicated to the seismic resistance design of structural and NSE elements; additionally, seismic design is also considered in the existent normative for CW design. In the case of the U.S., the west coast of North America is an area with a high degree of seismic risk because the Pacific and North American plates meet along the state of California, the place where the relative recent Northridge earthquake took place. To solve this problematic, institutions such as the Federal Emergency Management Agency (FEMA) and the National Earthquake Hazard Reduction Program (NEHRP) elaborated the seismic design provisions FEMA 450 for buildings and other structures based on existent requirements provided by the American Society of Civil Engineers (ASCE) and the American Architectural Manufacturers Association (AAMA). Finally, the Japanese regulations are considered because the country is located in the high seismic risk zone known as “The Pacific Ring of Fire”. Along the years, several earthquakes have affected the territory, and one of the most destructive and intense took place in the last decade a M_L 9,1 in Tohoku (2011), destroying cities and even causing structural damages to a nuclear plant [52]. To counter the high incidence and damages caused by earthquakes, strict regulations must be

followed in Japan regarding seismic design; in this chapter the “Japanese Architectural Standard Specification (JASS) 14 Curtain Wall” is described. After brief description of the standards mentioned, a final discussion comparing similarities between the codes is included.

2.3.1 Eurocodes

In this section a description of CW requirements, verification procedure and tests are described. A match between the codes EN 13830: “Curtain Walling Product Standard” and EN 1998-1: “Eurocode 8 – Design of structures for earthquake resistance – Part 1:1” is done because EN 13830 refers to Eurocode 8 provisions when considering seismic resistance requirements; finally, it is important to consider that Eurocode 8 includes CWs in the NSE category.

2.3.1.1 Requirements

In EN 13830 three requisites are approached: general requisite, safety in use, and serviceability [54]. The general requirement establishes that A CW must be able to resist a seism with a higher probability of occurrence than the design seismic action, without causing human risks and limitations of use. Safety limit states that CWs shall resist the inertial forces triggered by the design seismic action and accommodate movements to prevent failure of the glass unit, framing connections or anchorage system. Finally, for the serviceability limit, it is required to satisfy the limits established in the norm for air permeability and watertightness after a seismic action of shorter return period than the design seismic action.

2.3.1.2 Verification

A verification procedure is proposed in section 4.3.5 from Eurocode 8 (2004) to verify the resistance of a NSE (including its components and connections) to a horizontal seismic force acting at the centre of mass of the element [53].

$$F_a = \frac{S_a * W_a * \gamma_a}{q_a} \quad (2.3)$$

Where:

F_a : Horizontal seismic force at the mass centre of the element in the most unfavourable direction

S_a : Seismic coefficient applicable to the non-structural elements

W_a : Weight of the element

γ_a : Importance factor of the element, Eurocode 8

q_a : Behaviour factor of the element.

The seismic coefficient is calculated with Equation 2.4:

$$S_a = \alpha * S * \left[\frac{3 \left(1 + \frac{z}{H}\right)}{1 + \left(1 - \frac{T_a}{T_1}\right)^2} - 0,5 \right] \quad (2.4)$$

Where:

S_a : Seismic coefficient applicable to the non-structural elements

S : Soil factor

z : Height of the NSE above the level of application of the seismic action

H: Building height measured from the foundation

T_a : Fundamental vibration period of the NSE

T_1 : Fundamental vibration period of the building in the relevant direction.

Requisites for NSE to adjust displacement are not present in the current Eurocode 8, but a damage limitation requirement, which can be related to the general requirement in EN 13830, provides a limitation of inter-storey drift (section 4.4.3.2) for buildings with NSE of brittle components fixed to the main structure (2.5).

$$d_r * V \leq 0,005h \quad (2.5)$$

Where:

d_r : Designed inter-storey drift

h : Storey height

V : Reduction factor which considers the lower return period of seismic action associated with damage limitation

2.3.1.3 Tests

In the Annex B of the European Curtain Walling Product Standard, a real size mock-up with an in-plane racking test is recommended as an option to check if a CW satisfies the safety and serviceability limit criteria. The test procedure is done with 3 cycles of movement, where the unit is moved to one extreme position, then, it is moved to the other extreme position, and finally it returns to its original position. The displacement applied is defined according to the limit criteria considered, and both seismic limits are defined as the angular rotation of a mullion from the in-plane vertical direction [53].

2.3.2 FEMA 450

FEMA 450 gives provisions for “architectural components”, including CWs, these provisions can be described as a compilation of ASCE and AAMA requirements. For calculations such as seismic forces and drift capacity, FEMA refers to ASCE-7. For tests, it refers to AAMA 501.4 and AAMA 501.6 protocols.

2.3.2.1 Requirements

Only requirements regarding the structural performance are mentioned in FEMA 450. However, serviceability and ultimate limits are given by the tests performed according to AAMA standards and will be described in test section. The provisions require non-structural wall panels (CW) fixed to the main structure to resist inertial forces and to accommodate seismic movements. The design of the anchor system shall consider the loss of load bearing capacity in case of significant yielding, and it shall permit a relative movement between stories in function of the story drift [55].

2.3.2.2 Verification

To verify an “architectural component” against seismic action, seismic forces and seismic drifts shall be considered. Seismic forces are determined with a procedure similar to the one defined in Eurocode 8. In section “6.2.6 Seismic forces”, to verify the strength and stiffness of a CW

and its components, a horizontal design seismic force shall be calculated and applied in the in-plane centre of gravity of the unit, see Equation 2.6 [58].

$$F_p = \frac{0,4a_p * S_{DS} * W_p}{\frac{R_p}{I_p}} \left(1 + 2 * \frac{z}{h}\right) \quad (2.6)$$

Where:

F_p : Horizontal seismic design force

a_p : Component amplification factor

S_{DS} : Spectral response acceleration at short period

W_p : Component weight

R_p : Component response modification factor

I_p : Component importance factor

z : Height of the NSE above the level of application of the seismic action

h : Storey height

With:

$$F_p \geq 1,62S_{DS} * I_p * W_p \quad (2.7)$$

$$F_p \leq 0,3S_{DS} * I_p * W_p \quad (2.8)$$

Where:

F_p : Horizontal seismic design force

S_{DS} : Spectral response acceleration at short period

I_p : Component importance factor

W_p : Component weight

Regarding the displacement considerations, exterior wall panels should be able to accommodate the relative inter-storey movement (D_p), Equation 2.9.

$$D_p = \delta_{xA} - \delta_{yA} \quad (2.9)$$

Where:

D_p : Design inter-storey drift

δ_{xA} : Deflection at level x of structure A

δ_{yA} : Deflection at level y of structure A

With:

$$D_p = (X - Y) \frac{\Delta_{aA}}{h_{sx}} \quad (2.10)$$

Where:

D_p : Design inter-storey drift

X : Height above the base of the upper support attachment (at level x)

Y : Height above the base of the lower support attachment (at level y)

Δ_{aA} : Allowable story drift for structure A

h_{sx} : Storey height used in the definition of the allowable story drift

Moreover, an additional provision for glass within a CW is considered. The glass infill must be able to address the relative displacement in Equation 2.11,

$$\Delta_{fallout} \geq 1,25 * I_p * D_p \quad (2.11)$$

Where:

$\Delta_{fallout}$: Relative displacement (drift) at which glass fallout from a curtain wall

Where $\Delta_{fallout}$ is determined with AAMA 501.6 provisions. However, if sufficient clearance between glass and framing is provided (Equation 2.12) no actions shall be taken.

$$D_{clear} \geq 1,25 * D_p \quad (2.12)$$

Where:

D_{clear} : Relative horizontal displacement, which causes initial glass-frame contact.

Where D_{clear} can be calculated according to Bouwkamp and Meehan by following Equation 2.1 and 2.2.

2.3.2.3 Tests

The guideline for seismic performance tests is provided by AAMA. Two different types of tests are described, one to determine the (serviceability) resistance against air leakage and water penetration after a horizontal displacement is applied (AAMA 501.4), and the other one to determine the maximum drift capacity before the glass fallout (AAMA 501.6).

According to the ASCE manual for CW systems [47], the test method AAMA 501.4 consists of a static racking test, which evaluates the behaviour of a CW exposed to an imposed lateral displacement. The test is performed with a full size test specimen subjected to an imposed displacement applied through a hydraulic beam, see Figure 2.13. The displacement has to be 0,01 times higher than the adjacent story heights and shall be applied in 3 cycles [55]; a cycle is defined as a full lateral displacement in one direction followed by the return to its original position, and, finally, a full lateral displacement in the other direction. The mock-up must be at least one story high for single-story buildings, and at least two storeys high for multi-storey buildings. All the elements used in the mock-up shall be made with real-size elements. The test focuses on the serviceability of the CW which may change as a result of the displacement applied. This evaluation is done by a pass/fail criteria, which includes the next provisions: functionality and visible damage, glass cracking, and post-performance [56].

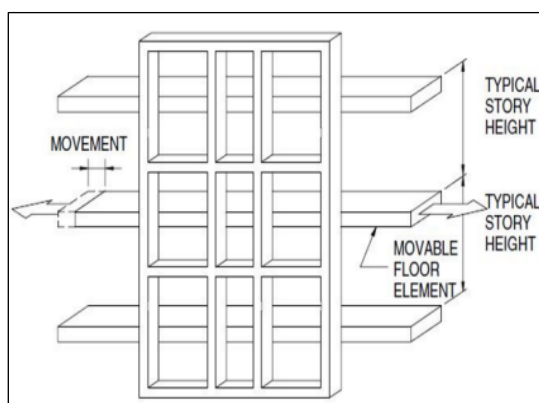


Figure 2.13 Typical multi-storey mock-up (AAMA 501.04) [56].

A dynamic racking test is proposed in AAAMA 501.6 to evaluate the drift provoking glass fallout from a CW unit (Δ_{fallout}) [57]. In other words, it focuses on the ultimate limit state of the glass infill. The dynamic racking or crescendo test, consists of installing full size CW units on a dynamic test system which moves horizontally with sinusoidal motions gradually and progressively increasing [56], see Figure 2.14. The loading starts with a frequency of 0.8 Hz, until it reaches an amplitude of 75 mm, and changes to 0.4 Hz for amplitudes greater than 75 mm. The test is accomplished when one out of the next three conditions is reached: glass fallout, the drift index over the glass infill is 0,10, or when a displacement of ± 150 mm is reached [57]. The lowest drift amplitude value obtained at the moment of glass fallout is selected as the Δ_{fallout} value for the CW [56] and is used in Equation (2.11).

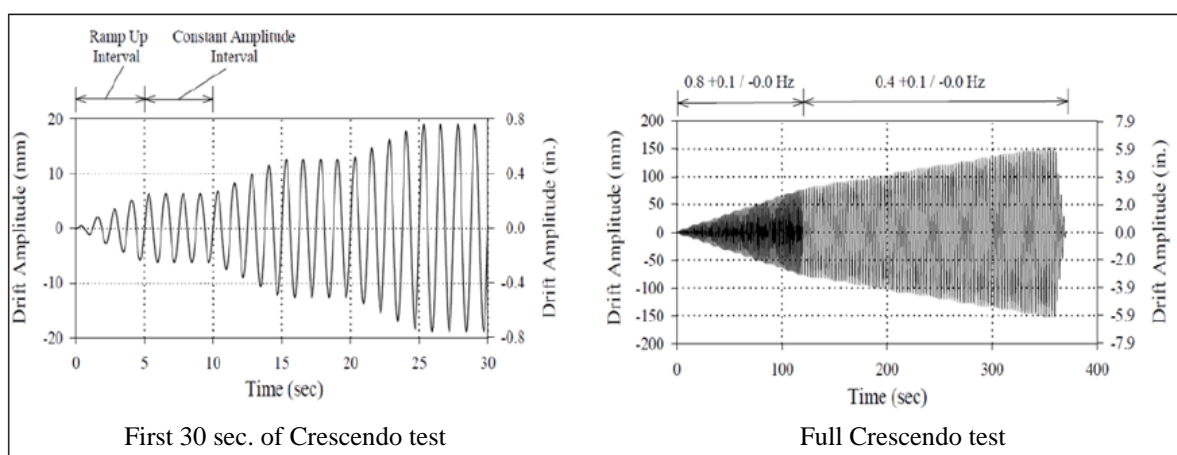


Figure 2.14 Example of a dynamic crescendo test. Starting with 0,8 Hz [57].

2.3.3 JASS 14

JASS 14 approach is focused on inter-storey relative displacements and considers various levels of performance.

2.3.3.1 Requirements

Despite its main approach related to inter-storey drifts, the standard requires a CW unit and its components to withstand the inertial forces originated by seismic action in two directions, horizontal and vertical. Moreover, a specific provision is mentioned in relation to inter-storey drifts, where different requirements shall be taken based on three different seismic intensity levels, see Table 2.4.

2.3.3.2 Verification

To calculate the resistance against inertial forces JASS 14 requires the application of a seismic design force at the centre of mass of the CW, to evaluate its strength and stiffness. The seismic force applied depends on the seismic primary and secondary waves [59], see Equations 2.13 and 2.14.

$$F_{P,V} = W * S_P \quad (2.13)$$

$$F_{P,H} = W * S_P \quad (2.14)$$

Where:

$F_{P,V}$: Vertical seismic force acting at the mass centre of the element

$F_{P,H}$: Horizontal seismic force acting at the mass centre of the element

W: Weight of the element

S_P : Seismic coefficient in vertical direction

To verify the performance based on the inter-story drift, 3 levels of performance and the respective requirement can be seen in Table 2.4.

Table 2.4 JASS 14 provisions for inter-storey displacements [59].

Limit	Max. inter-storey drift (m)	Potential hazard	Probability of occurrence
Level 1	H/300	No damages to internal and external components	Frequent
Level 2	H/200	Stresses in all external components must not exceed the allowable limits	Largest scale earthquake occurred in the past
Level 3	H/100	No damage of glass and no dropout of any component allowed	Greatest earthquake expected in 100 years

H = floor height (m)

2.3.4 Summary

A summary of the described seismic regulations is provided pointing the similarities and differences between them.

The Eurocodes 8 and 13830, and the North American provision FEMA 450 have apparently similar requirements. Both documents emphasize the necessity of performing a resistance check of the CW unit and its components using a horizontal seismic design force based on a response spectrum, importance factors, and seismic coefficients, which differs from the Japanese code where a horizontal and vertical forces are calculated with seismic coefficients only.

The three situations analysed address in different manners the inter-storey displacements. The limitations are reduced to an inter-storey displacement limit in Eurocodes for buildings with NSE with brittle components fixed to the structure. FEMA 450 provisions establish a limitation of the maximum drift of the structure considering the relative displacement of the glass within a CW. On the other hand, the focus of JASS 14 on displacements is addressed by seismic drifts, establishing limitations in distinct levels according to the potential hazard and probability of occurrence.

Regarding the suggested tests methods, there are not specific requirements mentioned in JASS 14, but Eurocode 13830 and FEMA 450 (AAMA 501.4 and 501.6) present some laboratory performance assessments. Eurocodes recommend a static racking test of a full-size mock-up, to evaluate both serviceability and safety limits of a CW unit. The North-American provisions FEMA 450 makes a reference to AAMA to describe two different tests to assess serviceability and the ultimate limit states. The standard AAMA 501.4 is similar to the one mentioned in the

European standard, consisting of a static racking test where a displacement of 0,01 times the story height is applied to test the service limits in function of water- and air-leakage post-seismic tests. Moreover, to check the ultimate limit stage of a CW, a procedure according to AAMA 501.6 is given in function of the glass panel fracture when submitted to dynamic displacements.

Finally, the limitations proposed in the three provisions can be grouped into two limit stages. A serviceability limit state, similar to the one considered in Eurocode and AAMA 501.4, where the CW shall guarantee functionality providing the interior of the structure with a barrier against air and water (Eurocode and AAMA 501.04), and without compromising any of its components (JASS 14). At last, an ultimate limit state combining the limitations given by the Eurocodes, AAMA 501.6 and JASS 14 can be reduced to the fact that a CW shall resist the inertial seismic forces and displacements imposed by the structure without glass fallout nor component drop-out.

3

Case Studies

This chapter will describe and present the two case studies analysed in this research. The description will include details about the CW specimens, monitoring systems, tests performed, and regulations followed, and testing sequence. Additionally, special attention will be given to the test carried out during the year 2022 at Permasteelisa Group installations. The reason of this focus is the fact that this is the latest seismic campaign performed and will be the base for a more detailed seismic performance analysis of a glazed CW. Nonetheless, for the test campaign of 2011, a brief explanation with fundamental information will be included. Relevant outcomes to this research will be provided in Chapter 5: Results and Discussion.

3.1 Case study 1 (2011)

To accomplish the objective established for this research, it is essential to consider case study 1 as a first step in the numerical model development. This case is selected because the geometry of the CW specimen analysed is relatively simpler than the specimen described in Case Study 2, displacement results of the overall behaviour of the façade were already processed, and a numerical model of a single CW unit is already available in the thesis report made by Umberto Galli (2011). Therefore, the relative easiness of the project and the immediate availability of data made this case a good starting point to introduce a first approach to evaluate the performance of the connections under seismic loads locally and globally.

3.1.1 Introduction

The specimen was assembled with four CW units with structural silicone, and it was designed and manufactured for its installation at the Manchester Metropolitan University Business School in November 2009, see Figure 3.1. It was later used in a test campaign carried out by Permasteelisa in Italy, starting in July 2010, and finalizing in January 2011. The purpose of these set of tests was to evaluate the behaviour of two distinct types of structural silicone: Sika SG500 and Sika SG550. At the same time, the results obtained were used for the development of a numerical model representing the seismic behaviour of a CW unit presented in the research made by Umberto Galli. Now, the displacement data previously obtained and processed is used to evaluate the global performance and calibrate a FEM of the specimen when submitted to a seismic imposed displacement by implementing a detailed analysis of the connection's performance.



Figure 3.1 Manchester Metropolitan University [14]

A set of static racking tests were performed measuring the absolute displacements of the glass infill, aluminium frame, and anchorage system with displacement transducers. The displacement transducers were located strategically to measure the displacements of two adjacent units with different type of SSG, see Figure 3.2. Similar to the description given in the Literature review, the mock-up tested consisted of a real representation of the façade, which was constructed and fixed as if it was going to be installed in a building. The static racking test consisted in the application of five full displacement cycles by means of a seismic beam, capable of moving in-plane (horizontally and vertically) and out-of-plane. To determine the magnitude of the displacements applied, JASS 14 provisions were adopted, and three seismic levels had to be checked. Seismic level 1 with displacement cycles of 12,50 mm, level 2 with 18,75 mm and level 3 with an imposed displacement of 37,50mm [14]. After each seismic level test, a sequence of test was carried out to determine if serviceability was compromised (e.g., air leakage test)

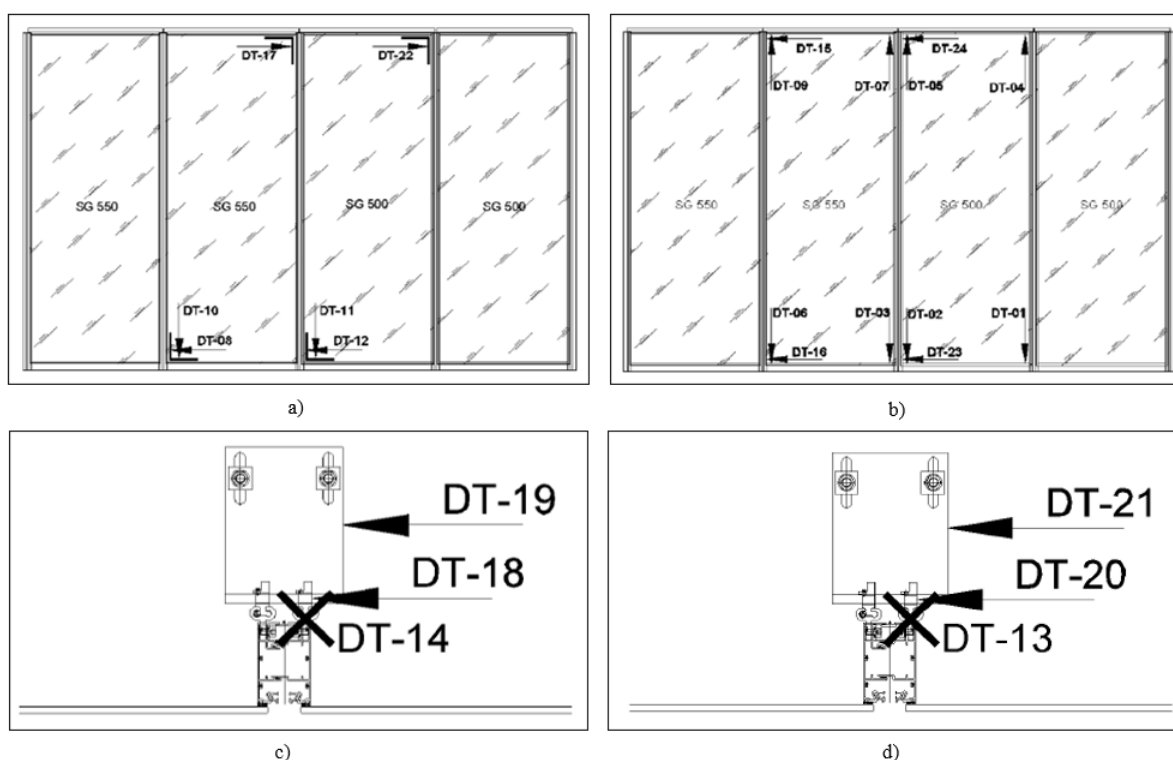


Figure 3.2 Displacement transducers. a) Over external glass b) Over the framing c) Upper anchorage SG550 d) Upper anchorage SG500

3.1.2 Specimen details

As described by Galli U., the specimen consists of four CW unitized units assembled with two types of structural silicon Sika: SG500 and SG550 with a cross-section of 10 mm x 6 mm and 6 mm x 6 mm respectively [14]. The dimensions of the glass panels are 1452 mm x 3752 mm, and the frame dimensions corresponding to one unit are 3800 mm x 1490 mm. The alloy used for the profiles is EN AW - 6063 T6 (EN 1999-1-1) and male-female joints are used to link the adjacent frame elements to each other [14]. The anchorage system holds the CW units from the top and consist of aluminium brackets, hooks, and steel bolts. At the bottom of the CW, the bottom transom is connected to the starter sill, which is fixed to a bottom bracket to prevent out-of-plane movements but allowing in-plane displacements.

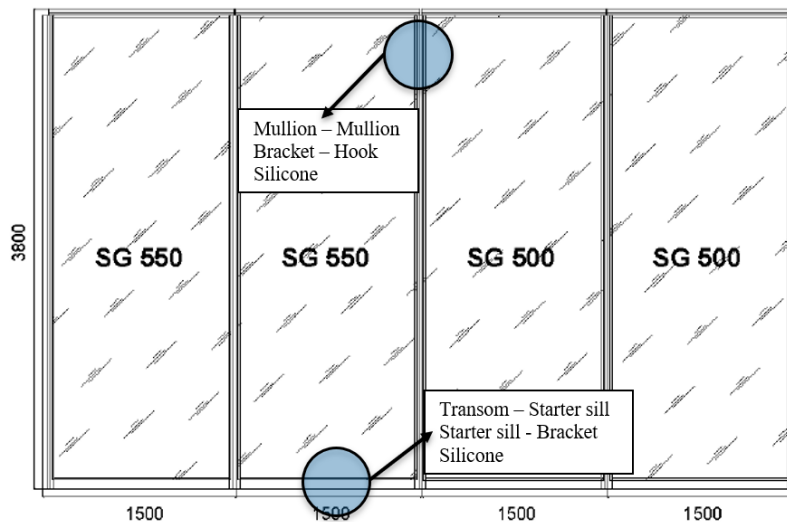


Figure 3.3 Specimen overall view and connection's location

The connections in analysis for case study 1 are: Mullion - Mullion, Transom - Starter sill, Starter sill - Bottom Bracket, Top bracket - Hook. Moreover, a study of the structural silicon behaviour is done to analyse its influence restraining the infill in-plane movement. Figures 3.3 and 3.4 provide an overall view of the of the connections in analysis and their locations.

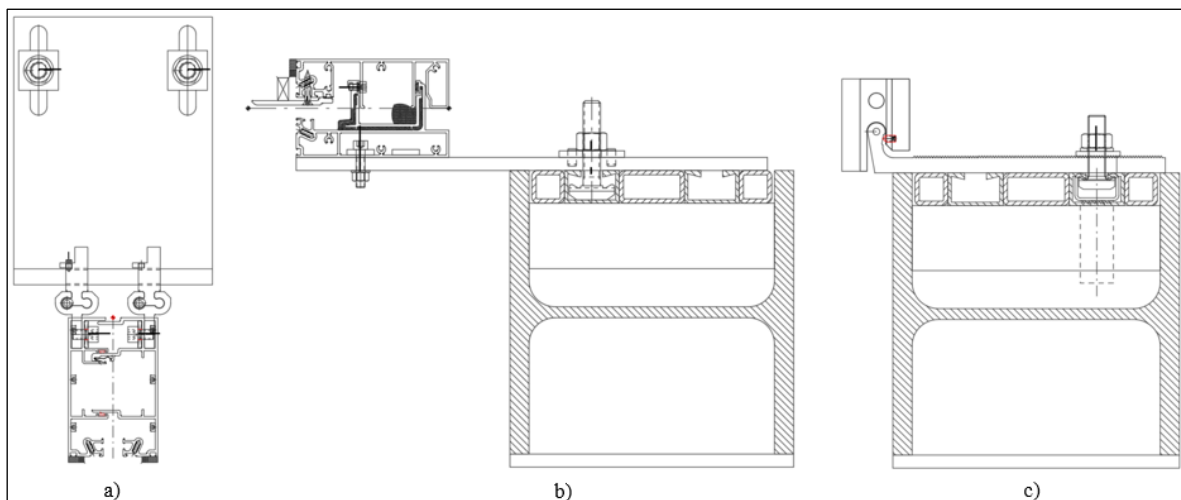


Figure 3.4 Connections cross-sections. a) Mullion, bracket, and hooks (top view) b) Transom, starter sill, bracket (lateral view) c) Bracket and hook (lateral view)

3.2 Case study 2 (2022)

The present case study presents a global and local evaluation of the seismic performance of a glazed CW of a more complex framing geometry. Similarly, to case study 1, in this case the displacements of the specimen were measured (global behaviour), but additional experiments testing the stiffness of the connections were also carried on (local behaviour). This analysis represents a further step in the numerical model due to the possibility to evaluate the connections individually without being restricted to global displacements checks. Moreover, few information about connections (tests and numerical models) is available in CW literature, where most of it is based on observations post seismic testing of the specimens; therefore, the purpose of this research to explore and reduce the gap of relevant information about seismic performance of the connections within a glazed CW. As a last point, this second case study is presented as a basic guide showing the multiple full-scale experiments required to evaluate seismic performance according to the serviceability limits provided by the codes.

3.2.1 Introduction

In 2022 Permasteelisa and TU Delft started an experimental campaign to support the research project "Seismic Safety and Energy efficiency: Integrated technologies and multi-criteria performance-based design for building Facades" (SAFE-FACE) Marie Curie research project [69]. The experimental campaign consists in the evaluation of four different types of specimens submitted to seismic actions following the available seismic regulations from which JASS 14 was selected to define the drift levels. The experimental layout initially consisted on testing the four different façade types in three phases comparing different glazing options. By the meantime, the testing campaign corresponding to phase one is already accomplished, and phases two and three are expected to be completed in the following months. Phase one consisted of testing two specimens from façade type 1 under seismic levels 1 and 2 according to the Japanese regulations, see Figure 3.5. The façade type selected was engineered, designed, and manufactured by Permasteelisa Group located in the region of Veneto, Italy. This CW was part of a façade renovation project of about 80.000 m² of the National Electricity Board (Enel) headquarters in Italy [23], see Figure 3.6.

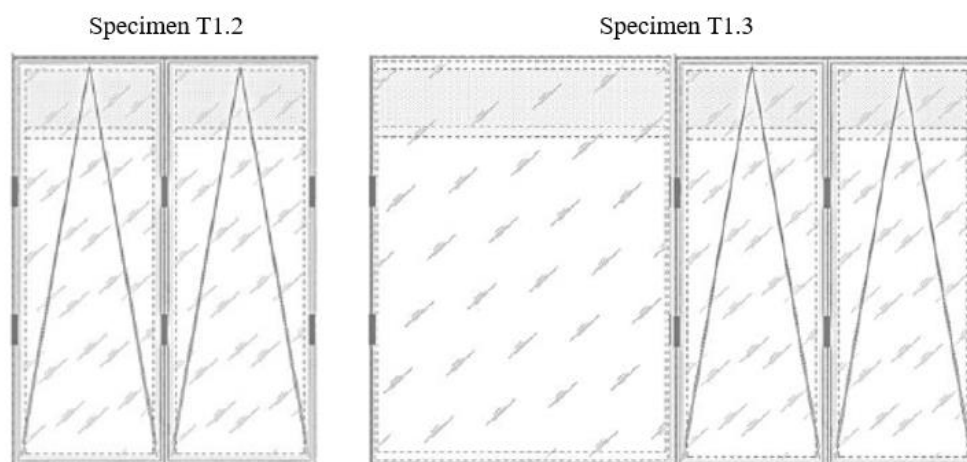


Figure 3.5 Facade type 1. Specimens T1.2 and T1.3

According to Bianchi S., the objectives of this experimental phase involve a: performance assessment of the façade, testing protocol validation, comparison between wet and dry glazing systems, and FEM calibrations [69]. The performance verification pretends to evaluate the response of the façade in function of its original configuration; the verification is achieved once the sample is submitted to a testing sequence according to the seismic levels established. The testing protocol or testing sequence is established to evaluate and compare air permeability, water resistance and structural integrity at different seismic drift levels according to the Japanese standard. For the two wet and dry glazing systems respectively, the comparison pretends to evaluate how they accommodate inter-storey drifts, but also considering their performance influence on other elements of the façade. Finally, this campaign intends to improve the modelling strategies with the calibration and validation of numerical models based on experimental results.



Figure 3.6 Enel's headquarters [23]

To accomplish phase one, two test sequences were prepared. The first test sequence involved specimen T1.2, and it was the key to determine the experimental sequence of specimen T1.3 because it was carried out as a control sample in order to establish a baseline for the elaboration of the final testing protocol. The test sequence of sample T1.2 included: seismic in-plane horizontal and out-of-plane displacements, and water penetration and air permeability tests. Once the tests concluded, a testing protocol for all the specimens was defined where an in-plane vertical displacement and a wind resistance test were included. With the testing protocol defined, a second test sequence was conducted to evaluate the seismic performance of the specimen T1.3. It is important to mention that both test sequences were evaluated according to seismic level 1 and 2 defined by the Japanese regulation JASS 14. The displacements applied to the CW can be seen in Table 3.1 where no damage is expected on the components for seismic level 1 and no exceedance of allowable stresses is expected for level 2. Moreover, additional tests were carried out to evaluate the connections within a CW; in this case the connections evaluated corresponded to the specimen T1.3. Due to the availability of information for the tested specimen T1.3, case study 2 is focused on the study of this specimen with special attention to its connections.

Table 3.1 Displacement applied to the specimens according to JASS 14

Limit	Max. inter-storey drift	Displacement (mm)	Potential hazard
Level 1	H/300	12	No damages to internal and external components
Level 2	H/200	24	Stresses in all external components must not exceed the allowable limits

3.2.2 Specimen details

The facade T1.3 consist of three CW units assembled together in a horizontal layout. Two out of the three units are openable with the next dimensions 1,25 m width and 3,43 m height, and for the third unit the width is increased up to 2,5 m but keeping the height of 3,43 m. The infill of the two small units was attached to the frame with a 4-SSG system by using the structural silicone DOWSIL 993EU with a silicone bite of 26 mm on transoms and mullions. On the other hand, the larger infill was attached to the frame with a dry-glazing system by means of mechanical restrains (gaskets). Centre to centre dimensions of the façade can be observed in Figure 3.7 together with a photograph of the façade specimen tested by Permasteelisa.

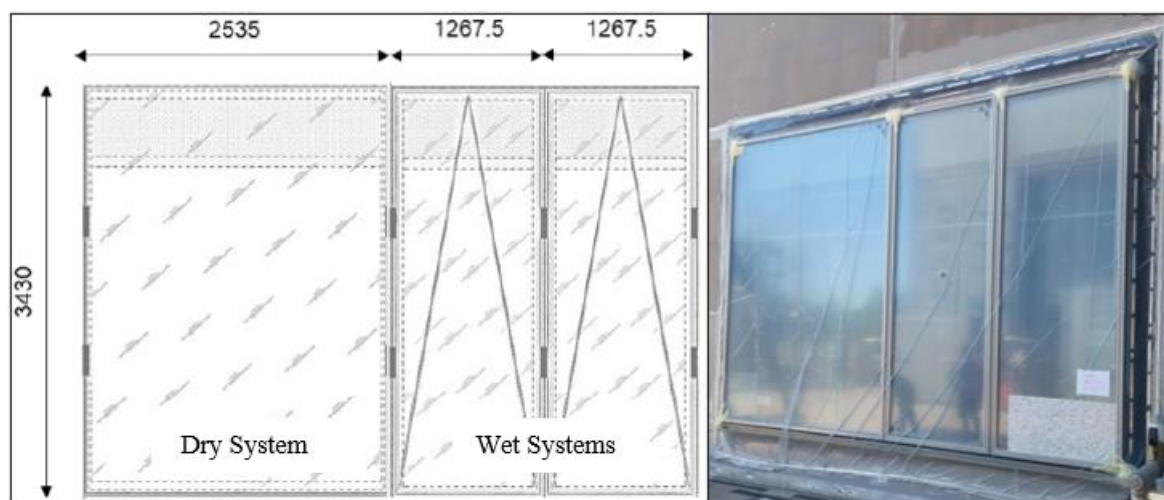


Figure 3.7 Sketch and photograph of specimen T1.3 [69]

Regarding the framing system, mullions and transoms are aluminium extrusions made with the alloy EN AW - 6063 T6 with mechanical properties specified by “Eurocode 9: Design of aluminium structures - Part 1-1” (EN 1999-1-1). The joint between adjacent profiles is addressed by male-female connections allowing the individual movement of the CW units up to a certain degree. At the lower part of the CW, the bottom transom is connected to the starter sill, which is fixed to a steel bracket to prevent out-of-plane movements but allowing in-plane displacements, see Figure 3.9. The specimen is connected to a seismic beam at the top through the anchorage system which consist of an aluminium bracket (EN AW - 6005 AT6), hooks (EN AW - 6082 T6), channels, and steel bolts as showed in Figure 3.10.

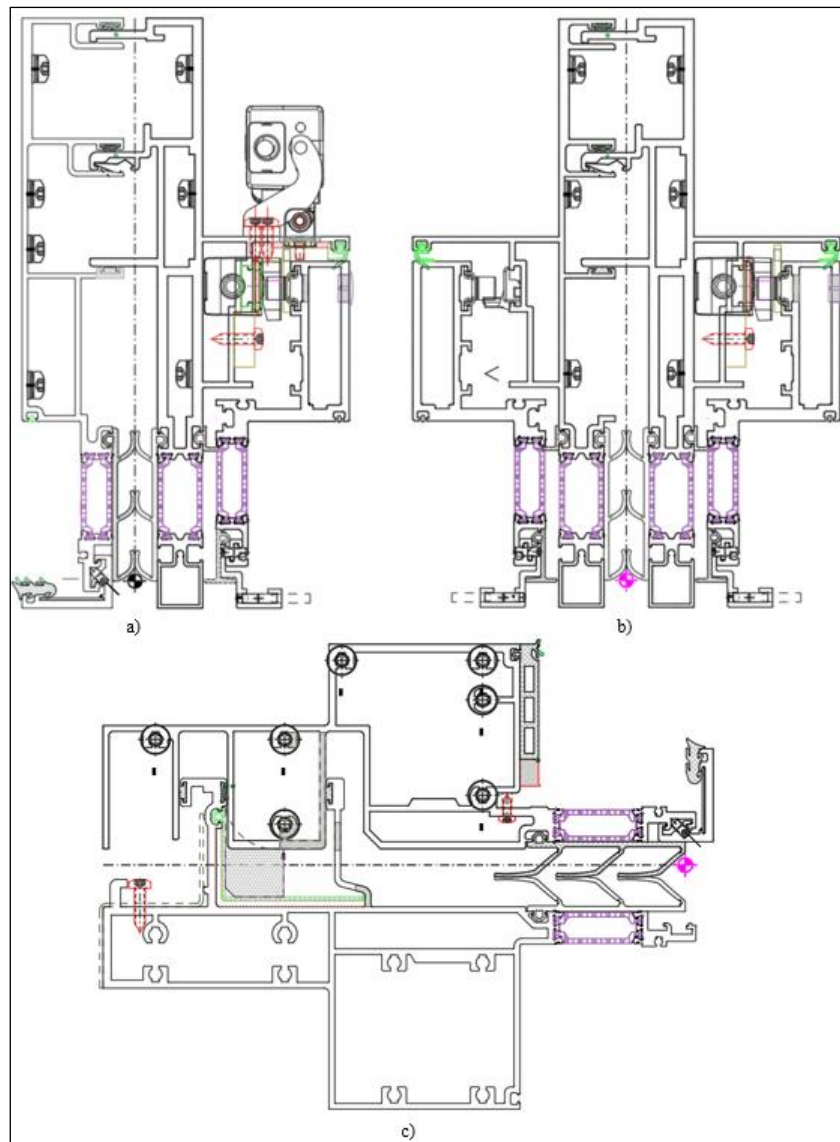


Figure 3.8 Frame cross-sections and connections. a) Large - small transom (top view) b) Small - small transom (top view) c) Bottom transom - starter sill (lateral view)

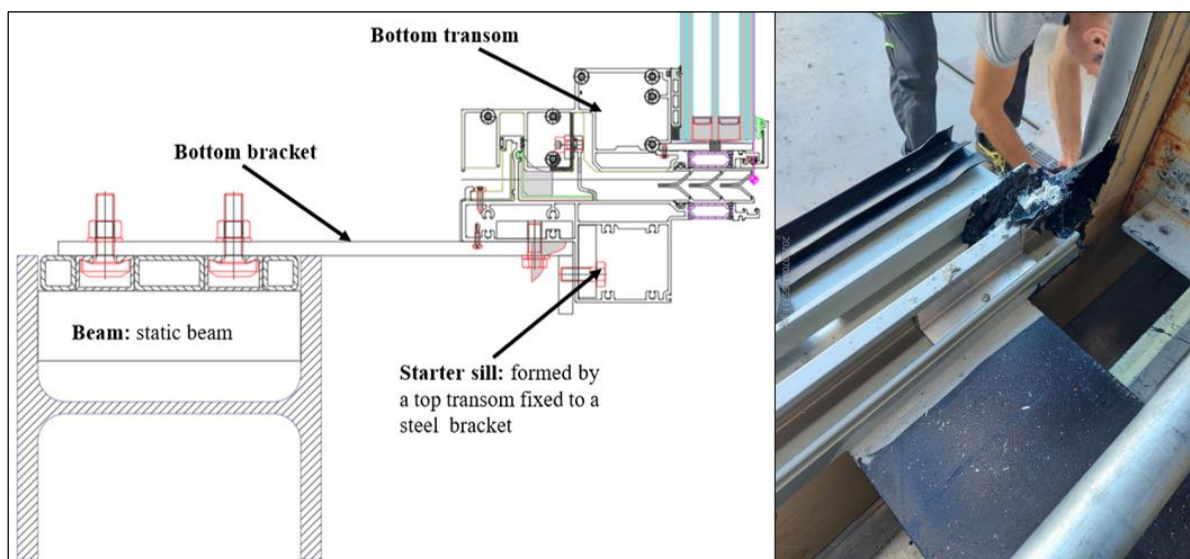


Figure 3.9 Starter sill and bottom bracket

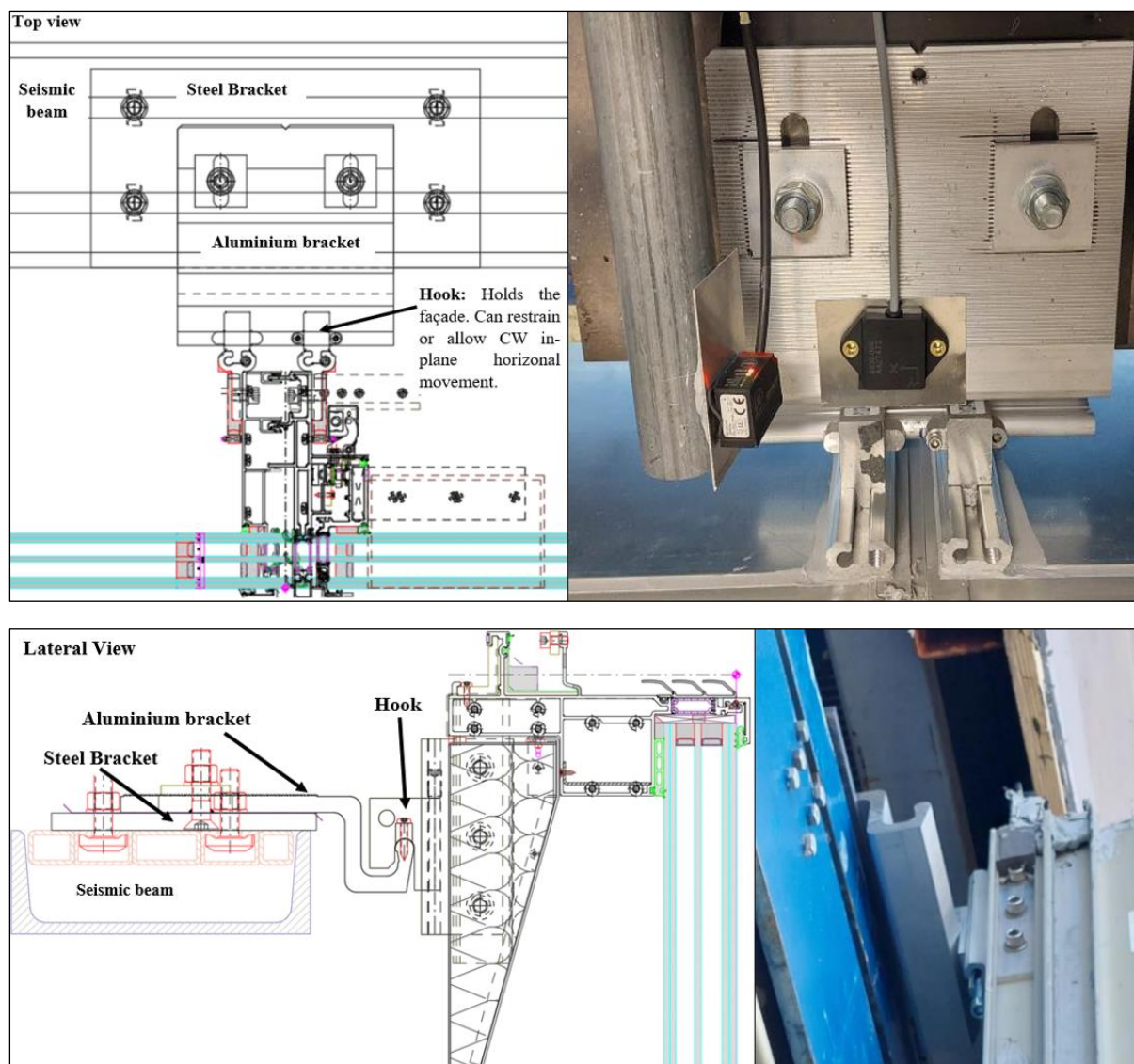


Figure 3.10 Anchorage system top and lateral view

3.2.3 Experimental sequence and experimental tests

Two testing sequences were carried out to understand the seismic behaviour of the façade. The first experimental sequence was established to determine the global behaviour of the façade submitted to different seismic intensities: level 1 and level 2. Table 3.2 shows the order and types of tests performed, which can be divided into three groups: pre-seismic, seismic level 1 and seismic level 2. Pre-seismic tests were carried out to determine possible air and/or water infiltrations that could affect the outcome of the testing sequence. Seismic level 1 and 2 experiments evaluated the structural integrity and the barrier function of the façade during and after the seismic action. To determine if the structural integrity of the specimen was satisfied, after the seismic induced displacements, wind load resistance tests were performed to evaluate the structural behaviour of the specimen. Moreover, after the seismic displacements two tests: air permeability and water penetration resistance were conducted to check the functionality of the façade unit.

Table 3.2 Testing sequence specimen T1.3 (7th of July 2022)

Sequence	Test
1	Pre-seismic: Air permeability with and without tape (600Pa) EN12152 – EN 12153
2	Pre-seismic: Water penetration resistance – static pressure (900Pa) EN12154 – EN 12155
3	Pre-seismic: Wind Load Resistance – static pressure 1500Pa – static suction 1900Pa
External Sensors Set-up	
4	Seismic Level 1: X Direction (± 12 mm, 10 cycles)
	Seismic Level 1: Z Direction (± 12 mm, 10 cycles)
	Seismic Level 1: Y Direction (± 6 mm, 10 cycles)
5	Seismic Level 1: Air permeability with and without tape (600Pa) EN12152 – EN 12153
External Sensors Dismantling	
6	Seismic level 1: Water penetration resistance – static pressure (900Pa) EN12154 – EN 12155
External Sensors Set-up	
7	Seismic Level 2: X Direction (± 36 mm, 10 cycles)
	Seismic Level 2: Z Direction (± 24 mm, 10 cycles)
	Seismic Level 2: Y Direction (± 12 mm, 10 cycles)
8	Seismic Level 2: Air permeability with and without tape (600Pa) EN12152 – EN 12153
External Sensors Dismantling	
9	Seismic Level 2: Water penetration resistance – static pressure (900Pa) EN12154 – EN 12155
10	Seismic Level 2: Wind Load Resistance – static pressure 1500Pa* – static suction 1900Pa*

* Increased by safety factor of 1,5

Finally, the second assessment sequence evaluated the connections that are presumed influence the seismic behaviour of the façade. The connections and the evaluation methods were selected by considering their relevance within the design and movement restrictions; the connections analysed are employed to evaluate the FEMs and can be observed in Table 3.3.

Table 3.3 Connections testing sequence.

Test connection type	Date	Number of tests conducted
Mullion To Mullion Out-of-plane inwards/outwards	11/10/2022	3 inwards and 2 outwards
Transom To Transom Out-of-plane inwards/outwards	13/10/2022	3 inwards and 2 outwards
Transom To Transom In-plane vertical	17/10/2022	3 downwards
Mullion To Mullion In-plane Horizontal	18/10/2022	2
Aluminium Top Bracket In-plane Horizontal	19/10/2022	4 with hook and 4 without hook
Steel Bottom Bracket In-plane Horizontal	19/10/2022	6
Steel Bottom Bracket In-plane Vertical	20/10/2022	4 upwards and 3 downwards
Aluminium Top Bracket In-plane Vertical	20/10/2022	4 downwards
Silicone Joints under shear, tension, and compression	25/10/2022	3 shears, 2 tension, and 1 compression

All the assessments of a CW require the use of a full-size façade mock-up assembled as if it was installed in-situ under controlled laboratory conditions. To understand the testing protocol proposed and the relation between each sequence of experiments conducted to analyse Specimen T1.3, it is important to describe the tests performed.

3.2.3.1 Seismic test

The seismic performance test is similar to a typical static racking test where a seismic beam imposes a displacement to the CW at the top side with the bottom side fixed. The proposed test differs from the other because the specimen is submitted to 10 cycles of displacement applied in three paths: in-plane horizontal, in-plane vertical, and out-of-plane. Each cycle follows only one path and consists of moving the CW from its initial position to one side, then, to the opposite side, and finally returning to its initial position. To determine the displacements applied, the CW standard JASS 14 is followed, resulting in three of seismic levels which can be applied to evaluate three different scenarios.

3.2.3.2 Connection test

The connections are tested individually, and the testing method consists on subjecting the connections to a distributed load applied to simulate the in- and out-of-plane movement of the connections by considering their movement restrictions. The load is applied by means of a pressure piston and measured by a pressure transducer, and the displacements are measured with two Micro-epsilon lasers. For the frame-to-frame connections specimens of 500 mm are used, and for the top aluminium and bottom steel brackets the real size elements are considered, the test is conducted until a total failure of the connection is reached. As a result of these tests a Force vs. Displacement diagram is obtained in order to be compared with the numerical results. Figure 3.11 presents an example of the connection tests carried out for a frame-frame and the top aluminium bracket connection.



Figure 3.11 Connection test. Left: Transom-transom in-plane. Right: Top aluminium bracket and hook

3.2.3.3 Air permeability test

The air permeability test is conducted according to the European standards EN 12152 and EN 12153, and it measures the quantity of air that penetrates the façade due to positive or negative air pressure [70]. It consists of the progressive increment of pressure where the volume of air passing, expressed in cubic meter per hour (m^3/h), is measured until reaching a pre-established pressure. The airflow entering is then related to the total area of the CW or to the metre length of the joint for future analysis. For openable CWs, the air permeability test must be performed with and without covering the openings to determine possible deficiencies in performance due

to a poorly sealed openable element. These tests were included in the experimental campaign because it can provide information about serviceability loss, in terms of airtightness, that may occur after seismic event.

3.2.3.4 Water penetration resistance – static pressure test

This test is carried out to check possible water penetration to the inside face of the façade or its parts designed to stay dry. The principle of this test relies on the application of a constant and specific amount of water combined with an increasing positive static pressure applied over the CW specimen [72]. Spray bar nozzles separated at no more than 400 mm from each other and located at no more than 250mm from the outside face of the façade are used to spread 2l/m² of water over the façade, creating a constant a continuous water film as it can be observed in Figure 3.12 [71]. The maximum pressure applied, and the application sequence must be defined according to EN 12154. The evaluation of this type of test is made by observation, and it is considered successful when no water penetration is observed.



Figure 3.12 Water penetration resistance – static pressure test

3.2.3.5 Wind load resistance – static pressure test

This test pretends to evaluate the structural integrity of the façade post-seismic action. This test pretends to replicate the action of wind loads by applying positive and negative pressure to the CW. According to EN 12179, the wind load shall be applied in terms of pressure in four increments equal to the 25% of the load until reaching the full design load [74]. Performance requirements related to frontal deflection and frontal displacement of fixing or frame elements shall be accomplished before a second test under an increased load is executed. The additional test consists of an increment of 1,5 times the design wind load; a successful accomplishment of this test requires no permanent damage of the framing elements, glass infill, fastener, or anchors [73].

3.2.4 Monitoring system

During the testing of the CW façade T1.3, the global behaviour of façade was monitored with different type of sensors to record its displacements and the acceleration introduced to the system. All the sensors were selected in function of their availability in the laboratories of Permasteelisa, Italy. The number and type of sensor used are showed in table 3.4. The sensors

were located to measure the differential displacement of the glass and the frame, with special considerations to the corners where the large and small CW units meet. The location of the sensors can be observed in Figure 3.12 and Figure 3.13. Moreover, recordings of pixel patterns attached to the glass corners were taken for the calculation of displacements through Digital Image Correlation (DIC) technique. Additionally, photos and videos capturing the global and local behaviour (joints) of the façade were taken during the full process.

Table 3.4 Sensor's part of the monitoring system

Sensor type	Number	Symbol
Potentiometer – Gefran 50 mm	8	PT
Potentiometer – Gefran 100 mm	16	PT
LVDT sensor – 200 mm maximum stroke	6	LT
Laser sensor	3	LS
Draw wire	4	DW
Accelerometer	6*	AC

LVDT: Linear variable differential transformer

* 5 bi-directional, and 1 tri-directional installed on seismic beam

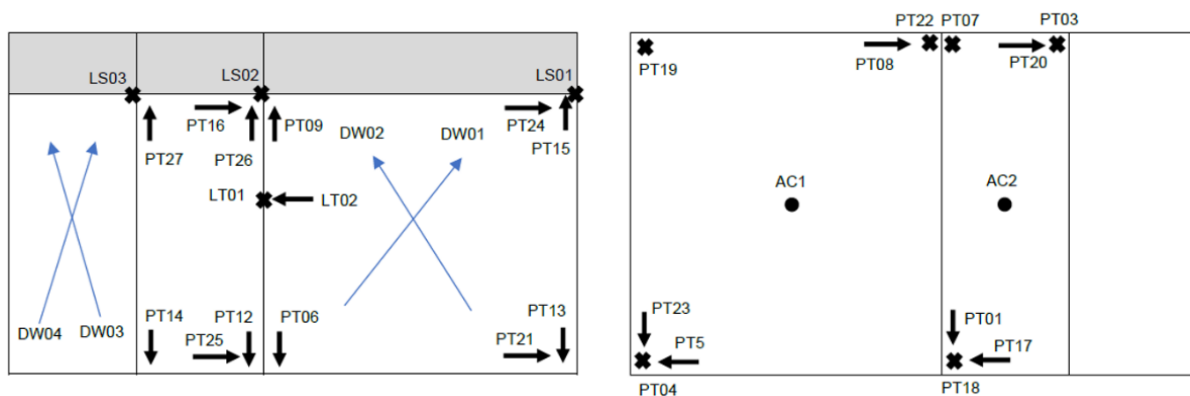


Figure 3.13 Sensor location. Left: Over aluminium frame (internal view) Right: Over glass panels (external view) [69]



a)



b)

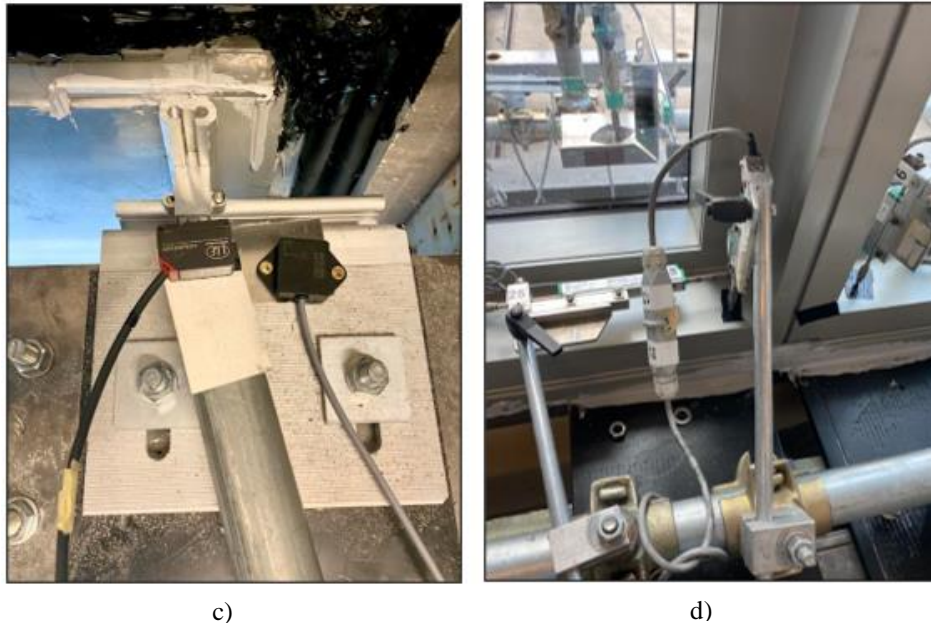


Figure 3.14 Monitoring system for specimen T1.3 a) Draw wires at the bottom-left corner b) Pixel pattern located at bottom-right corner for DIC c) Laser and accelerometer sensors located at the top-right upper bracket d) displacement sensors located on small and large frame

4

Finite Element Model

This chapter aims to introduce a general guideline for the elaboration of FEM capable of replicate the behaviour of the connections within a CW unit. This chapter gives guidelines based on real connection tests elaborated in Permasteelisa and explained in Chapter 3: “Case study 2”. An initial brief explanation of the software selected, and the main modelling considerations used during each analysis are described. It is worth to mention that the most relevant connections models are presented in this Chapter to avoid redundancy; nevertheless, the rest of the connections analysed will be presented in Annex A. A description of the connections modelled, as well as, material properties, boundary conditions, type of analysis and information about the load steps and convergence criteria is given.

4.1 FEM software and considerations

Nowadays, the application of finite element methods in engineering is essential. Modelling processes for research and understanding the response of structural and NSEs have become a major concern in research. In this sense, the finite element analysis has been acquiring greater importance in several applications of problems related to civil engineering such as structural optimization, contact mechanics, analysis of composite materials, etc. This numerical assessment approach is necessary when a necessity to solve and treat complex engineering problems arises.

In the development of this research the software DIANA FEA [75] was selected as the finite element modelling tool for the analysis of the connections within a CW. The purpose of the analysis presented is to better understand the mechanical seismic behaviour of connections. The FEMs of this section are focused on the in- and out-of-plane behaviour of the connection between mullion-mullion, transom-starter sill, top bracket and hook, and starter sill-floor bracket, but also it presents a model of the expected interaction of the structural silicone and the CW frame. The models showed in this Chapter are solved with non-linear considerations and a displacement control analysis. Moreover, it is worth to mention that some analyses are considered as highly non-linear problems due to the fact that their solution depends mainly on the contact between elements. Having mentioned this, it is considered important to start with some essential principles to be considered when modelling with DIANA FEA and other finite FEM software.

4.1.1 Geometric Non-linearity

For modelling of the CW connections, geometric non-linear effects are considered. Geometric non-linearity shall be considered when the geometric configuration of the model in analysis changes due to "large" deformation or rotations as a result of a load applied. On the contrary, a model behaving geometrically linear establishes equilibrium equations by considering an undeformed geometry and linear functions for the strain calculations which relies on nodal displacements, and restricts its applicability to small displacements, rotations, and strains [75]. Figure 4.1 (a) shows an example of a large displacement occurring in a flexible beam, where the displacement is larger than beam thickness; in this case, the force can be countered by the geometrically non-linear stress stiffening phenomenon. Figure 4.1 (b) presents an example of large rotations, which would be neglected in a geometrical linear model because the analysis considers an undeformed geometry for the force calculation, causing an improper estimation of the compression force in the bar; in the case of a geometrically non-linear analysis, the rotation is accounted and the estimation of the compression force in the bar is calculated considering the spring contribution. Geometric non-linearity is a requirement when modelling contact and hyper-elastic materials (silicone) in DIANA because of the expected large deformations and rotations occurring during contact and the large deformation of hyper-elastic materials.

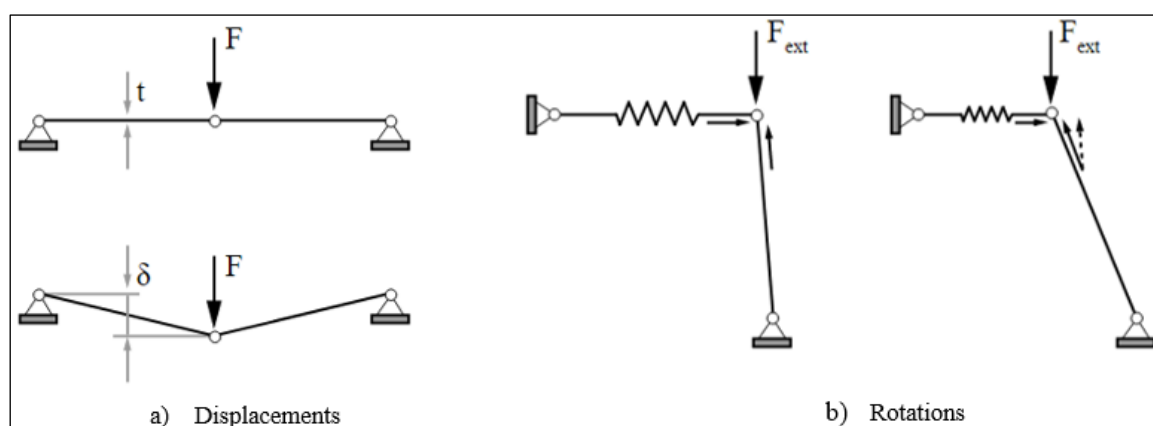


Figure 4.1 Large displacements [75]

4.1.2 Contact elements

An option presented in DIANA to model contact between different geometries is to use contact elements. Contact elements are special interface elements for modelling possible contact zones with a no-penetration condition which creates an extra set of conditions to formulate the equilibrium equations [75]. In contact analysis, contact zones must be defined using two types of elements: contacter and target elements, where the nodes of a contacter cannot penetrate target elements, see Figure 4.2. Moreover, it is possible to define different contact sets in function of the different contact zones to differentiate zones with different contact interaction, increasing the contact assessment performance. Once contact is reached, a contact force normal to the plane is generated; this normal force leads to a tangential friction force, which follows the Coulomb friction law.

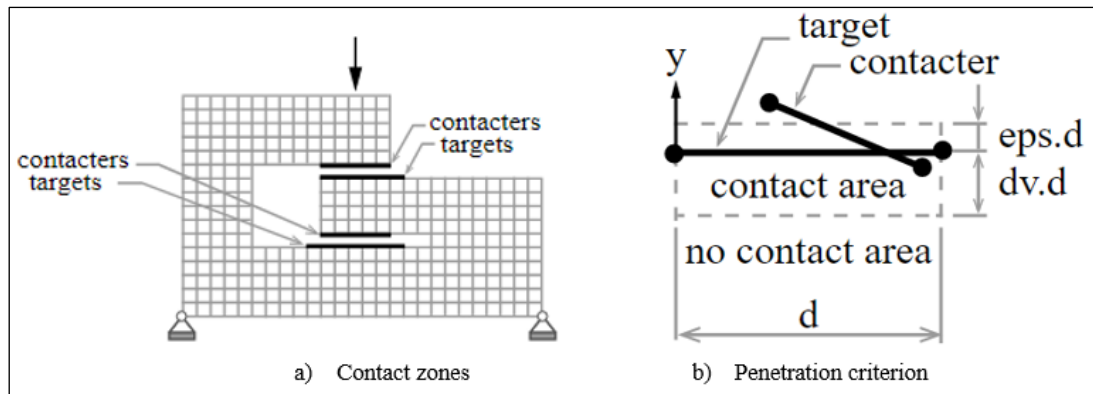


Figure 4.2 Contact behaviour [75]

Where:

dv: relative maximum depth for which DIANA check if a contacter element penetrates the target element

eps: relative distance from the target face at which DIANA defines contact

d: dimension of the target element (defined by the mesh size)

DIANA assumes contact when a contacter node is located in the range between $\text{eps} \cdot d$ and $\text{dv} \cdot d$ from the "outside" of the target. Apart of the above-mentioned parameters, the cut-off traction stress, Coulomb friction coefficient, and cohesion shall be specified when defining a target element. The "cut-off traction stress" is the cut-off stress for the contact stress between contacter and target surfaces; if the contact stress exceeds the cut-off stress, then DIANA assumes that the contacter node is not in contact [75]. To model the connections using contact elements, important considerations were necessary to guarantee the convergence of the model, which will be mentioned during the modelling procedure description.

4.1.2.1 Constitutive model

To describe the mechanical characteristics of the contact elements, DIANA uses displacements to derive Cauchy stresses and forces. For the 2-dimension elements used in this research, the basic displacement variables in the nodes are the translation u_x and u_y in the global X and Y directions, see Equation 4.1.

$$u_e = \begin{Bmatrix} u_x \\ u_y \end{Bmatrix} \quad (4.1)$$

The primary stresses derived are Cauchy stresses in the local element x and y axes (Equation 4.2).

$$\sigma = \begin{Bmatrix} \sigma_{xx} \\ \sigma_{yy} \end{Bmatrix} \quad (4.2)$$

From the Cauchy stresses distributed forces are derived (Equation 4.3)

$$f = \begin{Bmatrix} q_{xx} \\ n_{yy} \end{Bmatrix} \quad (4.3)$$

Where:

u_e : displacement of the node

u_x : displacement in the global X direction
 u_y : displacement in the global Y direction
 σ : Cauchy stresses
 σ_{xx} : Cauchy stresses in the local x axis
 σ_{yy} : Cauchy stresses in the local y axis
 f : total distributed force in the element
 q_{xx} : distributed forces in the local x axis
 n_{xx} : distributed forces in the local y axis

4.1.3 Structural interface elements

DIANA uses interface elements to model the connection interaction between two different geometries. Structural Interfaces are sub-shapes defined with respect to their shape and connectivity into nodal, two-dimensional line (edge), or plane (face) interface elements. The interaction between geometries is described in terms of normal stiffness, shear stiffness and relative displacements across a predefined node, line, or face. The configuration of a 2D line interface can be seen in Figure 4.3, and its linear elastic material model in Equation 4.4. The interface zone created between two geometries does not vary during the analysis, and it is not recommended for models with large slip [75].

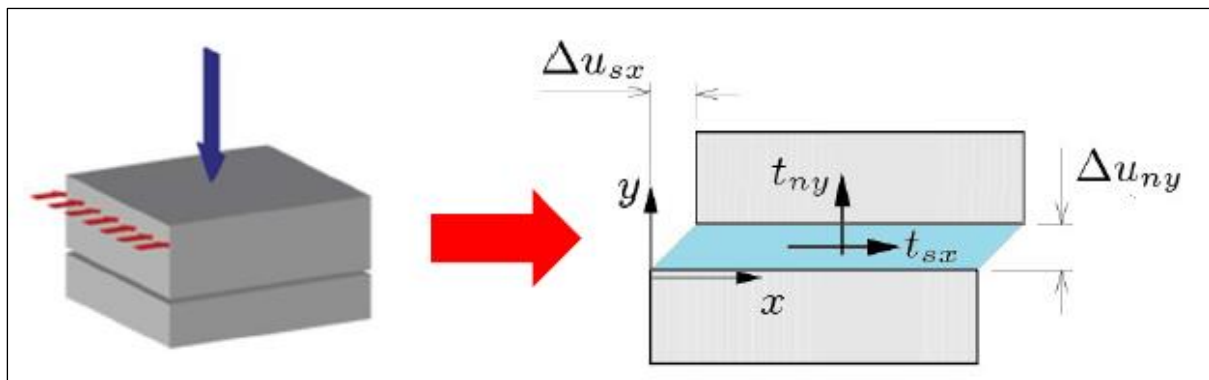


Figure 4.3 2D line interface configuration [75]

$$\begin{Bmatrix} t_{ny} \\ t_{sx} \end{Bmatrix} = \begin{bmatrix} D_{ny} & 0 \\ 0 & D_{sx} \end{bmatrix} * \begin{Bmatrix} \Delta u_{ny} \\ \Delta u_{sx} \end{Bmatrix} \quad (4.4)$$

Where:

t_{sx} : shear traction tangential to the interface
 t_{ny} : normal traction perpendicular to the interface
 D_{ny} : elastic normal interface stiffness
 D_{sx} : elastic shear interface stiffness
 Δu_{ny} : normal relative displacement Y direction (opening)
 Δu_{sx} : shear relative displacement X direction (slip)

In this research, to provide more flexibility in terms of model definition and analysis procedures, structural interface elements were selected for contact simulation in models where large slips were not expected; for example, the in-plane interaction of between the transom-stater sill or mullion-mullion connections. In terms of model definition, the use of structural interface elements makes it possible to adapt the interface stiffness to help the convergence

process; in terms of analysis, it gives the possibility of using Line Search tools, reducing the computational work of the iteration process.

A basic requirement during modelling is that interface elements must not be the source of significant additional deformations in the elastic regime; this means that the interface behaviour (slip, opening) shall manifest during the non-linear regime. Some parameters are given in the software manuals to determine the shear and normal stiffness of the interface elements, see Equation 4.5 and 4.6. However, it is recommended to assess if these parameters are correctly calibrated by comparing the displacement result between two linear analyses, one with the interfaces and one without it.

$$D_{ny} \cong 100 \sim 1000 * \frac{\max(E_1, E_2)}{L_m} \quad (4.5)$$

$$D_{sx} \cong \frac{D_{ny}}{10 \sim 100} \text{ (usually 10x lower)} \quad (4.6)$$

Where:

L_m : Average mesh element size

E_1, E_2 : Young's moduli of the elements forming the interface

4.1.3.1 Constitutive model

The basic variables of structural interfaces are nodal displacements; from these displacements it is possible to derive relative displacements and tractions. Structural interface elements determine a relation between traction stresses and relative displacements along the interface. The aforementioned set of variables depend on the type of interface elements; in the elaboration of this research two types of interface elements were used: two-dimensional lines and three-dimensional surfaces.

The variables of two-dimensional lines can be observed in Figure 4.4 and in Equations 4.7, 4.8 and 4.9.

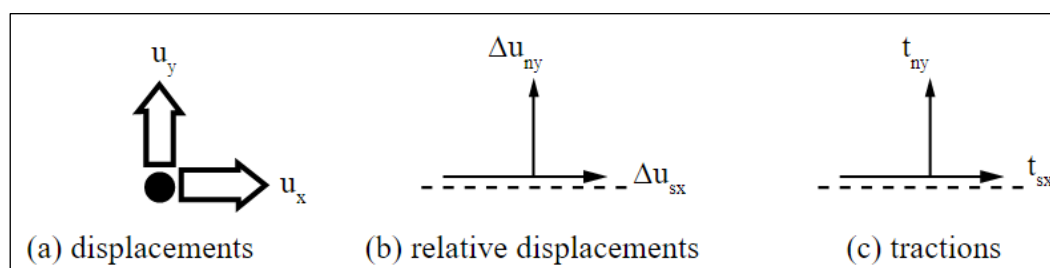


Figure 4.4 Variables of a two-dimensional line interface [75].

$$u_e = \begin{Bmatrix} u_x \\ u_y \end{Bmatrix} \quad (4.7)$$

$$\Delta u = \begin{Bmatrix} u_{sx} \\ u_{ny} \end{Bmatrix} \quad (4.8)$$

$$t = \begin{Bmatrix} t_{sx} \\ t_{ny} \end{Bmatrix} \quad (4.9)$$

The variables of three-dimensional surfaces can be observed in Figure 4.5 and in Equations 4.7, 4.8 and 4.9

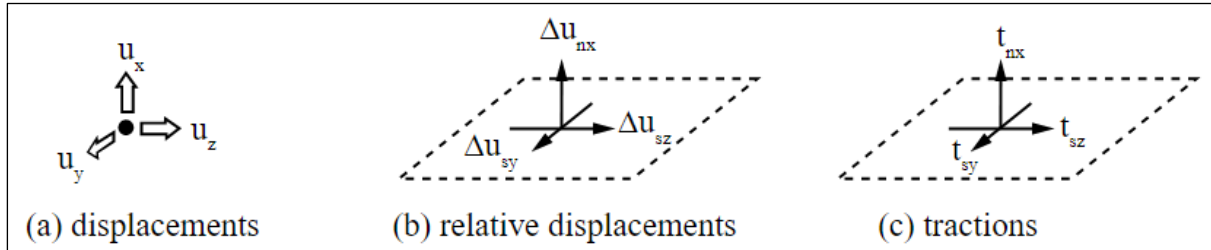


Figure 4.5 Variables of the a three-dimensional surface interface [75].

$$u_e = \begin{Bmatrix} u_x \\ u_y \\ u_z \end{Bmatrix} \quad (4.10)$$

$$\Delta u = \begin{Bmatrix} \Delta u_{sx} \\ \Delta u_{sy} \\ \Delta u_{nz} \end{Bmatrix} \quad (4.11)$$

$$t = \begin{Bmatrix} t_{sx} \\ t_{sy} \\ t_{nz} \end{Bmatrix} \quad (4.12)$$

Where:

u_e : displacement of the node

u_x : displacement in the local x direction

u_y : displacement in the local y direction

u_z : displacement in the local z direction

Δu : relative displacement

Δu_{sx} : relative displacement tangential to the interface (local x axis)

Δu_{sy} : relative displacement tangential to the interface (local y axis)

Δu_{nz} : relative displacement normal to the interface (local z axis)

t : traction stress

t_{sx} : traction stress tangential to the interface (local x axis)

t_{sy} : traction stress tangential to the interface (local y axis)

t_{nz} : traction stress normal to the interface (local z axis)

4.1.4 Finite elements

For a better understanding of the numerical model, a brief description of the finite elements used with their respective constitutive model is given.

4.1.4.1 Plane strain elements

Plane strain elements are commonly used in the analysis of cross-sections for structures with a larger depth compared to the other dimensions, see Figure 4.6. In this type of elements, the

strain components perpendicular to the element face are zero, and the depth of the model shall be specified in the project settings [75]. In this research, all the 2-D numerical analysis were designed with triangular and quadrilateral Standard plane stress elements. A summary of the specific finite element types used for each design and their characteristics is given in tables that can be found in the section "Element types" of each connection analysed.

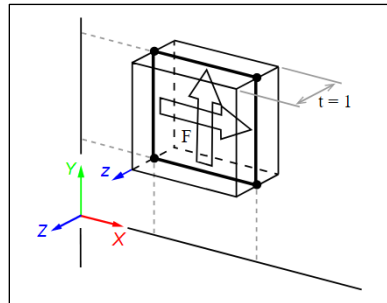


Figure 4.6 Plane strain elements [75].

Constitutive model

The basic variables of plain strain elements are the translation of the nodes u_x and u_y in the global X and Y directions, see Equation 4.4 and Figure 4.7.

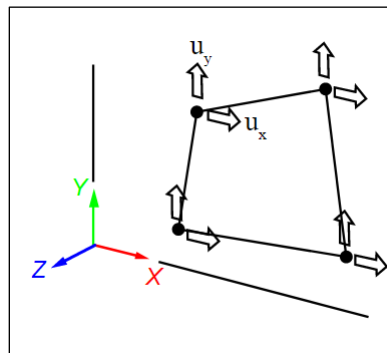


Figure 4.7 Nodal displacements of plane strain elements [75].

$$u_e = \begin{Bmatrix} u_x \\ u_y \end{Bmatrix} \quad (4.13)$$

From the displacements in the nodes deformations du_x and du_y are produced (Figure 4.8), and from these deformations Green-Lagrange strains are derived by DIANA in the local x, y, and z directions, see Equation 4.14.

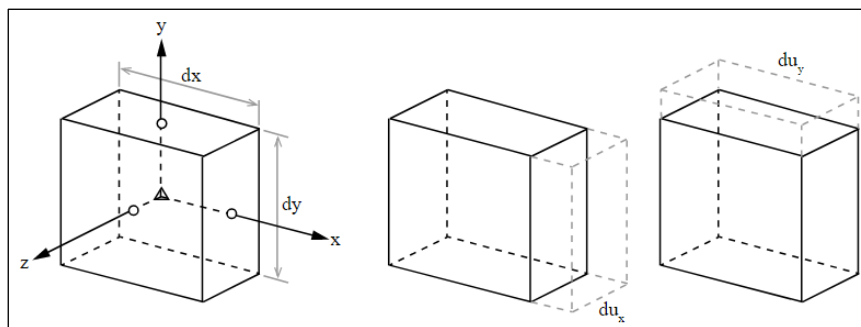


Figure 4.8 Deformations of plane strain elements [75].

$$\varepsilon = \begin{Bmatrix} \varepsilon_{xx} \\ \varepsilon_{yy} \\ \varepsilon_{zz} \\ \gamma_{xy} \end{Bmatrix} \quad (4.14)$$

With:

$$\varepsilon_{xx} = \frac{\partial u_x}{\partial x} \quad \varepsilon_{yy} = \frac{\partial u_y}{\partial y} \quad \varepsilon_{zz} = 0 \quad \gamma_{xy} = \frac{\partial u_x}{\partial y} + \frac{\partial u_y}{\partial x} \quad (4.15)$$

From the strain equations DIANA derives the Cauchy stresses, see Equation 4.16. Figure 4.9 shows the Cauchy stresses in their positive direction.

$$\sigma = \begin{Bmatrix} \sigma_{xx} \\ \sigma_{yy} \\ \sigma_{zz} \\ \sigma_{xy} = \sigma_{yx} \end{Bmatrix} \quad (4.16)$$

Where:

u_e : displacement of the node

u_x : displacement in the global X direction

u_y : displacement in the global Y direction

ε : Green-Lagrange strain

ε_{xx} : Green-Lagrange strain in the local x direction

ε_{yy} : Green-Lagrange strain in the local y direction

ε_{zz} : Green-Lagrange strain in the local z direction

γ : Green-Lagrange shear strain in the local coordinates

σ : Cauchy stresses

σ_{xx} : Cauchy stresses in the local x axis

σ_{yy} : Cauchy stresses in the local y axis

σ_{xy} : Cauchy shear stresses in the local coordinates

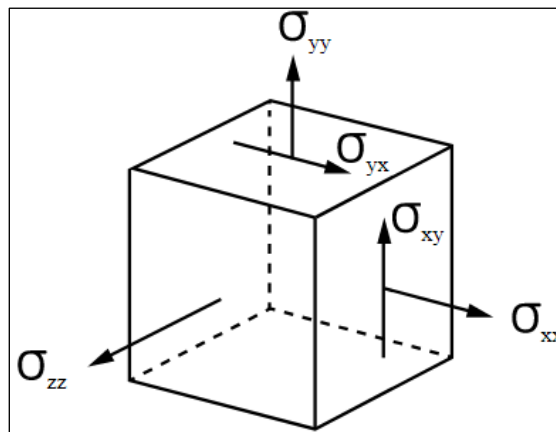


Figure 4.9 Positive direction of Cauchy stresses for a plane stress element on a unit cube [75].

4.1.4.2 Solid Elements

Solid elements are general purpose elements where the stress situation is three-dimensional, the loading may be arbitrary, and the dimension in X, Y and Z axial directions have the same magnitude, see Figure 4.10. In this research, brackets and silicone models were designed with tetrahedron, pyramid, wedge, and brick solid elements. A summary of the specific finite

element types used for each design and their characteristics is given in tables that can be found in the section "Element types" of each connection analysed.

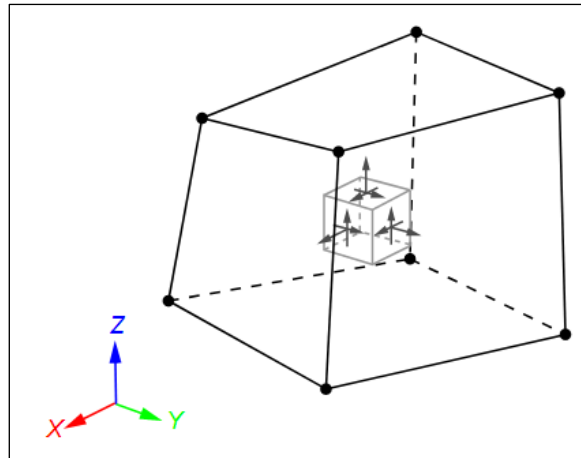


Figure 4.10 Characteristics of solid elements [75].

Constitutive model

Nodes translations in the local element directions x , y and z are the basic variables of solid elements (Equation 4.17)

$$u_e = \begin{Bmatrix} u_x \\ u_y \\ u_z \end{Bmatrix} \quad (4.17)$$

From the displacements in the nodes deformations du_x , du_y , and du_z are produced (Figure 4.11), and from these deformations Green-Lagrange strains are derived by DIANA in the local x , y , and z directions, see Equation 4.18.

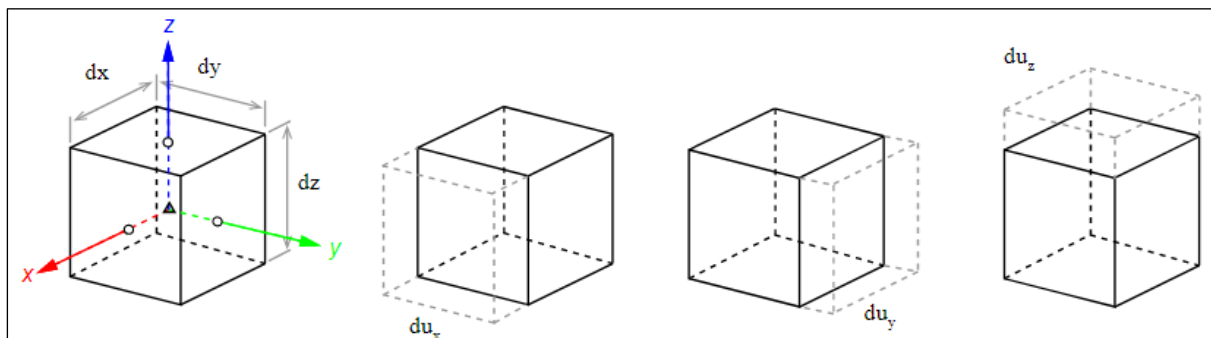


Figure 4.11 Deformation of solid elements [75].

$$\varepsilon = \begin{Bmatrix} \varepsilon_{xx} \\ \varepsilon_{yy} \\ \varepsilon_{zz} \\ \gamma_{xy} \\ \gamma_{yz} \\ \gamma_{zx} \end{Bmatrix} \quad (4.18)$$

With:

$$\begin{aligned} \varepsilon_{xx} &= \frac{\partial u_x}{\partial x} & \varepsilon_{yy} &= \frac{\partial u_y}{\partial y} & \varepsilon_{zz} &= \frac{\partial u_z}{\partial z} \\ \gamma_{xy} &= \frac{\partial u_x}{\partial y} + \frac{\partial u_y}{\partial x} & \gamma_{yz} &= \frac{\partial u_y}{\partial z} + \frac{\partial u_z}{\partial y} & \gamma_{zx} &= \frac{\partial u_z}{\partial x} + \frac{\partial u_x}{\partial z} \end{aligned} \quad (4.19)$$

From the strain equations DIANA derives the Cauchy stresses for all types of solid elements, see Equation 4.20. Figure 4.12 shows the Cauchy stresses in their positive direction.

$$\sigma = \begin{Bmatrix} \sigma_{xx} \\ \sigma_{yy} \\ \sigma_{zz} \\ \sigma_{xy} = \sigma_{yx} \\ \sigma_{yz} = \sigma_{zy} \\ \sigma_{zx} = \sigma_{xz} \end{Bmatrix} \quad (4.20)$$

Where:

u_e : displacement of the node

u_x : displacement in the local x direction

u_y : displacement in the local y direction

u_z : displacement in the local z direction

ε : Green-Lagrange strain

ε_{xx} : Green-Lagrange strain in the local x direction

ε_{yy} : Green-Lagrange strain in the local y direction

ε_{zz} : Green-Lagrange strain in the local z direction

γ : Green-Lagrange shear strain in the local coordinates

σ : Cauchy stresses

σ_{xx} : Cauchy stresses in the local x axis

σ_{yy} : Cauchy stresses in the local y axis

σ_{zz} : Cauchy stresses in the local z axis

σ_{xy} : Cauchy shear stress perpendicular to the x axis in y direction

σ_{yz} : Cauchy shear stress perpendicular to the y axis in z direction

σ_{zx} : Cauchy shear stress perpendicular to the z axis in x direction

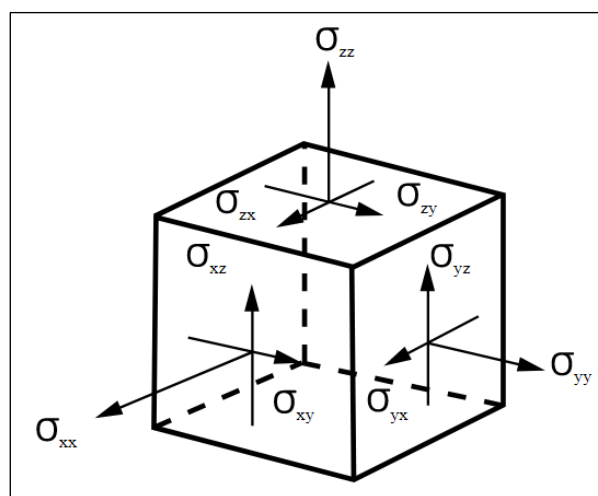


Figure 4.12 Positive direction of Cauchy stresses for a solid element on a unit cube [75]

4.2 Finite Element Models

As aforementioned, a summary with the description of the modelling procedure of the connections is presented in this report. This sub-chapter focuses on the description of the numerical models of the façade specimen 2, including information about elements type, material properties, boundary conditions, solution procedure, convergence criteria, and, finally, contact between elements and plastic strain plots are presented. Since the modelling process is redundant, only one in-plane and one out-of-plane example is given for the mullion-mullion, transom-starter-sill, and top and bottom brackets. For the silicone, extension and a shear model are presented. The boundary conditions and final deformation plots of the models from the Case Studies 1 and 2 not mentioned in this chapter are presented in the Annex.

The modelling objective is to develop a FEM capable to simulate the in- and out-of-plane behaviour of the connections within a CW in order to establish a modelling standard procedure that could be used for future studies. With the outcomes of the numerical model, a Force vs. Displacement curve for each connection is obtained for its further application in a full-size façade numerical model as interfaces, simulating the behaviour of each connection. Since the displacement applied was delimited by seismic loads Level 1 and Level 2, considered as serviceability limit levels, a full failure of the connection is not expected. Therefore, no stresses and strains beyond the elastic range are expected; in other words, all the connections shall behave within an elastic range. However, the models presented in this thesis exceed the elastic range but are limited in function of the test results and a maximum value of relative displacements. The results of the models will be presented and analysed in Chapter 5.

4.2.1 General material properties

Before describing the procedure to elaborate the FEMs of each connection a general description of the material properties is given for each group of connections.

4.2.1.1 Frame to frame connections

For the analysis of all frames to frame connections the material properties of aluminium AW 6063-T6 were obtained from the Eurocode 9. The material model chosen was Von Mises plasticity with strain-hardening once the elastic limit is reached. Hardening behaviour was defined in function of a Plastic strain – Yield stress diagram defined with analytical stress-strain models for aluminium alloys specified in the Annex E of EN 1999-1-1. A bi-linear model was selected to specify the hardening condition of the material according to section E.2.1.1 of the Eurocode. Figure 4.13 shows the stress-strain diagram proposed by the Eurocode.

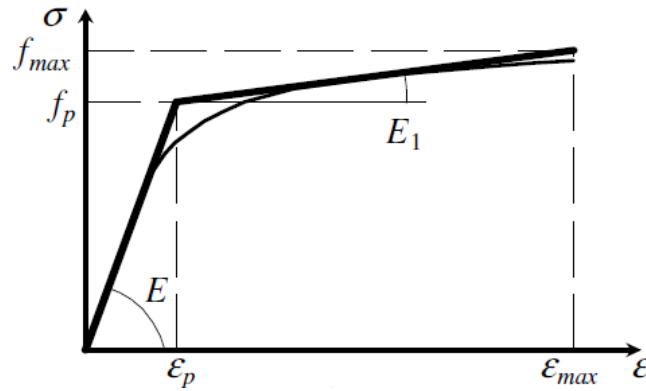


Figure 4.13 Bi-linear model diagram from Eurocode 9 [77].

To determine each point of the bi-linear model proposed in the Eurocode 9, the next equations are required:

$$f_p = f_o \quad (4.21)$$

$$f_{max} = f_u \quad (4.22)$$

$$\varepsilon_{max} = 0,5 * \varepsilon_u \quad (4.23)$$

$$\varepsilon_p = f_o/E \quad (4.24)$$

$$E_1 = (f_u - f_o)/(0,5 * \varepsilon_u - \varepsilon_p) \quad (4.25)$$

$$\sigma = E * \varepsilon \quad \text{for } 0 \leq \varepsilon \leq \varepsilon_p \quad (4.26)$$

$$\sigma = f_p + E_1(\varepsilon - \varepsilon_p) \quad \text{for } \varepsilon_p < \varepsilon \leq \varepsilon_{max} \quad (4.27)$$

Where:

f_p : conventional elastic limit of proportionality

ε_p : strain corresponding to the stress f_p

ε_{max} : strain corresponding to the stress f_{max}

E : elastic modulus

E_1 : hardening modulus

ε_u : nominal value of ultimate strain

f_o : characteristic value of 0,2% proof strength

f_u : characteristic value of ultimate tensile strength

To define the linear material properties of the interface: normal and shear stiffness, the Equations 4.5 and 4.6 were considered. However, due to the different conditions of each model a non-linear behaviour of the interface was selected, and it was necessary to indicate that no shear nor normal stiffness was expected if the cross-sections separated from each other. This condition can be applied in two ways: by diagrams or by using the condition "no-tension with shear stiffness reduction". An explanation of the condition selected in each model will be given when describing the modelling procedure.

To model contact with contact elements, it was necessary to define different material properties for each element to create different contact sets. This was made to obtain accurate results,

evaluating individually each contact zone between the cross-sections. The material definition for the contact elements is by default split into two: "contacter" and "target". "Contacters" do not require the assignment of any properties. On the other hand, for each "target" element it is necessary to specify additional information. For the definition of the "target" properties, friction is neglected in all cases.

4.2.1.2 Top and bottom brackets

For the analysis of the top aluminium bracket and hook the aluminium alloys were defined as AW 6005-AT6 and AW 6082-T6 respectively according to the Eurocode 9: Part 1-1. The bottom bracket is made of steel S235 with properties defined according to Eurocode 3. Von Misses plasticity criteria with a bi-linear hardening was defined for each of the 3-D models. The bi-linear diagram for the aluminium elements was already defined in the previous section, see Figure 4.13 and Equations 4.21 to 4.27, and the strain-hardening properties of the steel element was defined according to EN 1993-1-5 section C.6, see Figure 4.14.

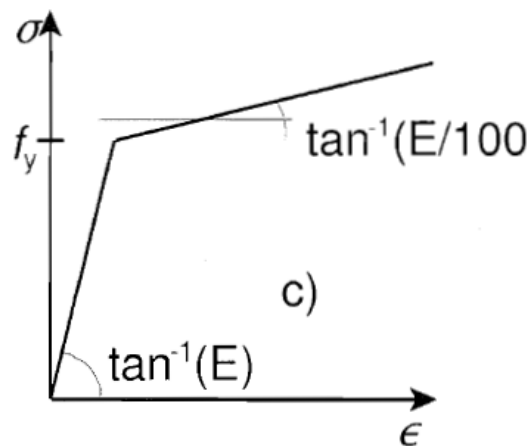


Figure 4.14 Strain-hardening model of steel elements [66].

Regarding the interface between the top aluminium bracket and the hook, only linear properties defined according to the Equations 4.5 and 4.6 were considered.

4.2.1.3 Silicone

Three material properties defined for the all the numerical models were: silicone hyper-elasticity, aluminium, and interface properties. For the aluminium, only linear elastic properties were assigned because the stress on the aluminium was expected to remain within the elastic range. Similarly, linear properties were assigned to the interface since detachment of both solids was not considered. The silicone properties were assigned in function of K_1 and K_2 constants for the application of Mooney-Rivlin hyper-elasticity equation in the solution of the problem, see Equation 4.28.

$$W_d = K_1(J_1 - 3) + K_2(J_2 - 3) \quad (4.28)$$

Where:

K_1 : constant depending of the type of silicone

K_2 : constant depending of the type of silicone

J_1 : invariant

J_2 : invariant

4.2.2 Transom - starter sill

The transom-starter sill connection is the first frame to frame connection analysed because it is used as a validation protocol for the whole procedure. In this case the connection tested, and the FEM share the same geometry, and boundary conditions applied in the model are similar to the tested conditions. The validation of the following models was carried out by comparing Force vs. Displacement diagrams obtained in the laboratory tests and the results of the numerical model. The outcome of this analysis is the connection stiffness behaviour in-plane vertical and out-of-plane inwards and outwards, see Figure 4.15. Therefore, 3 comparisons are made to validate this procedure and are discussed in Chapter 5. Regarding the numerical models, two models are presented in this section, one showing the procedure for the in-plane action and a last one showing the out-of-plane action of the elements. For the analysis, all the transom-starter sill cross-sections were divided in a mesh of approximately 1 mm per side; this selection was made considering the smallest dimensions of each cross-section, which is around 3 mm. Additionally, the decision was taken in order to reduce possible convergence problems by mainly having quadrilateral elements.

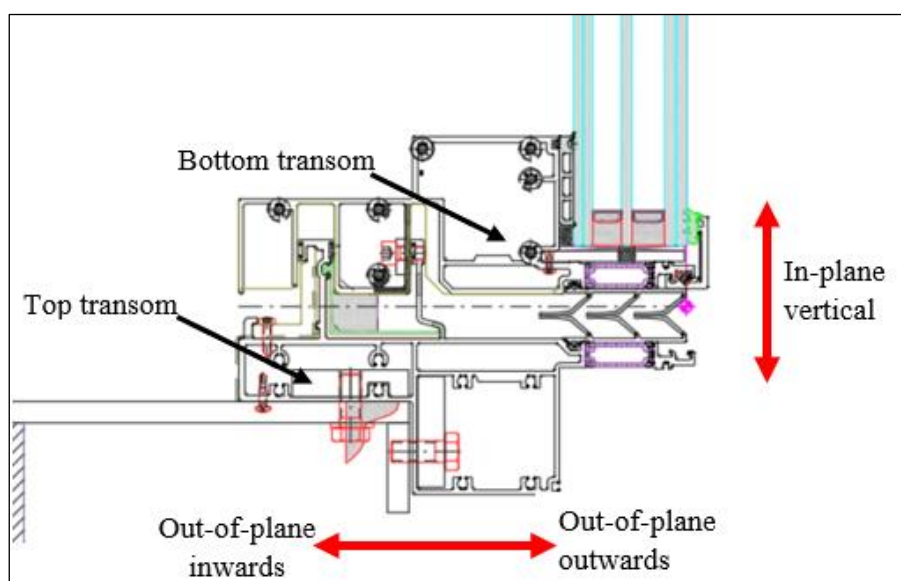


Figure 4.15 Transom-Starter sill displacement direction.

4.2.2.1 In-plane

The in-plane analysis of the connection consists of a 2D model of the connection between a bottom transom and a top transom fixed to the bottom bracket (starter sill) as shown in Figure 4.15. The model consists of a 2D plane strain analysis because it permits the analysis of long structures by evaluating 2D cross-sections with a previously specified depth. For the numerical analysis, 2D drawings of the cross-section were imported to DIANA from AutoCAD [76]. The geometries were simplified without rounded edges, gaskets, and thermal breaks as shown in Figure 4.16. Additionally, interface elements were used instead of contact elements to accelerate the iteration process. For the creation of interface elements, it was necessary to pre-

define the perimeter representing the real zone of contact between both cross-sections, see Figure 4.17.

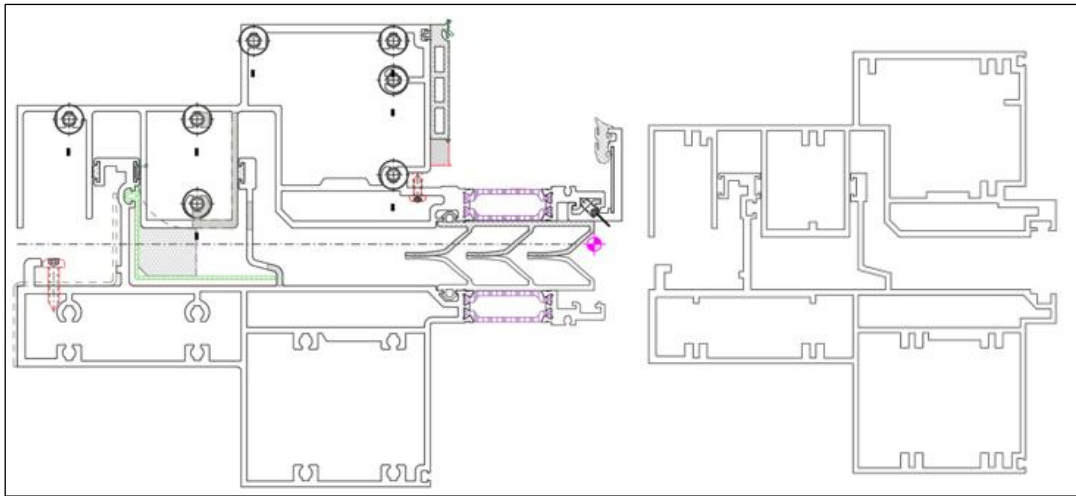


Figure 4.16 Drawing simplification for DIANA. Left: original geometry. Right: simplified geometry

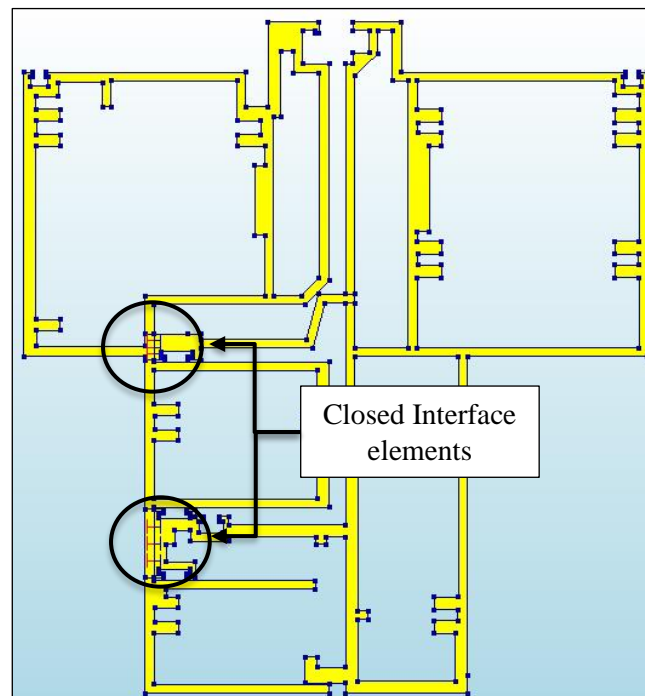


Figure 4.17 Interface elements location.

Material properties

For the analysis two material properties had to be defined: aluminium AW 6063-T6 and interface. The aluminium material properties were selected according to the afore mentioned in section 4.2.1.1. "General material properties".

Figure 4.18 shows the stress-strain diagram used in the numerical analysis of all frame-frame connections and Table 4.1 shows a summary of the properties.

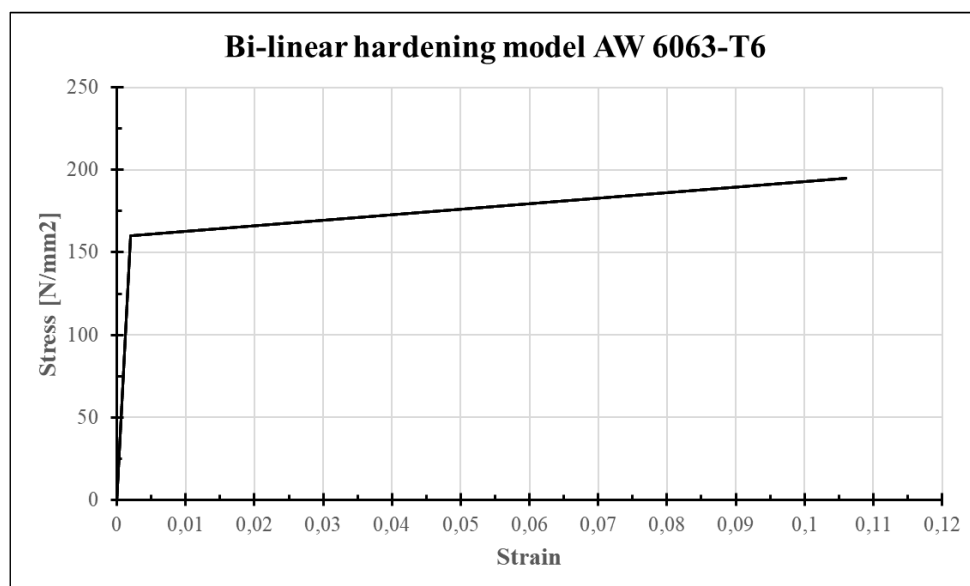


Figure 4.18 Bi-linear model diagram calculated

Table 4.1 Aluminium AW 6063-T6 summary of properties.

Material	Model	E [N/mm ²]	ν	ρ [kg/m ³]	f_o [N/mm ²]	f_u [N/mm ²]	ϵ_u
AW6063-T6	Hardening	70000	0,3	2700	160	195	0,212

In this specific case, two closed interfaces were selected since both zones of contact are reached simultaneously. Additionally, "no-tension with shear stiffness reduction" was selected, and the critical interface opening for the reduction of the normal and shear stiffness was set to 0,001 mm, see Table 4.3 Table 4.1 and 4.2.

Table 4.2 Interface linear properties. Transom – starter sill in-plane

Element	Normal stiffness modulus Y [N/mm ³]	Shear stiffness modulus X [N/mm ³]
Interface	7,00E+07	7,00E+05

Boundary and loading conditions

The boundary conditions adopted in the model intended to replicate the restraints used during the testing sequence. As it can be observed in Figure 4.19, the horizontal movement of the connection was restricted at the bottom part of the right element in the model, similarly to the test set-up. However, the vertical movement restriction of the element in the model differs from the experiment because it is necessary to fully restraint the vertical displacement of the numerical models to avoid convergence problems and inaccurate results. Regarding the load application, during the test a load was applied in the middle of the transom, see Figure 4.19 right, by means of a steel channel to distribute the load evenly along the frame's depth. In the model, the analysis was carried out by imposing a displacement to the transom, which was applied at approximately the same location. The value of the displacement applied was selected

according to the test results, imposing the model to a displacement of 3,5 mm after both cross-sections reach contact.

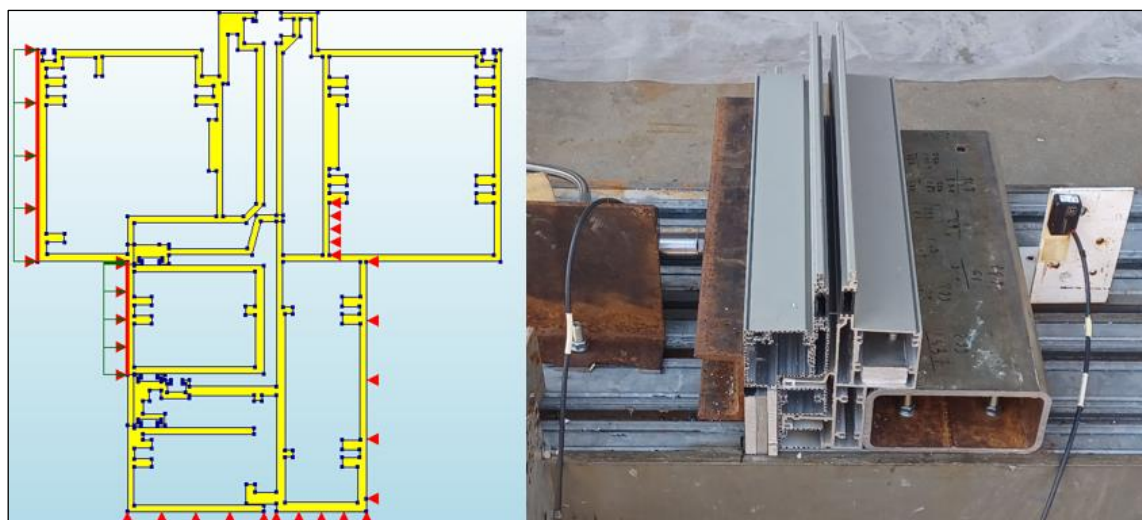


Figure 4.19 Transom- starter sill restraints and load application in-plane. Left: FEM. Right: test.

Finite element types

A summary of the finite element types presents in the model and the geometry to which they belong can be seen in Table 4.3.

Table 4.3 Finite element types and details.

Finite element type	Quadrilateral, 4 nodes (Q8EPS)	Triangular, 3 nodes (T6EPS)	Line, 2+2 nodes, 2D (L8IF)
DOF per node	2	2	2
Interpolation scheme	Linear	Linear	Linear
Integration scheme	2x2, Gauss	1- point, Area	3-point, Newton-Cotes
Dimension	2D	2D	2D
Geometry	Cross-section	Cross-section	Interface
Number of elements	4945	74	28

Solution procedure

To simplify the computational work due to the contact interaction, it was decided to simplify the numerical model joining both cross-sections to be already in contact. For the structural analysis set-up, it was selected a non-linear analysis considering the geometric non-linearities of the problem. For the equilibrium iteration, displacement and force convergence norms were selected, with line search activated. The total displacement of 3,5 mm was set to be reached in 40 steps. Finally, the force applied is obtained by summing the reaction values of the points where the imposed displacement was applied.

Figure 4.20 shows the final deformed shape after the 3,5 mm of displacement is applied. It can be noticed that the deformed shape is consistent with the formation of plastic strains along the cross-sections. Therefore, as an initial check it can be considered that the model works correctly. However, the results obtained must be contrasted with the experimental campaign to validate the modelling approach.



Figure 4.20 Transom-Starter sill in-plane. Final deformed shape and plastic strains.

4.2.2.2 Out-of-plane

The out-of-plane behaviour of the connection (Figure 4.15) was evaluated with similar considerations taken for the in-plane analysis. 2D geometries from Figure 4.16 were imported from AutoCAD and used to model both out-of-plane behaviours. Since both out-of-plane directions were analysed following the same principles, the examples in this section are focused on result of the out-of-plane outward analysis.

Regarding the model selection, a "Plane Strain model" was selected for the numerical analysis. The difference with the in-plane case relies in the use of contact elements to simulate the out-of-plane action of the connection since large slips were expected in this situation, and the accuracy of the results could be compromised with the use of structural interface elements. To elaborate the model with contact elements it was necessary to create line shapes on the edges of the possible contact zones between the two cross-sections and assign them the element class "contact". The contact elements of the cross-section can be observed in red in Figure 4.21.

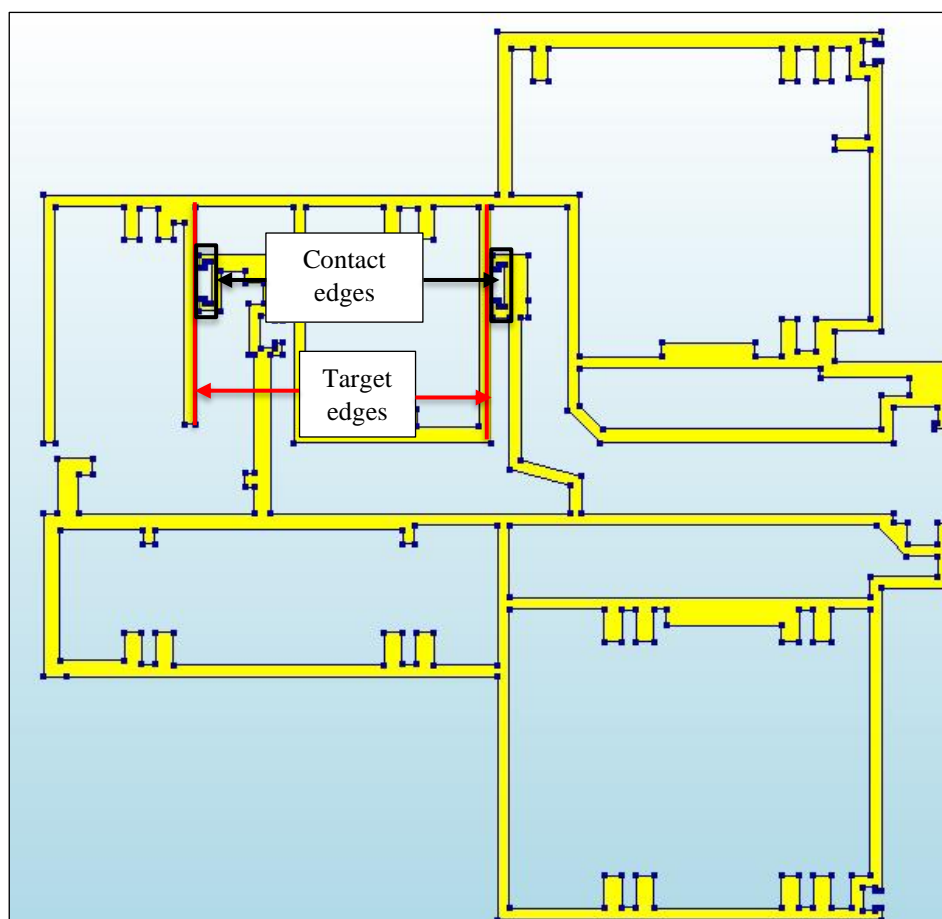


Figure 4.21 Location of contact elements. Transom-starter sill out-of-plane outwards.

Material properties

For the analysis, material properties for the aluminium AW 6063-T6 and contact elements were defined. The material model and properties of aluminium AW 6063-T6 are same as the defined in Table 4.1 and Figure 4.18. The properties assigned to the target elements can be seen in Table 4.4.

Table 4.4 Target material definitions transom - starter sill out-of-plane outward

Target material transom – starter sill Out-of-plane	
Relative maximum depth of target face	1
Relative distance above target face	0,01
Cut-off traction stress	1,00E-13
Coulomb Friction coefficient	0
Cohesion	0

Boundary and loading conditions

The restraints in the model were adopted following the test conditions to obtain results as similar as possible, see Figure 4.22. The load application in the experiment was done by means of a steel angle located at the left part of the upper transom. Similarly, an imposed displacement was applied at the same location in the FEM. The value of the displacement applied was limited to a relative displacement of 20 mm, even though the experimental layout reached higher levels

of displacement. This decision was made because a higher relative displacement range is not expected to occur for seismic levels 1 and 2.

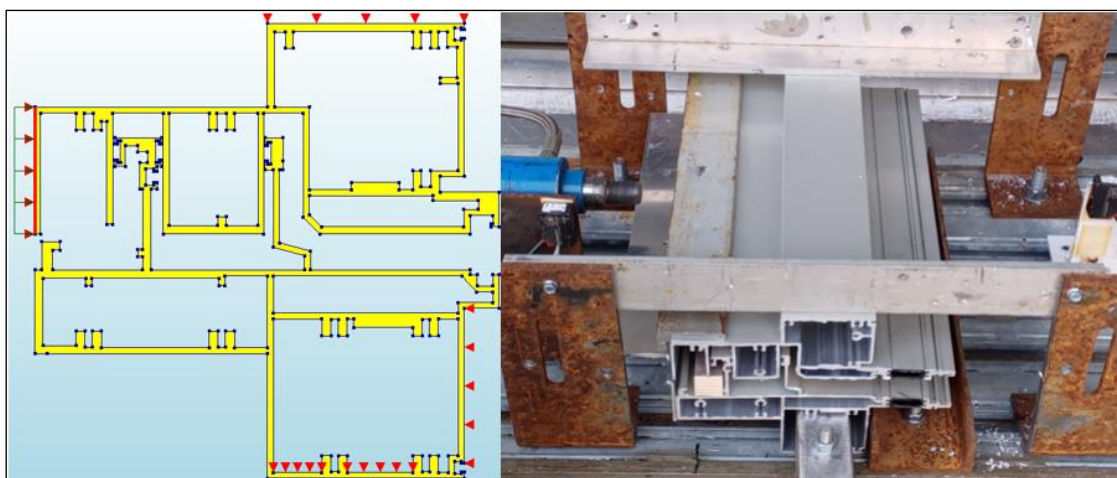


Figure 4.22 Transom-starter sill restraints and load application out-of-plane outwards. Left: FEM. Right: picture.

Finite element types

Table 4.5 presents a summary of the finite elements and the geometries to which they correspond.

Table 4.5 Finite element types and details.

Finite element type	Quadrilateral, 4 nodes (Q8EPS)	Triangular, 3 nodes (T6EPS)	Line, 2 nodes, 2D (LACT)
DOF per node	2	2	2
Interpolation scheme	Linear	Linear	Linear
Integration scheme	2x2, Gauss	1- point, Area	-
Dimension	2D	2D	2D
Geometry	Cross-section	Cross-section	Contact
Number of elements	4928	64	111

Solution procedure

To elaborate an accurate analysis, it was necessary to implement two target elements and a contactor element per contact zone. It was observed during the model elaboration that contact was produced independently of which edge was selected as "target" or "contactor". However, to simplify the analysis is preferred the smallest edges to be considered as "contactors" rather than the larger ones; this because it is easier to establish contact when the "contactor" elements have a smaller span between nodes during the contact analysis. The analysis was carried out with a non-linear analysis considering geometric non-linearities. The stability issues during the solution of contact problems with contact elements are caused by the high number of oscillations on residual forces [75]. Nevertheless, these problems can be reduced when selecting the equilibrium iteration properties. In case of contact, only energy was selected as the convergence norm, and the "Abort criterion" was increased from the default values up to $1e+15$ because according to DIANA Support Centre [75] the default value for "Abort criterion" for the energy convergence norm can be restrictive in these cases. Moreover, it was also necessary to divide the analysis in different blocks in order to establish contact first and stabilize

the model. The total displacement of 20 mm was set to be reached in four blocks of around 10 steps each. To define the size of the steps of each block it was necessary a combination of a trial-and-error procedure combined with automatic load steps. Figure 4.23 shows the final deformed shape with plastic strains formed for the out-of-plane outwards analysis.



Figure 4.23 Transom-starter sill out-of-plane outwards. Final deformed shape and plastic strains.

4.2.3 Mullion - Mullion

The process to evaluate the mullion-mullion connections followed the validated procedure from the transom-starter sill connection. This analysis pretends to evaluate the connection's performance in-plane horizontal and out-of-plane inwards and outwards, see Figure 4.24. A total of six models were made from the mullion-mullion connections. Three for the connection between the large and the small CW unit, and three for the connection between both small units. It is important to mention that in the laboratory tests, the tested connection corresponds to a mullion-mullion connection with two cross-sections from the large CW unit, and this type of connection does not exist in the real façade specimen. However, a discussion of the possible effects of the different geometry sizes can be found in Chapter 5. To avoid redundant information, only two models are presented in this section; one showing the procedure for the in-plane action and a last one showing the out-of-plane action of the elements. Both examples correspond to the analysis of the connection between the large and small CW units.

For the in-plane and out-of-plane analysis, 2D models with simplified cross-sections, neglecting rounded edges, gaskets, and thermal breaks, were imported from AutoCAD to DIANA. Moreover, for all the cases a "Plane strain" model was selected to capture the depth the elements in the experimental campaign. A mesh of approximately 1 mm per side is used

for the analysis of all the cross-sections; this selection was made in order to reduce convergence problems by mainly having quadrilateral elements.

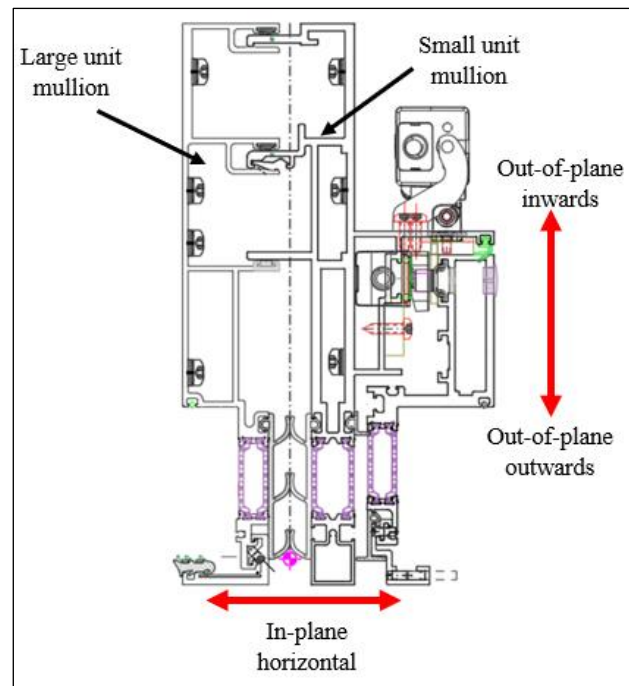


Figure 4.24 Mullion-Mullion displacement directions.

4.2.3.1 In-plane

As previously mentioned, the mullion-mullion in-plane model shown in this section consists of a 2D model of the connection between two mullions from the large and small CW units as shown in Figure 4.25. For the modelling of this connection, interface and contact elements were selected for the proper analysis of the contact behaviour between both elements.

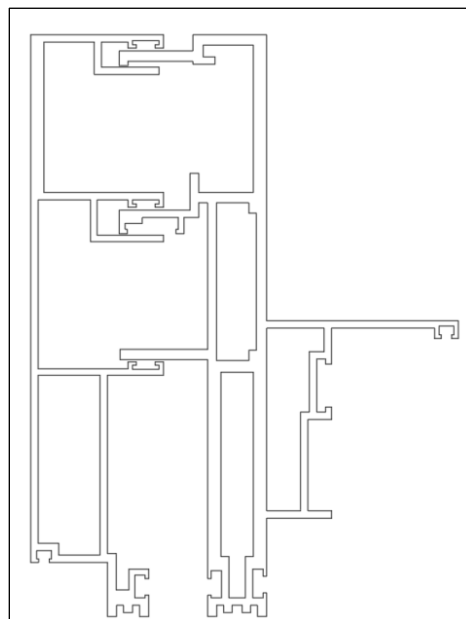


Figure 4.25 Mullion-mullion (large-small units) simplified geometry

Material properties

The aluminium properties are similar to the already defined for the transom-star sill connection and can be seen in Figure 4.18 and Table 4.1, respectively.

Moreover, two structural interface materials were defined: an open and a closed interface. The open interface properties were established in function the necessity to reduce a gap between both cross-sections to 0 before having contact, see Figure 4.26; to define this interface, a diagram Normal traction vs. Relative displacement was defined (Figure 4.27). The second interface was modelled with the condition "no-tension with shear stiffness reduction", specifying a critical interface opening for the normal and shear stiffness reduction of 0,001 mm. The linear material properties of both interfaces can be seen in Table 4.6.

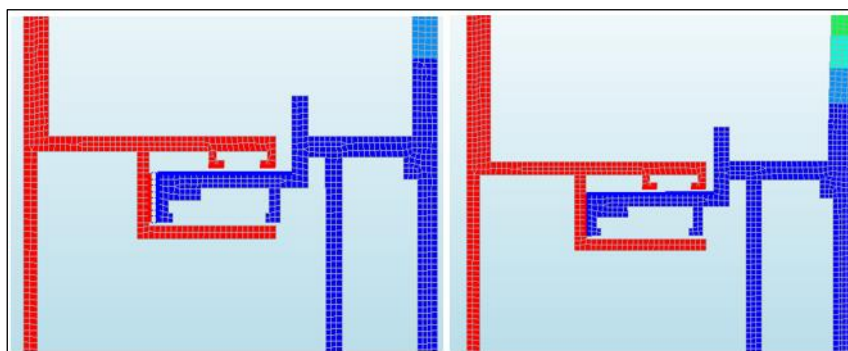


Figure 4.26 Structural interface non-linearity due to an opening. Left: before contact. Right: after contact.

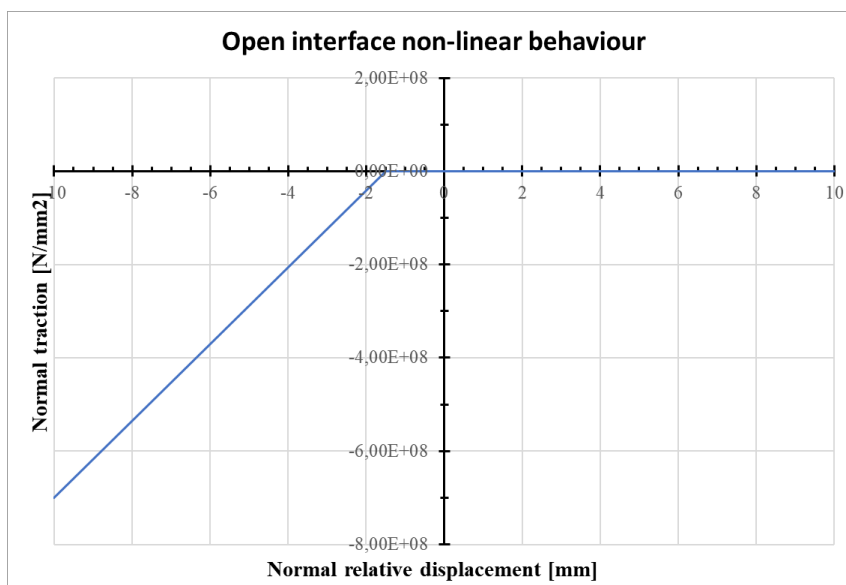


Figure 4.27 Open non-linear elastic interface diagram to reach contact.

Table 4.6 Mullion-mullion in-plane structural interface linear properties.

Element	Normal stiffness modulus Y [N/mm ³]	Shear stiffness modulus X [N/mm ³]
Closed Interface	7,00E+07	7,00E+05
Open Interface 2	7,00E+07	7,00E+05

For the contact elements, the material properties of the target element were defined according to the values shown in Table 4.2.

Table 4.7 Target material definitions mullion-mullion in-plane.

Target material mullion – mullion in-plane	
Relative maximum depth of target face	1
Relative distance above target face	0,01
Cut-off traction stress	1,00E-13
Coulomb Friction coefficient	0
Cohesion	0

Boundary and loading conditions

The restraints used in the model can be seen in Figure 4.28. During the experiment, the load was applied along the male mullion "evenly" through a steel channel. To match the load condition, it was set an imposed displacement at right mullion in the FEM, trying to replicate the application zone in the experiment. A value of 4 mm of displacement was applied to meet the maximum relative displacement reached in the experiment.

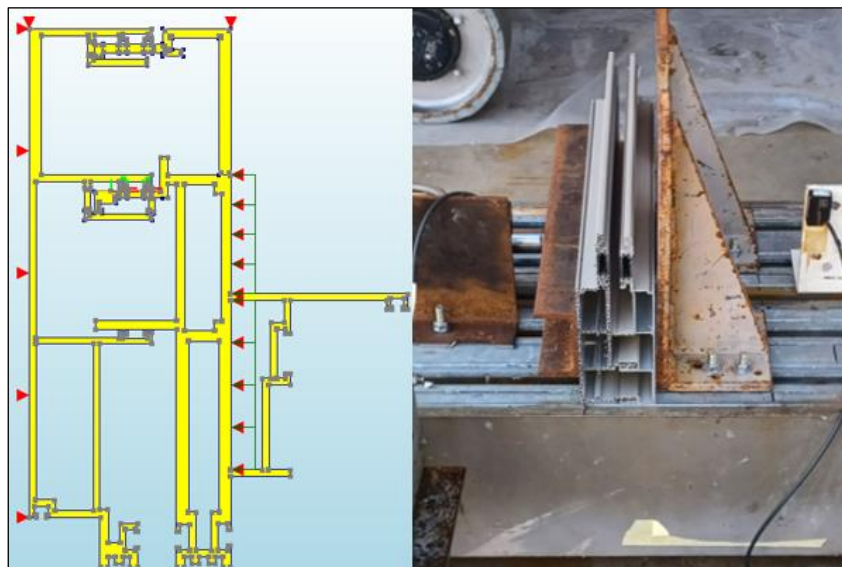


Figure 4.28 Mullion-mullion restraints and load application in-plane. Left: FEM. Right: Test picture.

Finite element types

Table 4.3 presents a summary of the finite element types and the geometries to which they correspond.

Table 4.8 Finite element types and details.

Finite element type	Quadrilateral, 4 nodes (Q8EPS)	Triangular, 3 nodes (T6EPS)	Line, 2 nodes, 2D (LACT)	Line, 2+2 nodes, 2D (L8IF)
DOF per node	2	2	2	2
Interpolation scheme	Linear	Linear	Linear	Linear
Integration scheme	2x2, Gauss	1- point, Area	-	3-point, Newton-Cotes
Dimension	2D	2D	2D	2D
Geometry	Cross-section	Cross-section	Contact	Interface
Number of elements	3759	54	30	12

Solution procedure

To elaborate an accurate analysis, it was necessary to combine interface and contact elements; Figure 4.29 illustrates the location of the interface and contact elements. It was previously observed that structural interface elements work perfectly when no large slip was expected, a correct assumption when modelling contact of elements in compression. Nevertheless, in this case large slips were also expected, and a model with only interfaces caused an unexpected behaviour of the structure increasing the stiffness of the connection and leading to sudden deformations of the cross-sections.

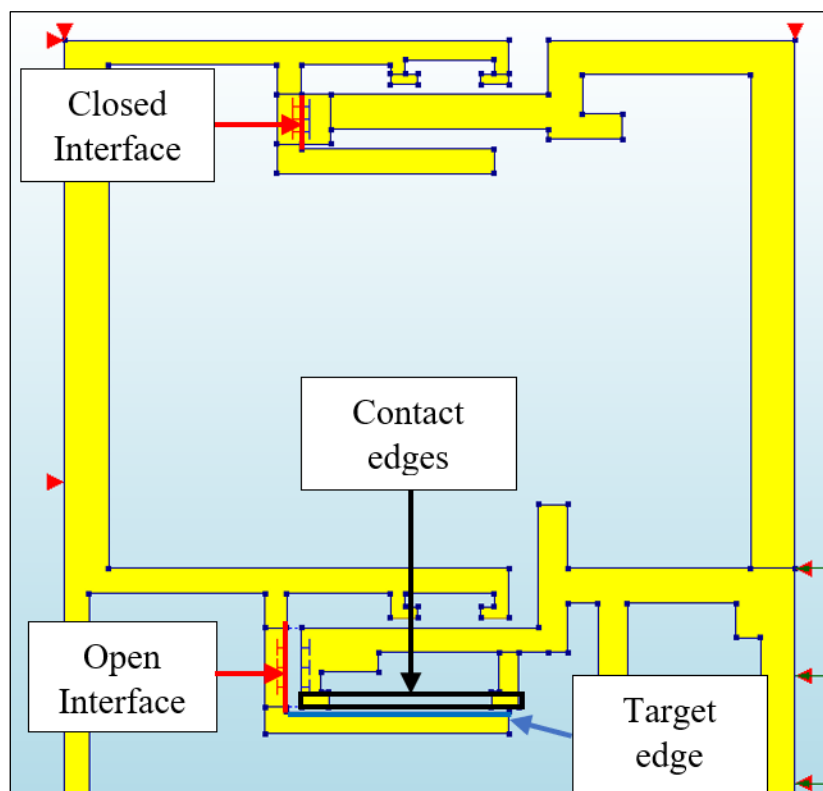


Figure 4.29 Mullion-mullion in-plane. Interface and contact elements location.

The structural analysis was set-up as a non-linear analysis considering geometric non-linearities. To reduce non-convergence issues, energy was selected as the convergence norm, and the "Abort criterion" was increased from 10000 to $1e+15$ according to the recommendations given by DIANA Support Centre [75]. Additionally, the application of the 4mm displacement was achieved dividing the analysis into three blocks with different step sizes and step numbers. After 47 load steps in total, the deformed shape, plastic strains, and connection stiffness values were obtained. Figure 4.30 shows the final deformed shape and plastic strains of the in-plane analysis.

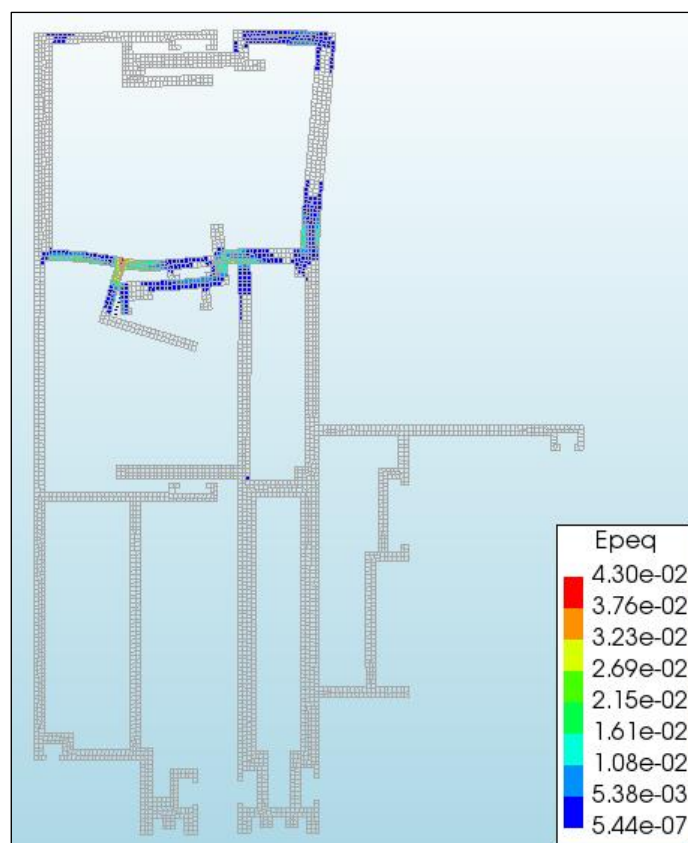


Figure 4.30 Mullion-mullion in-plane. Final deformed shape and plastic strains.

4.2.3.2 Out-of-plane

The out-of-plane behaviour of the connection was evaluated with similar considerations as the in-plane analysis. In this section only the out-of-plane outward behaviour is presented, see Figure 4.24 for reference; nonetheless, for both out-of-plane directions the analysis follows the same principles. Finally, it is important to remark that the out-of-plane analysis was carried out with contact elements only.

Material properties

The material properties of aluminium can be observed in Table 4.1 and Figure 4.18. For the contact elements, the properties of the target elements can be found in Table 4.9.

Table 4.9 Target material definitions mullion-mullion out-of-plane outward

Target material transom – starter sill Out-of-plane	
Relative maximum depth of target face	1
Relative distance above target face	0,01
Cut-off traction stress	1,00E-13
Coulomb Friction coefficient	0
Cohesion	0

Boundary and loading conditions

The restraints in the model were adopted in an attempt to follow the test conditions. In Figure 4.31, some differences between the load application in the model and in the test can be noticed. In the model the load is applied at the right part of the bottom cross-section, but in the test is

applied at the left side of the top cross-section; however, the results obtained from the specimen 1 models showed that the stiffness is independent of the place of load application (see Annex C). A 20mm displacement was applied in the model, which was considered enough to resemble the connection behaviour.

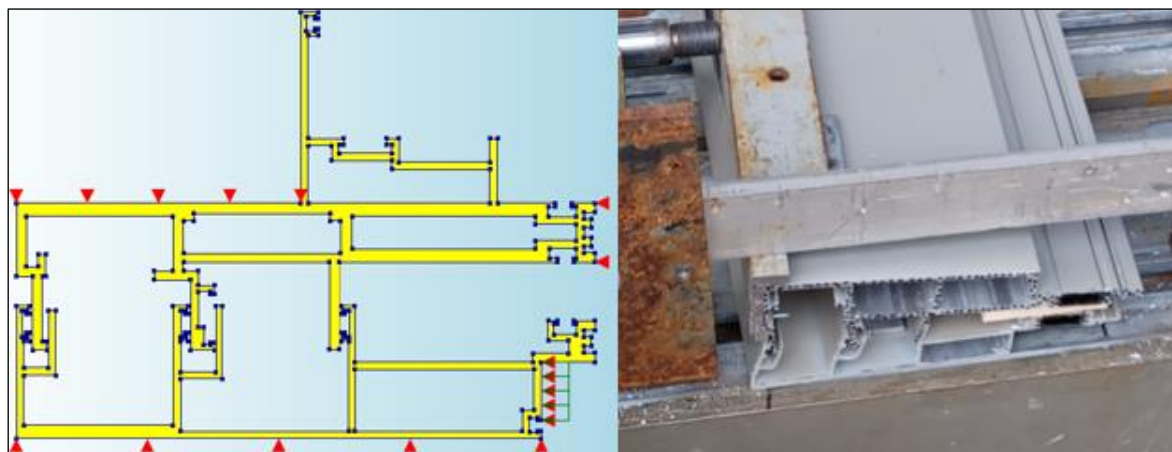


Figure 4.31 Mullion-mullion restraints and load application out-of-plane outwards. Left: FEM. Right: picture.

Finite element types

Details of the finite element types used in the analysis can be seen in Table 4.10.

Table 4.10 Finite element types and details.

Finite element type	Quadrilateral, 4 nodes (Q8EPS)	Triangular, 3 nodes (T6EPS)	Line, 2 nodes, 2D (L4CT)
DOF per node	2	2	2
Interpolation scheme	Linear	Linear	Linear
Integration scheme	2x2, Gauss	1- point, Area	-
Dimension	2D	2D	2D
Geometry	Cross-section	Cross-section	Contact
Number of elements	3739	50	85

Solution procedure

To get a solution that satisfies the connection performance it was necessary to define three target elements with one or two contacter elements per contact zone, see Figure 4.32. For the non-linear analysis geometric non-linearities and energy convergence norm were selected. Additionally, "Abort criterion" was increased from the default values up to $1e+15$. The analysis was divided into 3 blocks to establish contact and stabilize the model after contact. The total displacement of 20 mm was reached in approximately 40 load steps. Figure 4.33 shows the final deformed shape and the plastic strains formed after 20 mm of relative displacement.

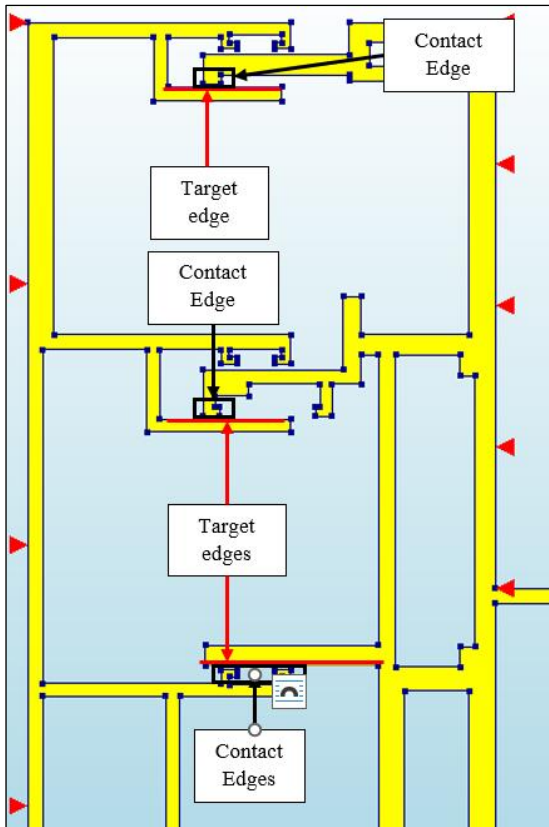


Figure 4.32 Mullion-mullion out-of-plane outwards. Contact elements.

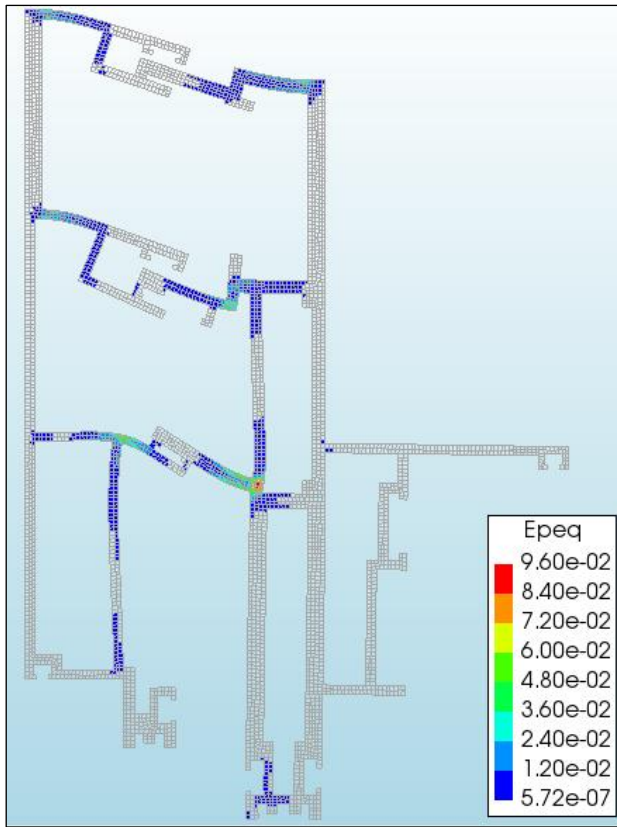


Figure 4.33 Mullion-mullion out-of-plane outwards. Final deformed shape and plastic strains

4.2.4 Top and Bottom brackets

The behaviour of the top and bottom brackets was analysed in-plane vertically and horizontally, see Figure 4.34. 3D models were used to analyse the aluminium bracket in-plane horizontal and vertical down performance, and the bottom bracket vertical up and down, and horizontal behaviour. The 3D models were analysed as "Structural solids" according to DIANA element class definitions, and the bolted connection was assumed as fully fixed. Since the analysis procedure followed was similar for top and bottom brackets, in this section only the vertical and horizontal analysis of the aluminium bracket is displayed. A mesh of approximately 10 mm per side was used for the analysis.

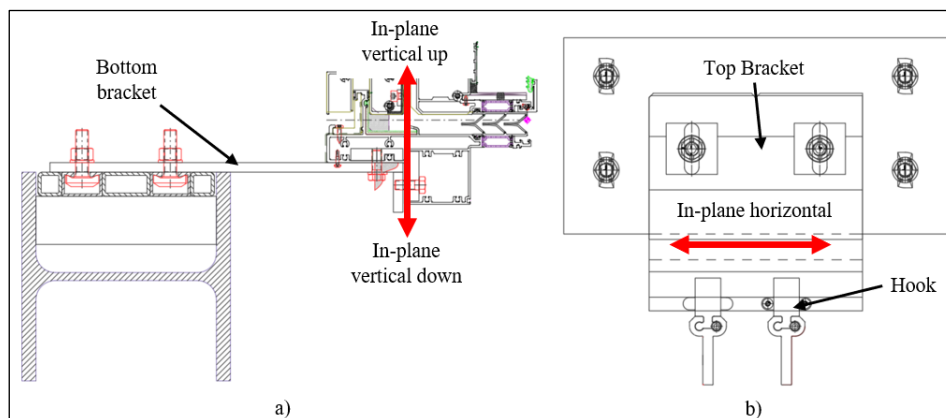


Figure 4.34 Brackets displacement directions. a) Bottom bracket b) Top bracket and hook.

4.2.4.1 In-plane horizontal

The horizontal analysis of the top bracket was carried out with a 3D model including the hook to check the interaction between both elements when applying a horizontal force at the hook and at the edge of the element, see Figure 4.35. Since the aforementioned analysis follow a similar procedure, the in-plane horizontal analysis presented describes only the analysis of the horizontal force applied at the edge of the bracket. An interface was created to set the contact interaction between the top bracket and hook.

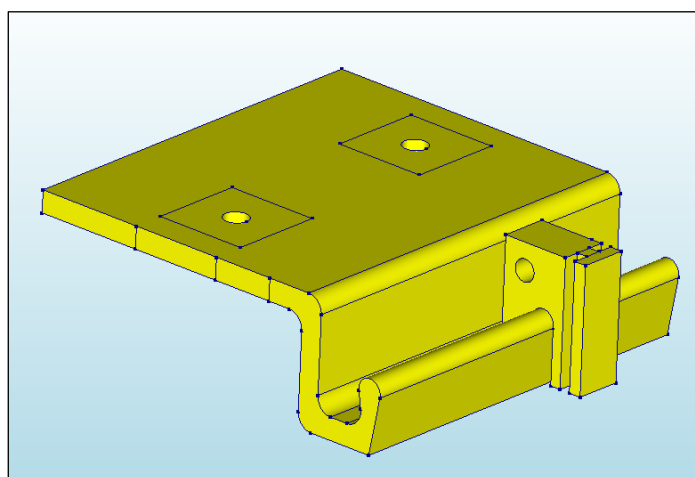


Figure 4.35 3D model top bracket + hook

Material properties

The material properties for the bracket and hook can be found in Table 4.11, and the bi-linear model in Figure 4.36, and the linear properties of the interface can be observed in Table 4.12.

Table 4.11 Aluminium alloys AL 6005-AT6 and AL 6082-T6 summary of properties.

Material	Model	E	ν	ρ	f_o	f_u	ϵ_u
		[N/mm ²]					
AW 6005-T6	Hardening	70000	0,3	2700	200	250	0,19
AW 6082-T6	Hardening	70000	0,3	2700	154	300	0,16

Table 4.12 Top bracket- hook interface linear properties.

Element	Normal stiffness modulus Y	Shear stiffness modulus X
	[N/mm ³]	[N/mm ³]
Interface	7,00E+06	7,00E+04

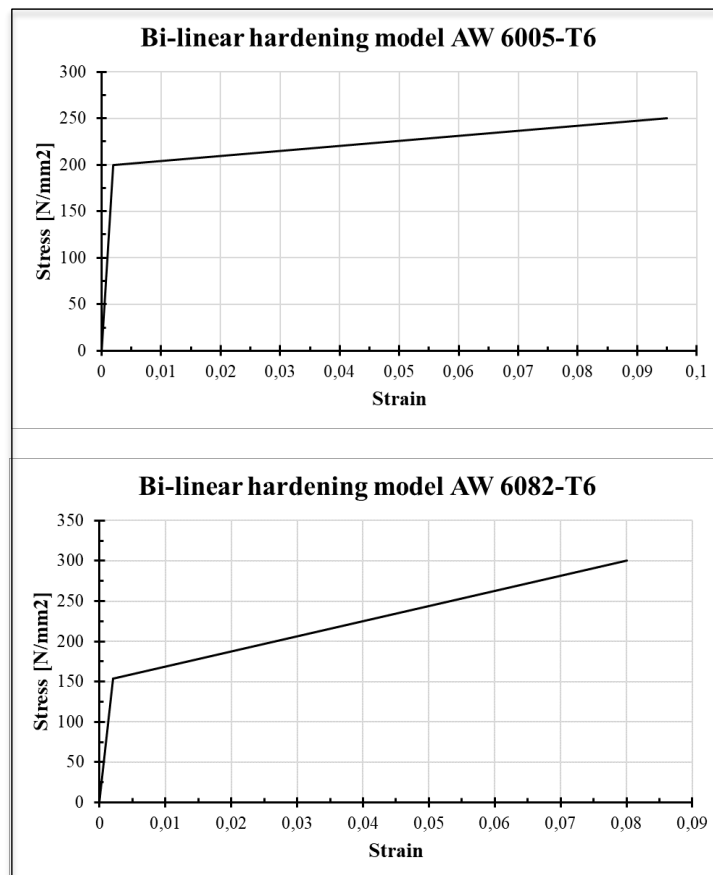


Figure 4.36 Bi-linear model aluminium alloys AW 6005-T6 and AW

Boundary and loading conditions

The restraints adopted in the model were: bolts fully fixed and vertical restraints along the edge in contact with beam used as support. Regarding the load application, for the model an imposed displacement of 1,5 mm was applied the right-outer side of the solid geometry, replicating the load application seen in Figure 4.38. A more complex restraint option can be considered, since the bolt connections shall behave with a rotational stiffness in function of the pressure exerted over the plate; however, a most sophisticated analysis is considered out of the scope of this research.

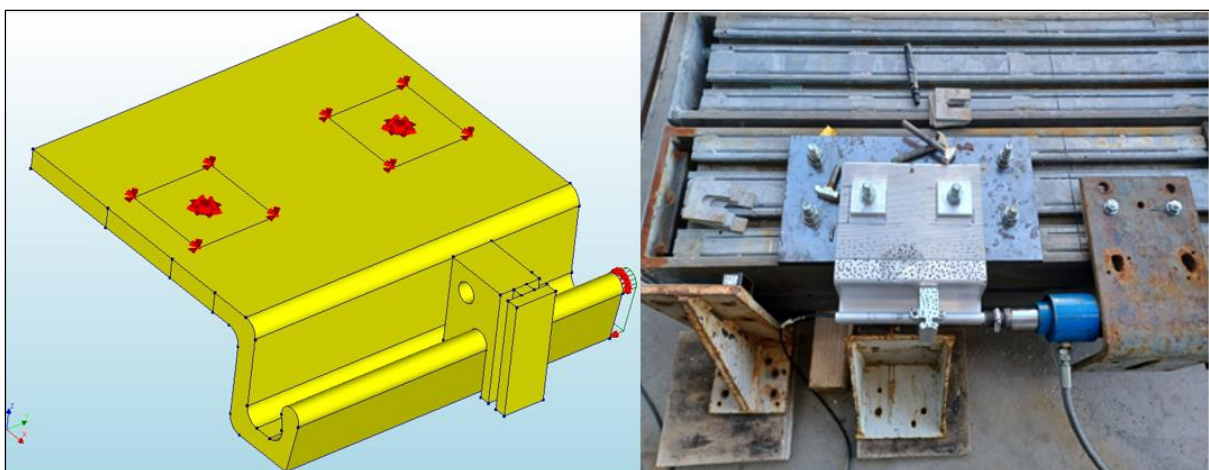


Figure 4.37 Top bracket-hook horizontal. Restraints and load application

Finite element types

Details of the finite element types used in the analysis can be seen in Table 4.13.

Table 4.13 Finite element types and details.

Finite element type	Brick, 8 nodes (HX24L)	Pyramid, 5 nodes (PY15L)	Tetrahedron, 3 sides, 4 nodes (TE12L)	Wedge, 6 nodes (TP18L)	Plane quadrilateral, 4+4 nodes (Q24IF)
DOF per node	3	3	3	3	3
Interpolation scheme	Linear	Linear	Linear	Linear: area/isoperimetric	Linear
Integration scheme	2x2x2, Gauss	Numerical	Numerical	1- and 2-point, Area	3x3 Newton-Cotes
Dimension	3D	3D	3D	3D	3D
Geometry	Bracket/Hook	Bracket/Hook	Bracket/Hook	Bracket/Hook	Interface
Number of elements	1413	737	498	196	18

Solution procedure

To find the lateral stiffness of the connection, it was submitted to a non-linear analysis with the next considerations: geometric non-linearity, and displacement and force convergence norms. For this analysis, only one execute block was required with 100 steps to reach 1,5 mm of prescribed displacement applied. Figure 4.39 shows the final deformed shape and the plastic strains formed after 1,5 mm of imposed displacement was applied.

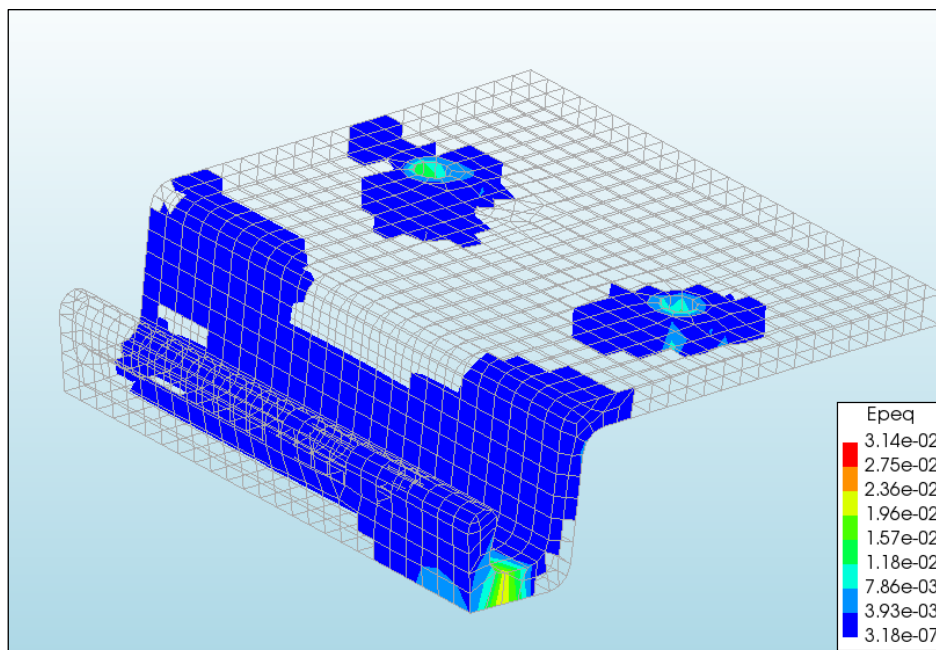


Figure 4.38 Aluminium bracket horizontal. Final deformed shape and plastic strains.

4.2.4.2 In-plane vertical

The vertical in-plane numerical model of the top bracket consisted of a 3D model including the hook to analyse the interaction between both the bracket and the hook when applying a vertical force on top of the hook (Figure 4.35).

Material properties

The material properties of the two aluminium alloys and interface are the same as the ones used for the horizontal analysis, see 4.2.3.1 In-plane horizontal.

Boundary and loading conditions

The restraints adopted in the model were: bolts fully fixed and vertical restraints along the edge in contact with beam used as support. The load application in the model differs from the load applied during the test because the sleeve connection was not considered in the 3D model. However, the aim of the analysis was to determine the vertical stiffness of the bracket. Thus, the application of an imposed displacement of 7 mm at the bottom edge of the cantilever was considered a good approach, see Figure 4.40.

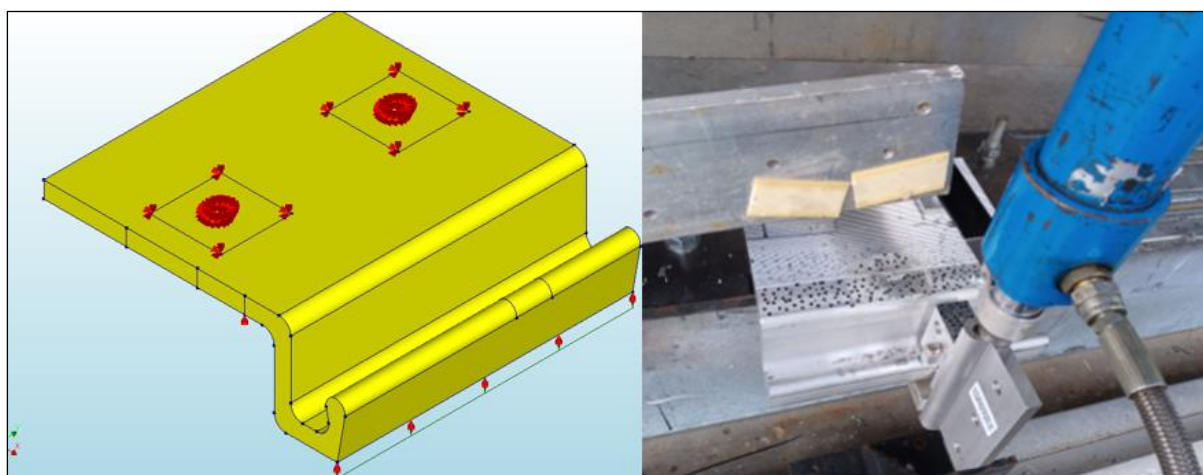


Figure 4.39 Top bracket-hook vertical. Restraints and load application.

Finite element types

No changes to the mesh were executed for the vertical evaluation. Thus, the same finite element types described in Table 4.13 apply for this analysis.

Solution procedure

To find the vertical stiffness of the connection, a non-linear analysis was carried out with the next considerations: geometric non-linearity, and displacement and force convergence norms. One executes block was sufficient to reach the 70 mm of prescribed displacement with 40 load steps. Figure 4.41 shows the final deformed shape and the plastic strains formed after 7 mm of imposed displacement applied.

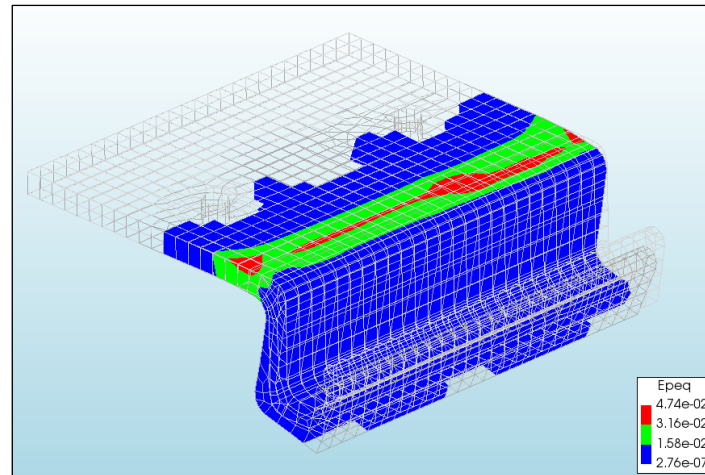


Figure 4.40 Aluminium bracket vertical. Final deformed shape and plastic strains.

4.2.5 Silicone

The silicone modelling objective is to determine its shear and tension stiffness of the silicone adhesive Dow Corning 993. To obtain results, a 3D model of the silicone was elaborated with the next dimensions: 184 mm depth, 8 mm width, and 25 mm height. Two directions of shear response were analysed as shown in Figure 4.42. The silicone element class was defined as "Rubber solid" with hyper-elastic material properties. For modelling reasons, the numerical model uses a bar of aluminium attached to the silicone for the load application, this is necessary to reproduce the test realized in the laboratories. For the mesh, the frontal faces of both elements were divided in a mesh of approximately 2 mm per side, and the lateral face was divided in a mesh of approximately 5 mm per side



Figure 4.41 Silicone shear. a) Vertical b) Horizontal

4.2.5.1 Tension

Material properties

Three material properties for the aluminium can be observed in Table 4.14. Similarly, the linear properties of the interface can be seen in Table 4.15. Table 1.6 provides information about the constants K1 and K2 required to define the hyper-elastic properties.

Table 4.14 Aluminium linear elastic properties.

Material	Model	E	v	ρ
		[N/mm ²]		[kg/m ³]
Aluminium	Linear	70000	0,3	2700

Table 4.15 Silicone-aluminium interface properties.

Element	Normal stiffness modulus Y	Shear stiffness modulus X
	[N/mm ³]	[N/mm ³]
Interface	1,40E+07	1,40E+06

Table 4.16 Mooney-Rivlin constants Dow Corning 993 [78]

Element	K1	K2
	[N/mm ³]	[N/mm ³]
Interface	1,40E+07	1,40E+06

Boundary and loading conditions

To simulate the silicone as it were attached at both sides, the free face of the silicone was fully restrained in all directions. Moreover, to ensure only a horizontal movement when applying the load two edges of the aluminium element had restraints in Y and Z directions. The load application was solved with 10 mm of imposed displacement applied at the four outer corners and the centre of the aluminium solid, see Figure 4.43.

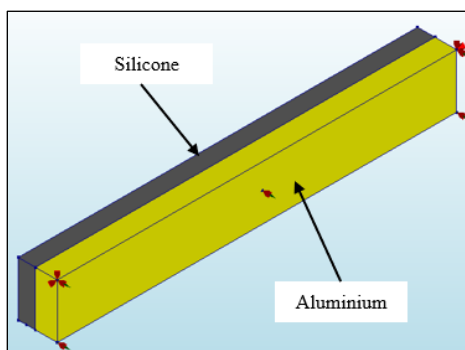


Figure 4.42 Silicone and aluminium boundary conditions

Finite element types

The details of the finite element types used in the analysis can be seen in Table 4.18.

Table 4.17 Finite element types and details.

Finite element type	Brick, 8 nodes (HX24L)	Pyramid, 5 nodes (PY15L)	Tetrahedron, 3 sides, 4 nodes (TE12L)	Wedge, 6 nodes (TP18L)	Plane quadrilateral, 4+4 nodes (Q24IF)
DOF per node	3	3	3	3	3
Interpolation scheme	Linear	Linear	Linear	Linear: area/isoperimetric	Linear

Integration scheme	2x2x2, Gauss	Numerical	Numerical	1- and 2-point, Area	3x3 Newton-Cotes
Dimension	3D	3D	3D	3D	3D
Geometry	Silicone/Alu	Aluminium	Aluminium	Aluminium	Interface
Number of elements	3069	758	603	253	481

Solution procedure

To find a solution for a hyper-elastic model, it is necessary to perform a non-linear analysis with geometric non-linearity considerations activated; moreover, displacement and force convergence norms were applied during the analysis. The full displacement of 10 mm was applied in on execute block with 100 load steps. Figure 4.44 shows the final deformed shape of the silicone its extension up to 10 mm.

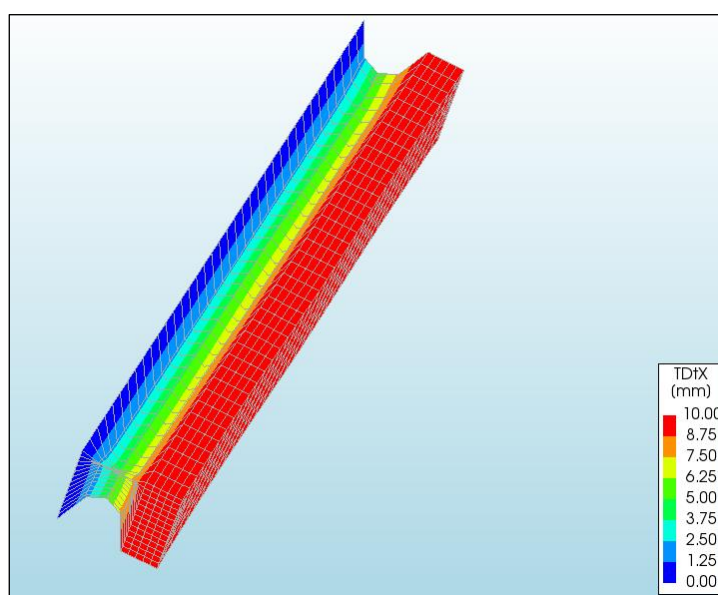


Figure 4.43 Silicone extension. Final deformed shape.

4.2.5.2 Shear

The modelling of silicone submitted to shear forces vertically and horizontally as defined in Figure 4.42 was carried out following the same directions for both cases. Therefore, to avoid redundancy in this section, only the vertical shear model is explained. The boundaries condition and deform shape of the other shear direction can be observed in Annex A.

Material properties

The same material properties defined for extension were used for shear analysis, see Tables 4.14, 4.15, and 4.16.

Boundary and loading conditions

To simulate the silicone as it were attached at both sides, the free face of the silicone was fully restrained in all directions. Moreover, to ensure only the vertical movement of the aluminium solid when applying the load, two edges of the aluminium element had restraints in X and Y

directions. The load application was solved with 20 mm of imposed displacement applied at the four top corners of the aluminium solid, see Figure 4.45.

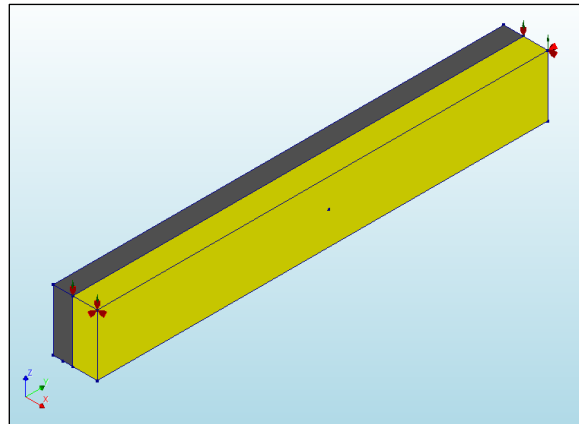


Figure 4.44 Silicone and aluminium vertical shear boundary conditions.

Finite element mesh

The mesh for the vertical shear analysis is the same defined for the extension analysis, see Table 4.18.

Solution procedure

To find a solution for a hyper-elastic model, it is necessary to perform a non-linear analysis with geometric non-linearity considerations activated; moreover, displacement and force convergence norms were applied during the analysis. The full displacement of 10 mm was applied in on execute block with 100 load steps. Figure 4.46 shows the final deformed shape of the silicone after the application of 20 mm of displacement to the aluminium solid.

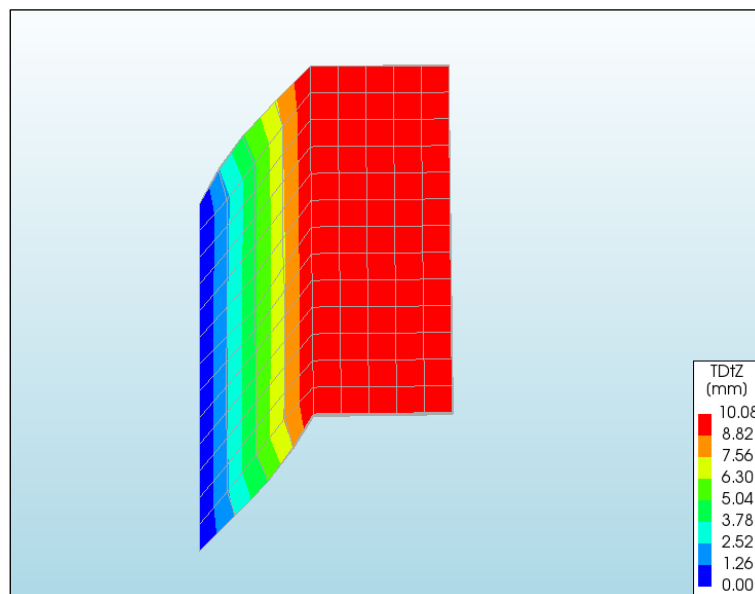


Figure 4.45 Silicone vertical shear. Deformed shape at 10 mm of displacement. front view.

5

Results and Discussion

This chapter is focused on presenting and comparing the results from the connections experimental campaign and the results from the numerical models. As aforementioned, the objective of this thesis is evaluating the performance of the connections within a CW with FEM in terms of Force vs. Displacement behaviour. In this Chapter, the numerical results are analysed and compared with the experimental results in order to be validated; moreover, the potential causes for the difference in the results will be evaluated. Finally, it is important to mention that the results showed in this section are selected according to their explanatory relevance.

5.1 Discussion and results

In this section, the test and numerical results of the analysed connections from Case study 2 are presented in the form of a Force vs. Displacement graph. The results displayed were selected in concordance with the section: Discussion. Moreover, the results not considered in this section will be presented in Annex B.

As aforementioned, earthquake activity represents a challenge for façade designers due to the potential hazard they represent to non-structural elements such as curtain walls. Moreover, seismic events can cause irreversible or reparable damages on façade elements, representing high economic losses and safety risks. Having emphasised this problematic again, it is noticed the importance to study the components of a CW and their seismic performance. To achieve the objectives of this thesis research, the connections that contribute to the seismic response of glazed curtain walls are evaluated with finite element models and validated with experimental tests.

To determine the connections that may influence the seismic performance of glazed CWs an extensive study of literature was carried out. As an outcome, it was understood that during a seismic event: the anchorage system shall be rigid enough to resist the weigh load of the CW façade, but ,additionally, should permit certain degree of rotation and translation when submitted to imposed displacements caused by earthquakes; the contact between two framing elements may cause plastic deformations according to the tests carried out by Memari A., et all. [67]; finally, it was described in the literature that silicone glazing gives glass the chance to accommodate cyclic displacement due to its adhesive properties and elastic behaviour. Therefore, the transom, mullion, top and bottom brackets, and silicone were the connections selected for this study. The evaluation of the performance of each connection was carried out

with the use of FEMs elaborated with the software DIANA and validated with connection tests carried out at Permasteelisa Group facilities in Italy.

Initially, the validation of the numerical models was intended to be carried out by comparing global displacements of a full-size façade specimen obtained with experimental tests with global displacements resulting from a FEM of the same façade specimen (global model) that included the local behaviour of the connections as parameters. To accomplish this goal, two façade specimens should have been evaluated: one with a "simple" geometry and another with a "more complex" geometry. Hence, two different sets of connections corresponding to each façade topology were about to be modelled in order to implement the local behaviour of the connections in each numerical global model of the facades. However, due to complexity and time limitations, the proposed modelling objective changed during the elaboration of this research. For this reason, an additional experimental campaign, evaluating the connections of the specimen tested in July 2022, was performed in October 2022. With this set of tests, a new validation protocol relying on the Load vs. Displacement comparison of the connections tested and modelled was established to evaluate the modelling approach.

The discussion is based on three points. First, a description of the results and an initial explanation of the behaviour observed in the Force vs. Displacement curve based on the result data obtained from DIANA. This initial discussion is followed by a comparison between the curves obtained during the tests and the numerical models; the comparison is mainly made in terms of the behaviour of the connection, which can be done by comparing the slope of the curves obtained during the testing campaign with the curve from the numerical result. Finally, a general summary of the possible reasons of discrepancy is given to explain the unexpected behaviour of the components. Nevertheless, if required, in specific cases the cause of the possible discrepancy will be discussed. Anyhow, despite the constant contact with the responsible personnel from Permasteelisa, the discussion of the results obtained is limited due to the fact that some details about boundary conditions, testing conditions and testing facilities of the testing campaign may be missing. Additionally, it is limited by the amount of information available in the literature, which made it difficult to compare the procedure and the results obtained with other sources. Finally, it is limited by amount of information that can be obtained from Load vs. Displacement curves, which can only be used to calibrate the model based on load results and not base on strains or stresses.

5.1.1 Transom – starter sill

The transom-starter sill connection is the most critical model comparison due to the fact that the numerical model and the tested connection share the same cross-sectional geometry. Thus, this analysis is used to determine the reliability of the modelling approach used to elaborate the all the frame-frame connection analysis, and a similitude between the numerical results and the experimental results is expected. In Figures 5.1, 5.3 and 5.5 the results obtained in the experimental campaign and the FEM can be observed.

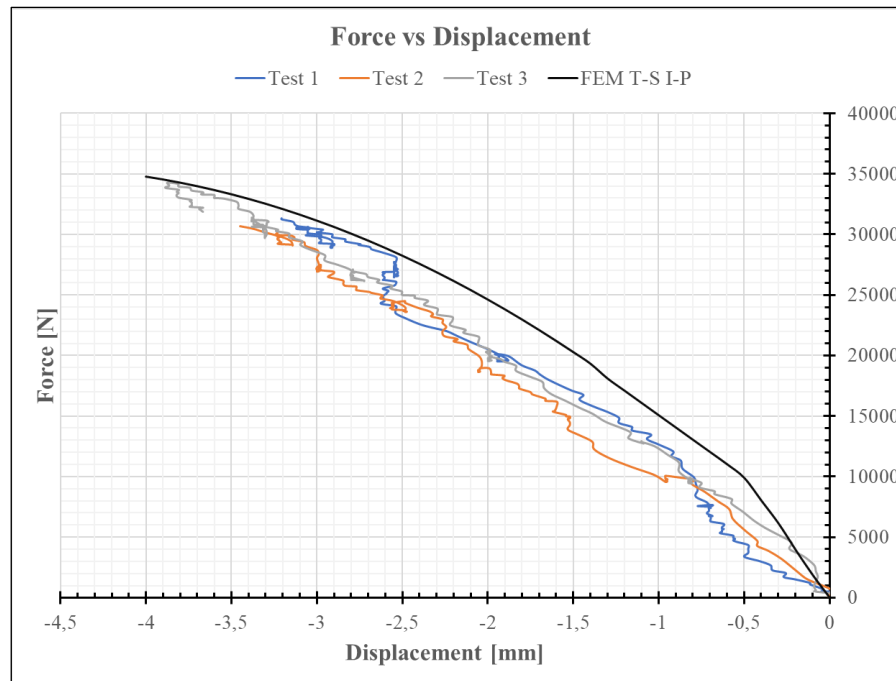


Figure 5.1 Transom-starter sill. In-plane. Force vs. Displacement.

As it can be noted in **Figure 5.1**, the numerical result of the stiffness evaluation in the in-plane vertical direction of the transom presents a linear behaviour until reaching 0,5 mm of displacement. The tendency to a further increase in stiffness remains until the cross-section reaches 4 mm of displacement corresponding to a force of around 35.000N for a cross-sectional depth of 500mm.

The linear behaviour observed in the model illustrates that the connection is working within the linear-elastic range until reaching 0,5 mm of displacement. The change of tendency seen after the 0,5 mm of displacement is caused by the first appearance of plastic strains (Figure 5.2), meaning that the connection entered to the plastic range and a slightly increase of stiffness is expected due to the hardening criteria used in the model. With respect to the comparison with the test results, it can be observed that the behaviour of the connection modelled is similar to the test results despite the FEM starts with a marginally higher stiffness until reaching the first 0,5 mm of deformation.

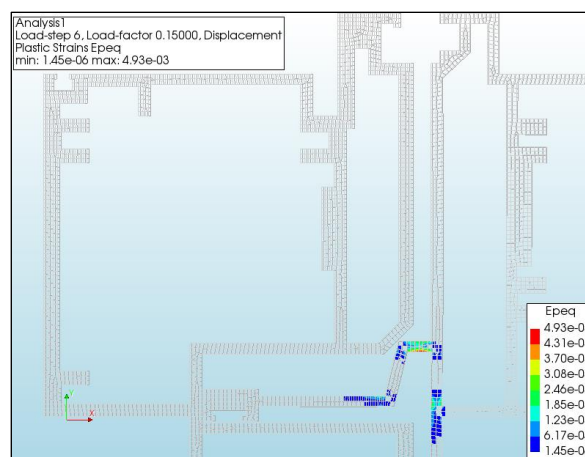


Figure 5.2 Transom-starter sill in-plane first plastic stain formed.

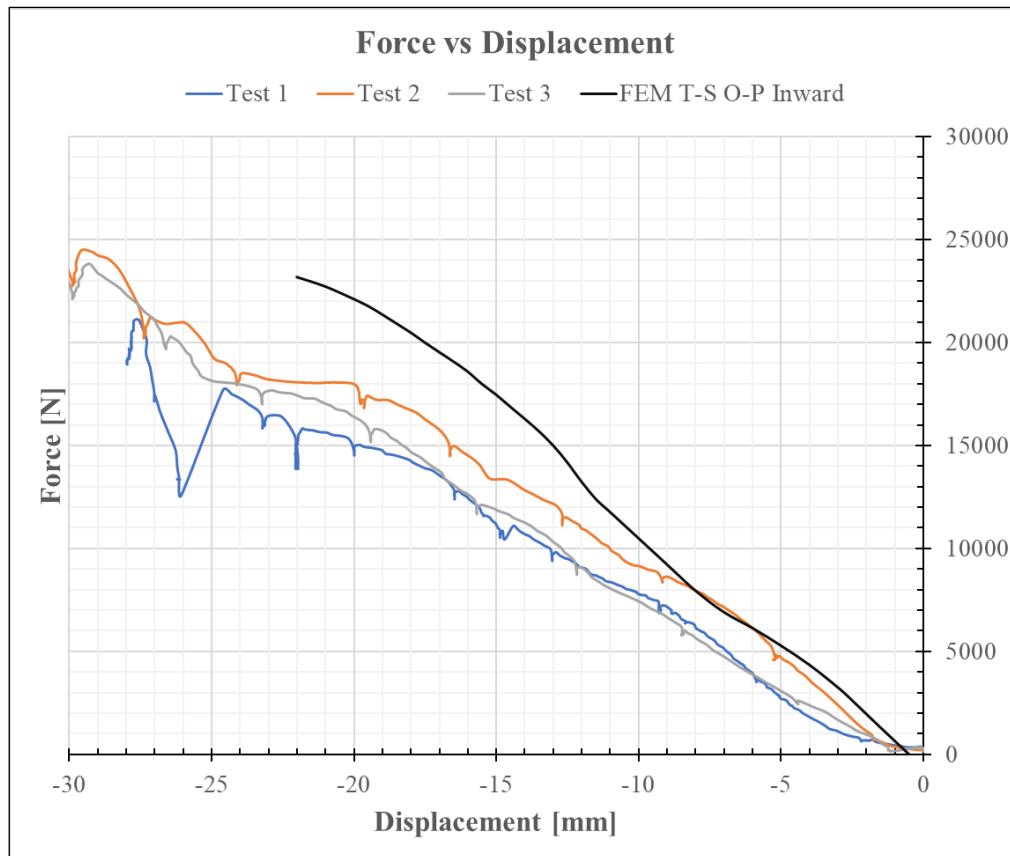


Figure 5.3 Transom-starter sill. Out-of-plane inward. Force vs. Displacement.

Figure 5.3 corresponds to the out-of-plane inward connection. It can be pointed out the fact that the connection starts being loaded after 1 mm of displacement, corresponding to the gap between the elements before contact. Moreover, it can be noticed that the FEM behaves linearly until the first 4 mm of displacement. Then, the curve starts to develop a non-linear tendency with two points of inflection. The first occurs at 7,5 mm of displacement and the second at 12 mm of displacement; after this, the tendency is stabilized until reaching 23 mm of displacement with 23.000N of force applied for a cross-sectional depth of 500mm.

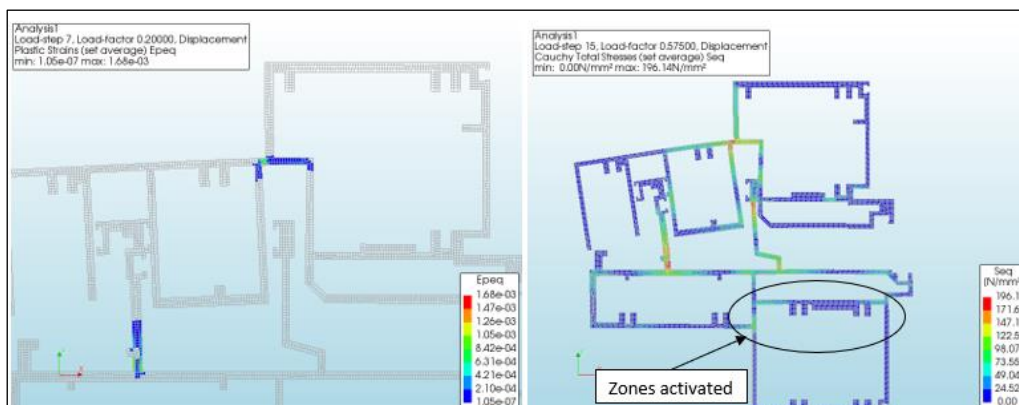


Figure 5.4 Out-of-plane inwards. Left: First plastic strains. Right: Stress diagram.

The linear behaviour seen in the model clearly shows that the connection behaves within the linear-elastic range until reaching 4 mm of displacement. The first change of tendency is caused by the formation of the first plastic strain (Figure 5.4 Left), meaning that the connection entered

to the plastic range and an increase of stiffness is observed due to the hardening criteria used in the model. The increase of stiffness at 7,5 mm is caused by the second contact between the cross-section at the right zone of the transoms. Moreover, the additional stiffness acquired when reaching 12 mm of displacement is caused by the "activation" of the other members of the cross-section which react against the pull-out forces caused by the displacement applied, see Figure 5.4 Right. When comparing the numerical results and the experimental results, it is possible to observe that the tendency is similar until the second contact is produced between both cross-sections at 7,5 mm. Then, the model starts to behave differently with respect to the curve tendency showed in the tests, reaching a difference of around 20% (4.000 N) in the force required to reach 20 mm of displacement.

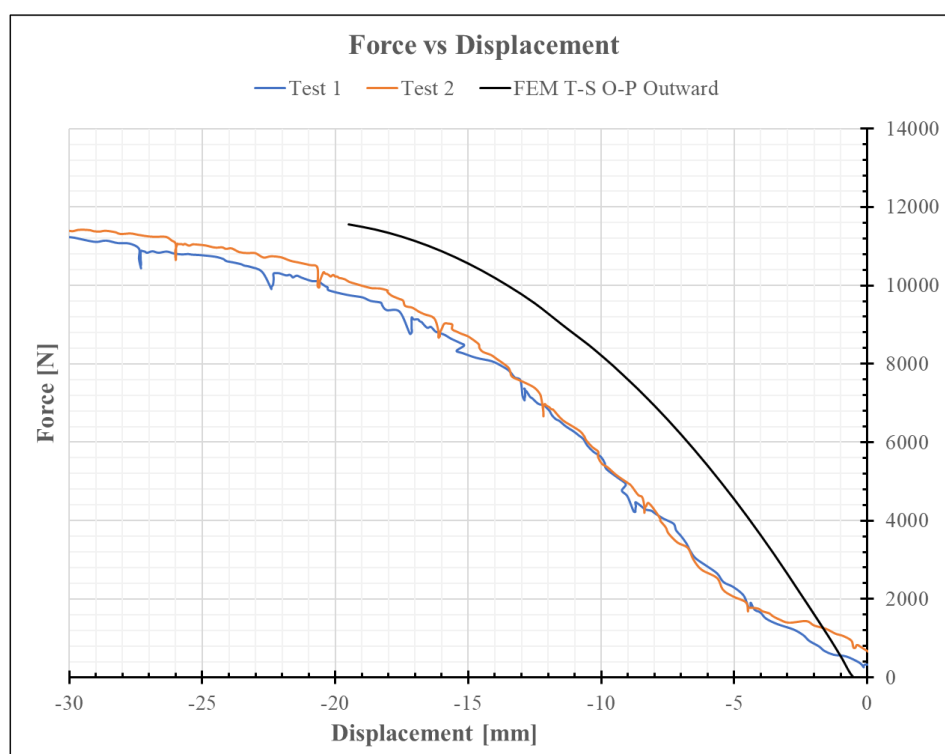


Figure 5.5 Transom-starter sill. Out-of-plane outward. Force vs. Displacement.

Finally, **Figure 5.5** corresponds to the out-of-plane outward action of the element. In the graph it can be noted that the connection is loaded after an initial 0,5 mm of displacement. Then, the curve starts with an initial linear tendency until reaching approximately 3 mm of displacement, where the curve starts showing a polynomial curvature. The cross-section analysis ends when the Force vs. Displacement curve of the connection modelled is close to reach its asymptote after 20 mm of displacement, with a force applied of 10.800 N approximately for a cross-sectional depth of 500mm.

As afore mentioned, a linear tendency of the curve represents the linear-elastic behaviour of the connection. From the data obtained with DIANA, it is possible to determine that the connection performs within the elastic range until reaching around 3 mm of displacement because the first plastic strains in the model appear at 3,5 mm of displacement, see Figure 5.6. Additionally, no changes in the stiffness of the connection are perceived for the reason that

contact between both cross-sections is produced twice but at the same time, resulting in a continuous curvature until the end of the analysis.

When comparing the computational results and the test results, it is feasible to observe the curves share a similar slope after 5 mm of displacement, being the initial behaviour of the model the main cause of difference with the experimental results. This difference could be caused by an initial accommodation of the displacements occurred until 5mm of displacement. At the end of the analysis (20 mm displacement), a difference of around 15% in the force required to reach 20 mm of displacement is observed.

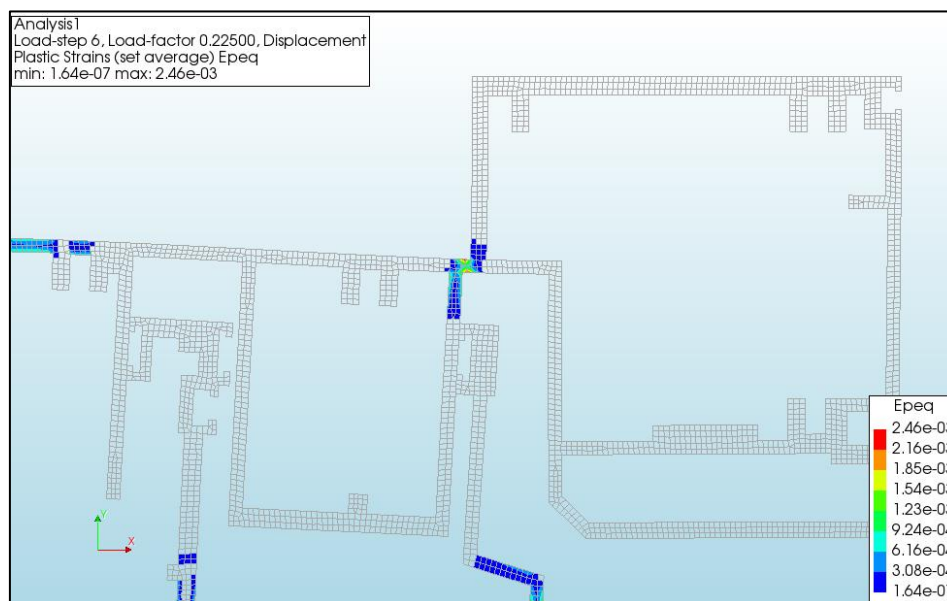


Figure 5.6 Out-of-plane outwards. First plastic strains.

5.1.2 Mullion-mullion

For the Mullion-Mullion connection only the out-of-plane inwards direction will be discussed. This decision is made because for both directions: out-of-plane inwards, and out-of-plane outwards the same principles can be applied to evaluate the tendency of the numerical and experimental results. Moreover, the in-plane connection was not considered because it was not possible to calibrate the model due to time restrictions. Finally, it is important to emphasize that the connections tested and modelled do not share the same geometry, see Figure 5.9.

From **Figure 5.7**, it can be observed that the out-of-plane inwards curve for the mullion connection between the large unit and the small unit (L-S) and the mullion connection between the two small units (S-S) are loaded after 1 mm of displacement. Additionally, it is observed that both curves start with a linear tendency until reaching 2 mm of total displacement and afterwards, the former straight lines adopt a curved shape. Finally, it is important to mention that for both curves the required load to reach 17 mm of displacement is 15.200 N and 24.200 N for the L-S and S-S connection, respectively.

From the FEM of the L-S connection, it is observed that at 2 mm of displacement plastic strains are formed, explaining why after 2 mm of displacement the curve adopts a non-linear tendency. Moreover, changes in the direction or the slope of the curvature are not observed because full

contact between both cross-sections already occurs during the 1 mm of free displacement. With respect to the S-S connection, after 2 mm of displacement plastic strains were already formed, see figure 5.8, and changes in the direction or slope of the curvature are not observed because contact is already developed after 1 mm of displacement. With both curvatures explained, it can be noticed that both connections behave within the elastic range until 2 mm of displacement is reached, and that a non-linear behaviour characterised by plastic deformations starts after the 2 mm of displacement applied.

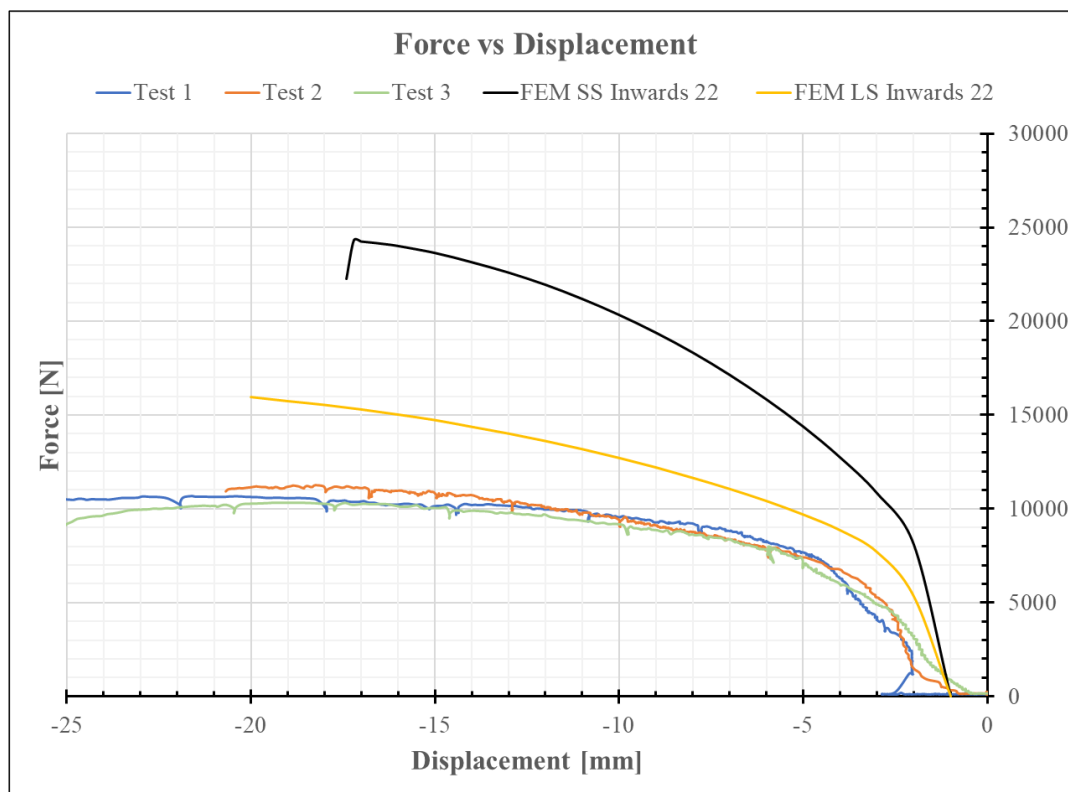


Figure 5.7 Mullion-Mullion. Out-of-plane inwards. Force vs. Displacement

Despite it is clear that the S-S connection can resist more load with less deformation, it is plausible to recognize that both connections share the same behaviour. If the curves from the model are compared with the curves from the experimental campaign, it is possible to observe that the L-S connection is around 1,5 times stiffer than the tested connection, and the S-S connection is around 2,5 times stiffer than the assessed connection during the experimental campaign. The reason for this behaviour relies on the size of the components; see Figure 5.8 showing the three connections and their distinct size. To illustrate, let's assume that each contact zone behaves as a cantilever beam. The amount of force required to produce a displacement of 1 mm will depend on the length of the cantilever, see Equation 5.1; in this way the force required to displace 1 mm the L-S and S-S connections will be higher than the required in the tested connection. The comparison illustrated in Figure 5.9 shows that the three connections compared have certain similitude in the behaviour, but it is influenced by the size of the connections.

$$\delta_{cant.max} = \frac{FL^3}{3EI} \quad (5.1)$$

With:

$\delta_{cant,max}$: maximum deflection at length L of a cantilever beam

F: force applied

L: length of the beam/span

E: Young's modulus

I: moment of Inertia

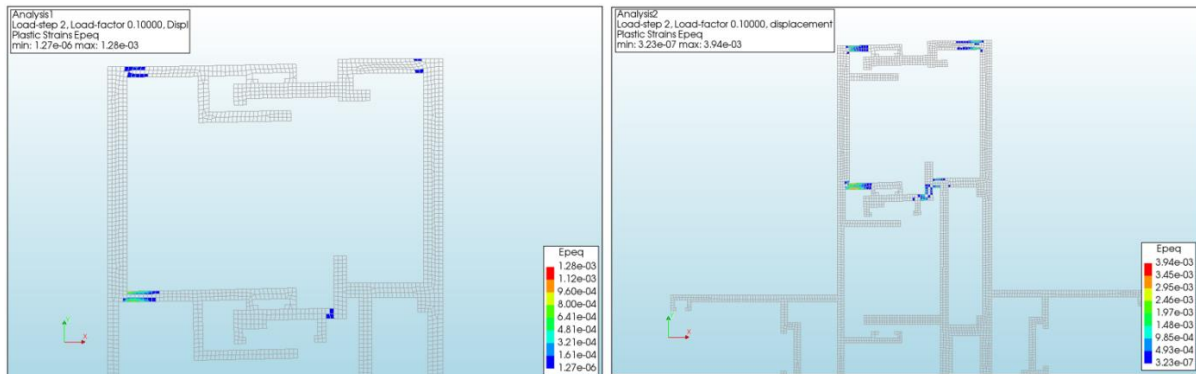


Figure 5.8 Out-of-plane inwards. Plastic strain formations. Left: L-S Right: S-S

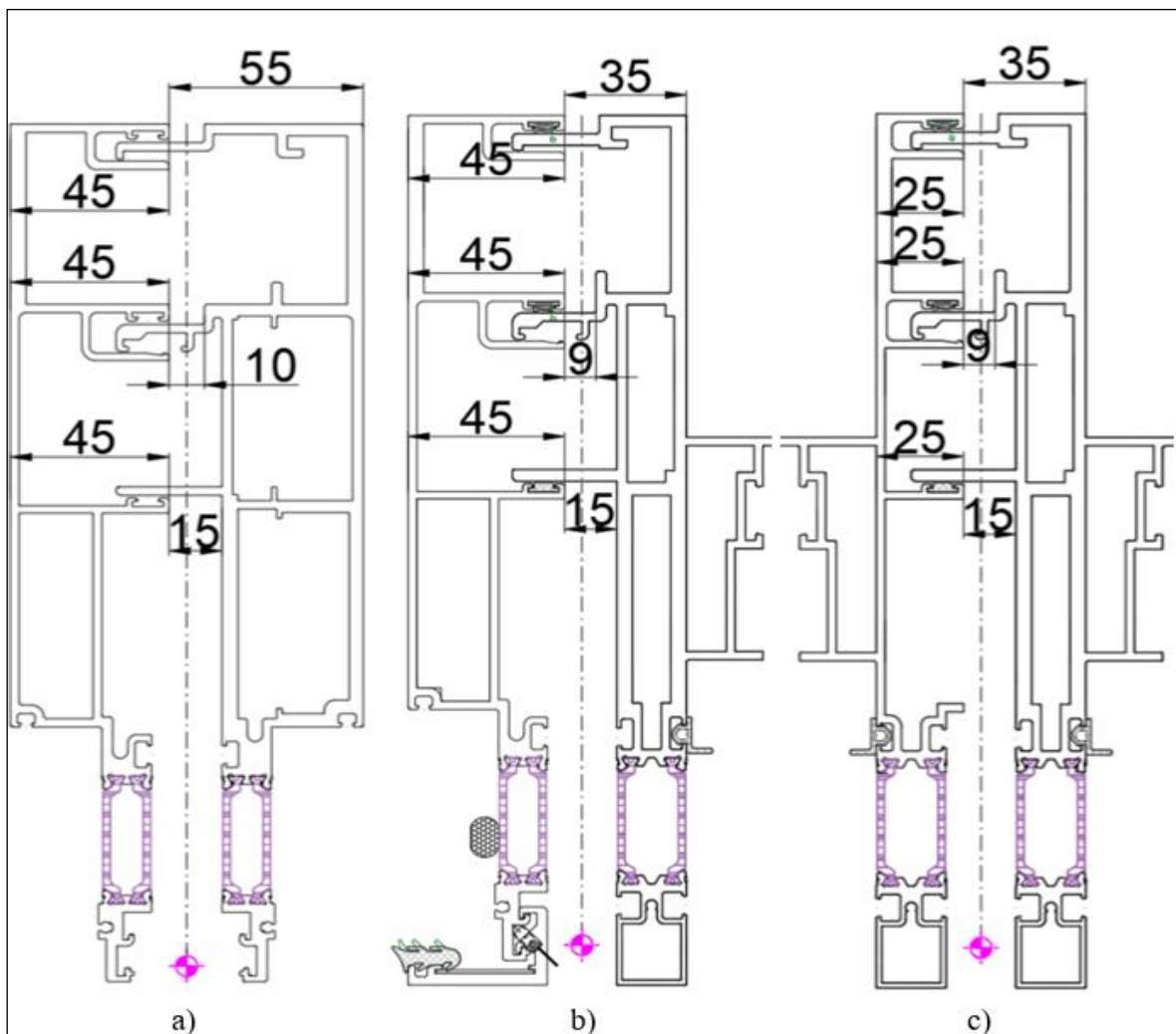


Figure 5.9 Mullion-Mullion connections. a) Tested b) L-S c) S-S

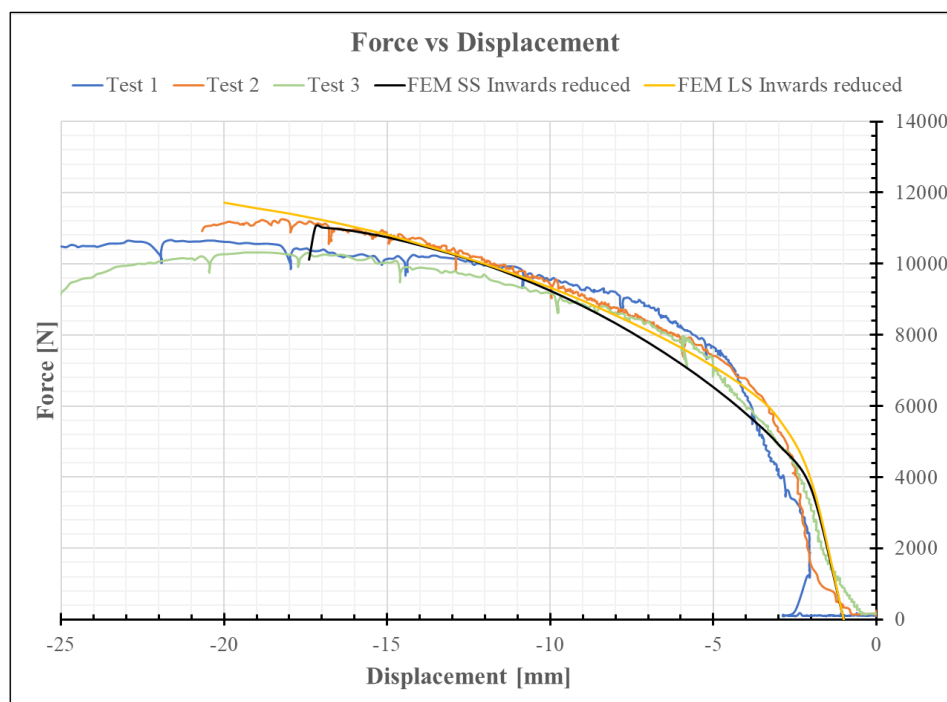


Figure 5.10 Mullion-Mullion out-of-plane inwards with reduced stiffness. Force vs. Displacement

5.1.3 Top aluminium bracket and hook

The top bracket and hook behaviour evaluated in this section only considers the load applied directly on the bracket. This decision was taken due to the high degree of uncertainty at the moment to elaborate a FEM with the load applied directly on the hook.

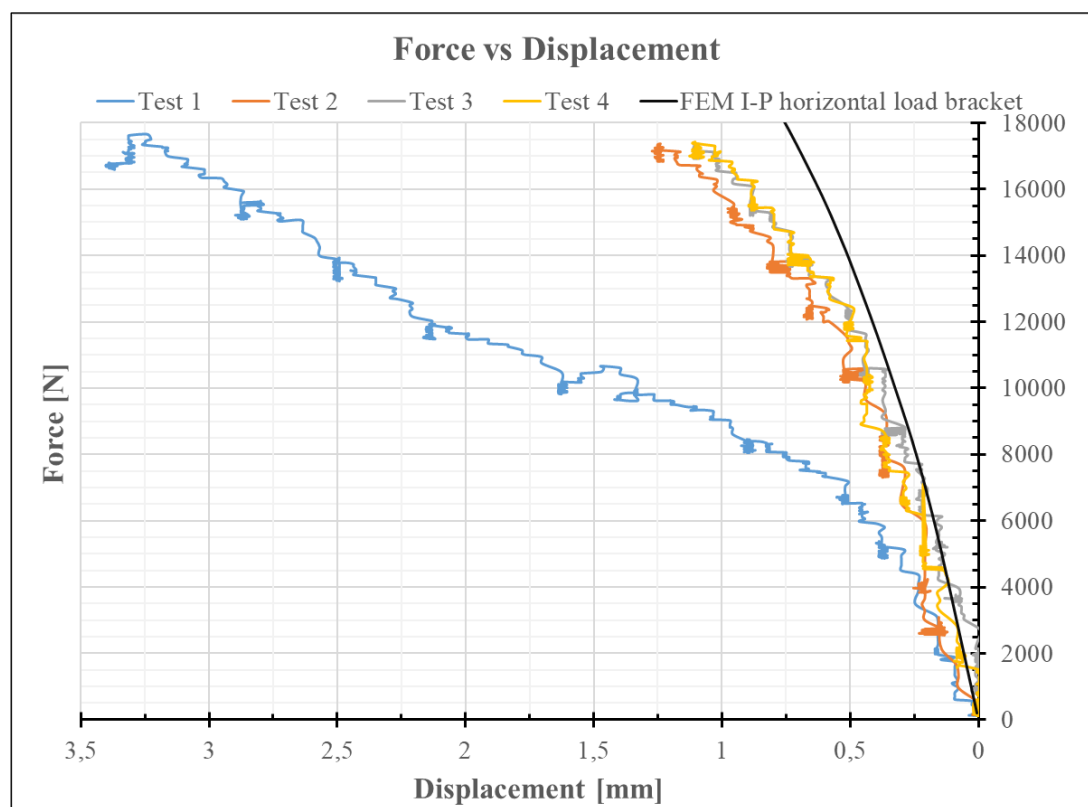


Figure 5.11 Top bracket and hook. In-plane horizontal (load on bracket). Force vs. Displacement.

Figure 5.11 shows clearly a linear behaviour of the bracket until 0,25 mm of displacement for the in-plane horizontal action. Then, it adopts a slightly curved shape until reaching 0,75 mm of displacement with a force of 18.000 N.

The straight line formed until 0,25 mm of displacement are reached represent the linear-elastic state of the aluminium bracket, which occurs without any plastic deformation. On the other hand, at 0,3 mm of displacement the first plastic strains start to arise on the bracket (Figure 5.12), justifying the small curvature observed in Figure 5.11.

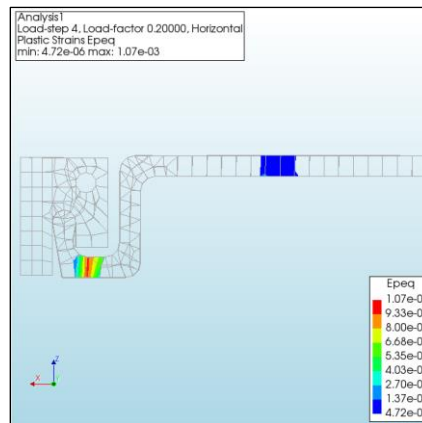


Figure 5.12 Top bracket and hook. In-plane horizontal. Initial Plastic strains

Comparing the numerical and the experimental results, it can be noticed that the initial stiffness of the model and the test results match until a force of 6.000 N is applied. It is possible to observe that forces exceeding the range of 6.000 N causes greater deformation in the tested connections when compared to the numerical model; moreover, it is clear that the largest displacements occurred during test 1. In this sense, the probable cause of the excessive deformation for test 1 can be caused by the rotation of the bracket due to the loss of tightness in the bolted connection, or/and due to the accommodation of displacements in the channel used to attach the bracket to the beam used as base for the test. Therefore, the difference between the FEM and the tests 2,3, and 4 can be caused by a small rotation of the bracket, causing the final difference in behaviour.

Moreover, it is important to emphasise that the numerical model was simplified by assuming a fully rigid connection between the bracket and the testing apparatus. The easiest option to consider this rotation during the design is the use of rotational springs instead of the assumed fully fixed connection. The rotational spring shall be modelled considering the first 6.000 N of rotational restriction before allowing rotation. Nevertheless, the test was carried out without the contribution of the CW's weight which can have an extra influence on the rotation of the connection, but it this evaluation is not part of the scope of this research.

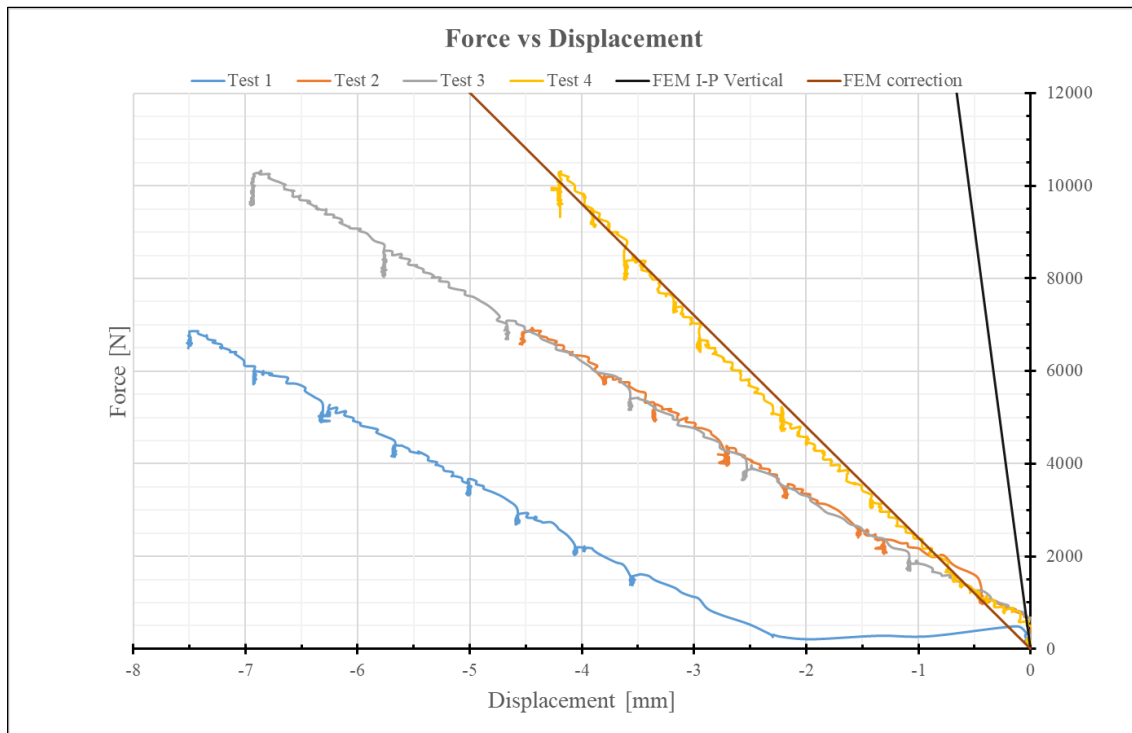


Figure 5.13 Top bracket and hook. In-plane vertical (down). Force vs. Displacement.

Figure 5.13 shows the Load vs. Displacement graph of the top aluminium bracket loaded vertically. It can be observed that the aluminium bracket follows a linear pattern of load and displacement until reaching 12.000 N with around 0,75 mm of displacement. This linear behaviour corresponds to the observed in the numerical model where plastic deformations start to appear after 2,1 mm of deformation when the load applied reaches 36.000 N of force, see Figure 5.19.

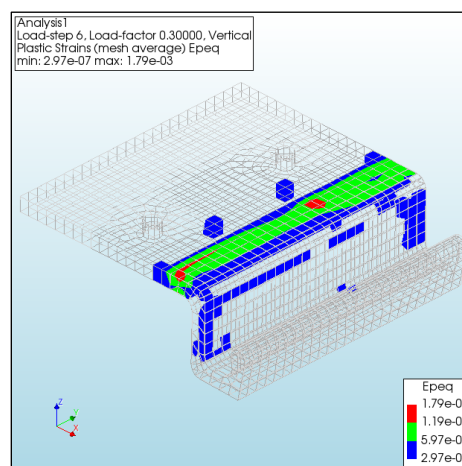


Figure 5.14 Top bracket and hook. In-plane vertical. Initial Plastic strains

From the numerical and the experimental results, it can be observed that the initial stiffness of the model and the test results does not match. After a discussion with the responsible of the testing sequence, it was concluded that the cause of the difference between the values obtained with the model and the values from the test, relied on the laser sensor location. In this way only test 4 was considered as a reference because it was located on a fixed position. However, it was also concluded that the beam to which the steel bracket was attached to was deflecting and

rotating due to the load applied through the aluminium bracket. Since the numerical results were required to match with the experiments, a calibration of the results obtained from the FEM was elaborated to match the conditions of the experimental test. This calibration was based on the addition of the deflection of the beam, which causes an additional vertical displacement, and the addition of a vertical displacement produced by the rotation of the beam. In this sense, the corrected curve was added to the Force vs. Displacement diagram, matching both curves. The correction of the vertical displacement can be found in Equation 5.2.

$$y_{corrected} = y + \frac{\delta_y * Load}{1000 N} + 200 * \sin(\text{beam}_{rot.}) * \frac{Load}{1000 N} \quad (5.2)$$

With:

$y_{corrected}$: corrected displacement in vertical direction

y : displacement obtained in the FEM

δ_y : Deflection of the beam per 1000 N

Load: load from the FEM results

$\text{beam}_{rot.}$: Beam rotational angle per 1000 N

5.1.4 Bottom steel bracket

The bottom bracket evaluation is similar to the one performed to the top bracket. Similar problems with similar possible causes were observed during these tests. However, two cases are included in the discussion.

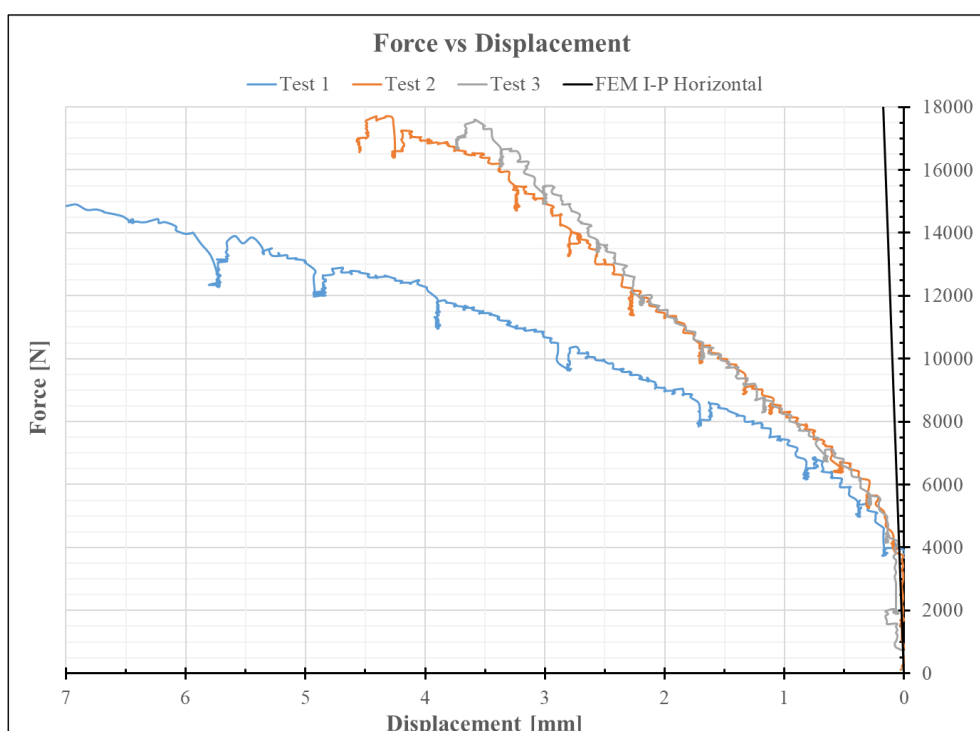


Figure 5.15 Bottom bracket. In-plane horizontal. Force vs. Displacement.

In **Figure 5.15**, it is possible to visualize the in-plane horizontal stiffness of the bottom steel bracket in terms of Load vs. Displacement. The steel bracket shows a linear behaviour until 18.000 N of force with a displacement of around 0,25 mm are reached. This linear behaviour corresponds to the elastic range. This information is contrasted with the numerical model

where plastic strains appears after 0,3 mm of displacement is applied with a force of 30.000 N (Figure 5.20).

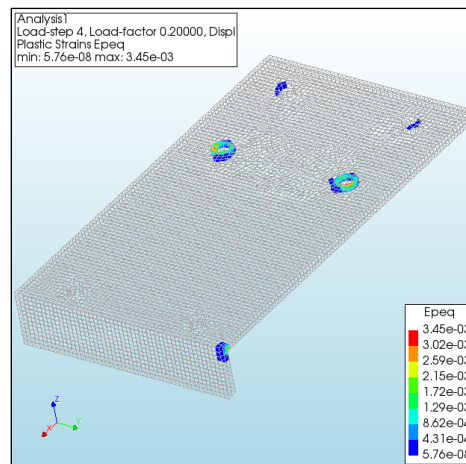


Figure 5.16 Bottom bracket. In-plane horizontal. Initial Plastic strains

With respect to the tests performed by Permasteelisa, the initial stiffness of the model and the test results are similar until the force applied reaches 4.000 N. By observing the graph, it is noticed that after a force of 4.000 N is applied, the connection's resistance against displacement is extremely reduced in all three tested cases. As observed before in the aluminium bracket connection, the causes of this exaggerated displacement can occur due to a loss of the fastening pressure between the bolt and the bracket, or due to the displacement of the bracket along the Halfen channel, used to fix the bracket to the beam where it is attached. Once again, to represent this behaviour in the numerical model the bolts shall be modelled as a rotational spring instead of using fully fixed restraints.

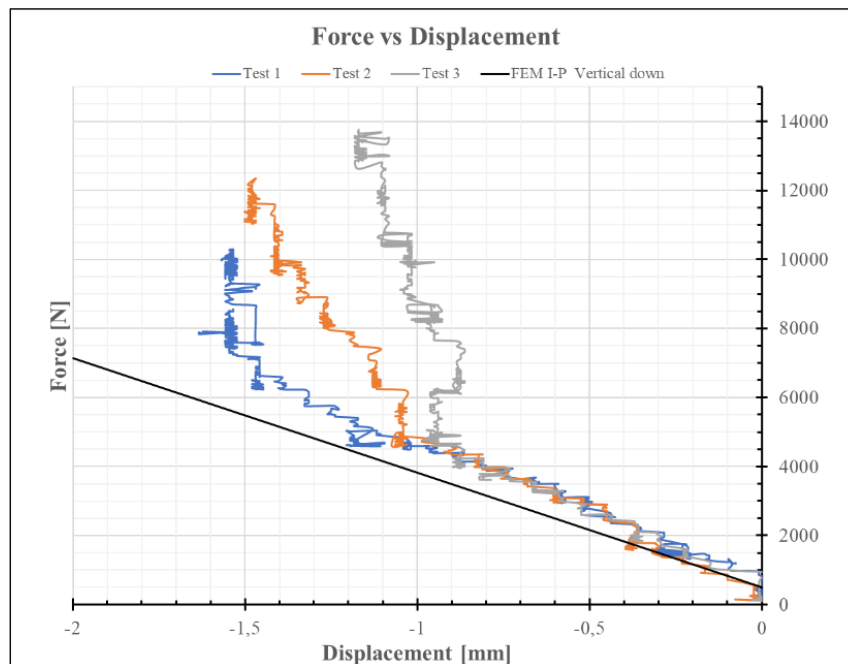


Figure 5.17 Bottom bracket. In-plane vertical (down). Force vs. Displacement

The Force vs. Displacement in-plane vertical down stiffness of the bottom bracket is displayed in **Figure 5.17**. The bracket shows a linear-elastic behaviour until it reaches 2 mm of displacement. This time, the model was only loaded with 2 mm of imposed displacement; therefore, there is no information about the moment when plastic strains start to appear. However, as it can be noticed from the graph that the calculated stiffness of the element is slightly smaller than the obtained by the experimental tests. This time, the comparison is limited by the test results since only information for the 1 mm of deformation was measured. Nevertheless, a comparison can be made between the force required to deform both elements by 1 mm; as a result, a 10% difference is found between the load applied at the bracket and the load from the numerical model.

5.1.5 Silicone

The last analysis performed were related to the silicone behaviour. This analysis was critical, since part of the research objective was the determination of the behaviour of a silicone connection with a numerical model for its further validation with laboratory tests. In this section, horizontal shear of the silicone will not be considered to avoid redundancy during the discussion.

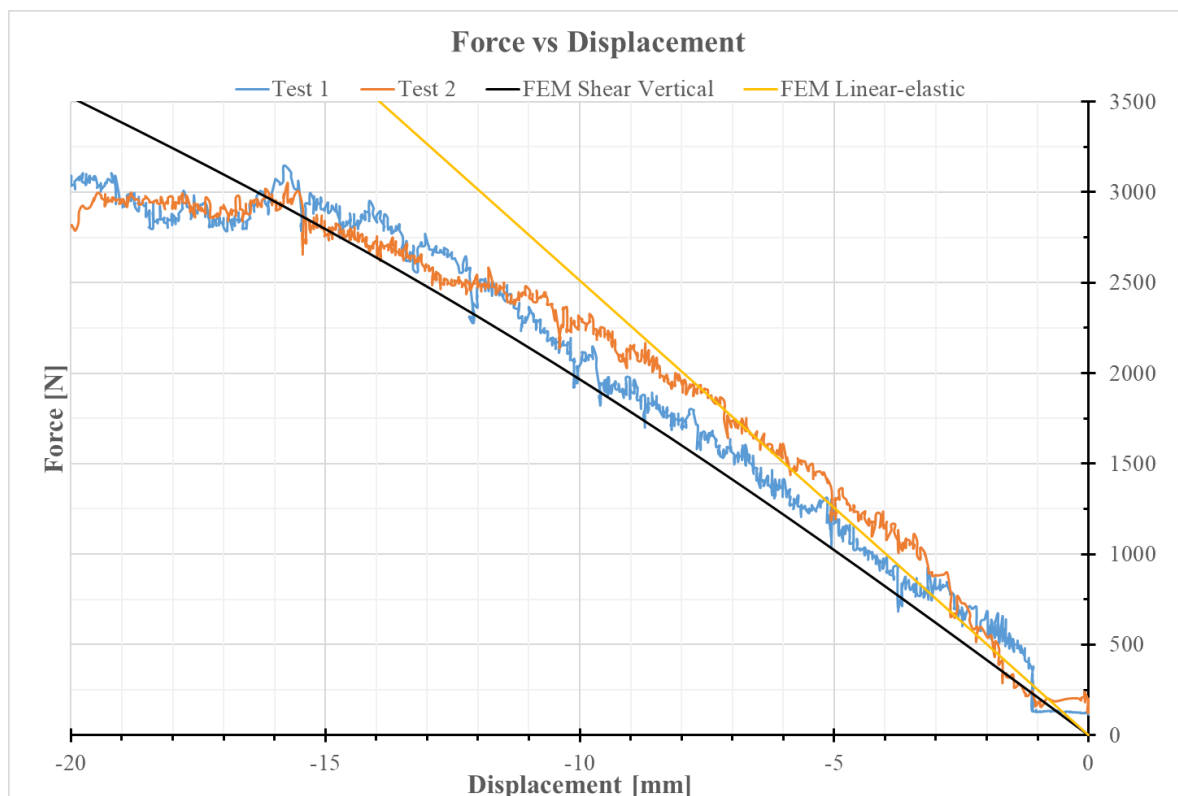


Figure 5.18 Silicone. Shear (vertical). Force vs. Displacement

Figure 5.18 shows the Load vs. Displacement curve of a silicone joint (8x25 mm with an effective length of 184 mm) submitted to shear action. In this scenario, two lines are plotted: one corresponding to a hyper-elastic model elaborated with Mooney-Rivlin constants as input data, and a second one using linear material properties; the data for the elaboration of both curves was obtained from a study elaborated by Silvestru V., et al. [78]. From graph, it is observed that behaviour of the hyper-elastic model elaborated with DIANA is almost linear. Moreover, it can be observed that the numerical model agrees with the experimental results

obtained during the testing campaign in the range between 0 and 16 mm of displacement. To corroborate this result, the paper titled “Investigations on Linear Silicone Joints for Glass-Metal Elements with Composite Structural Behaviour” were used to contrast the result obtained in this research. Silvestru V., et al. [78] tested three different samples of structural silicone Dow Corning 993 with the double-lap shear procedure; the results obtained in the tests were compared with numerical models elaborated using the Mooney-Rivlin hyper-elastic model and concluded that there is a good agreement between the results of the tested samples and the numerical model in the form of load vs. displacement curves. It can be observed in Figure 5.19 that the results obtained in this research for a silicone of 184x25x8 mm has a similar behaviour when compared to the silicone of 100x20x12 mm modelled by Silvestru V., et al.

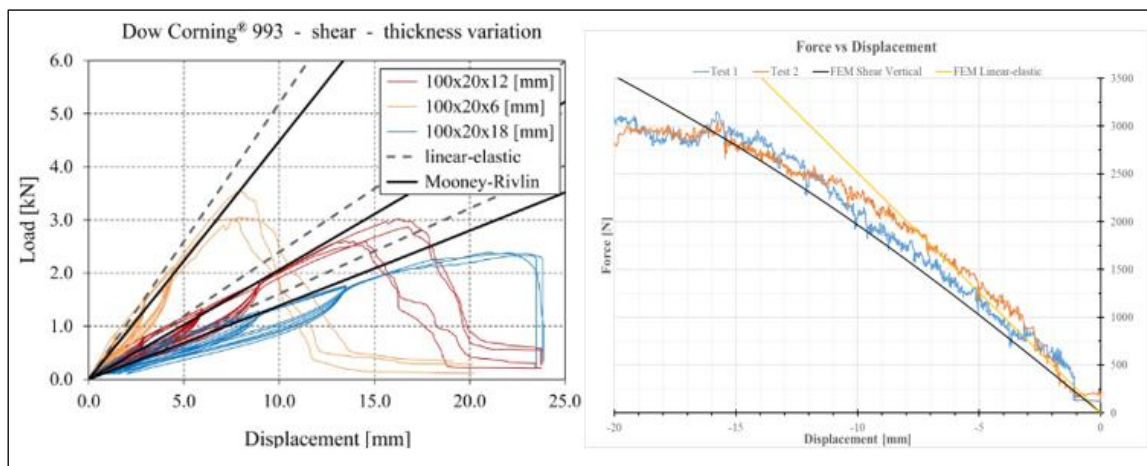


Figure 5.19 Load vs. Displacement Shear. Left: Silvestru V., et al results [78]. Right: research result

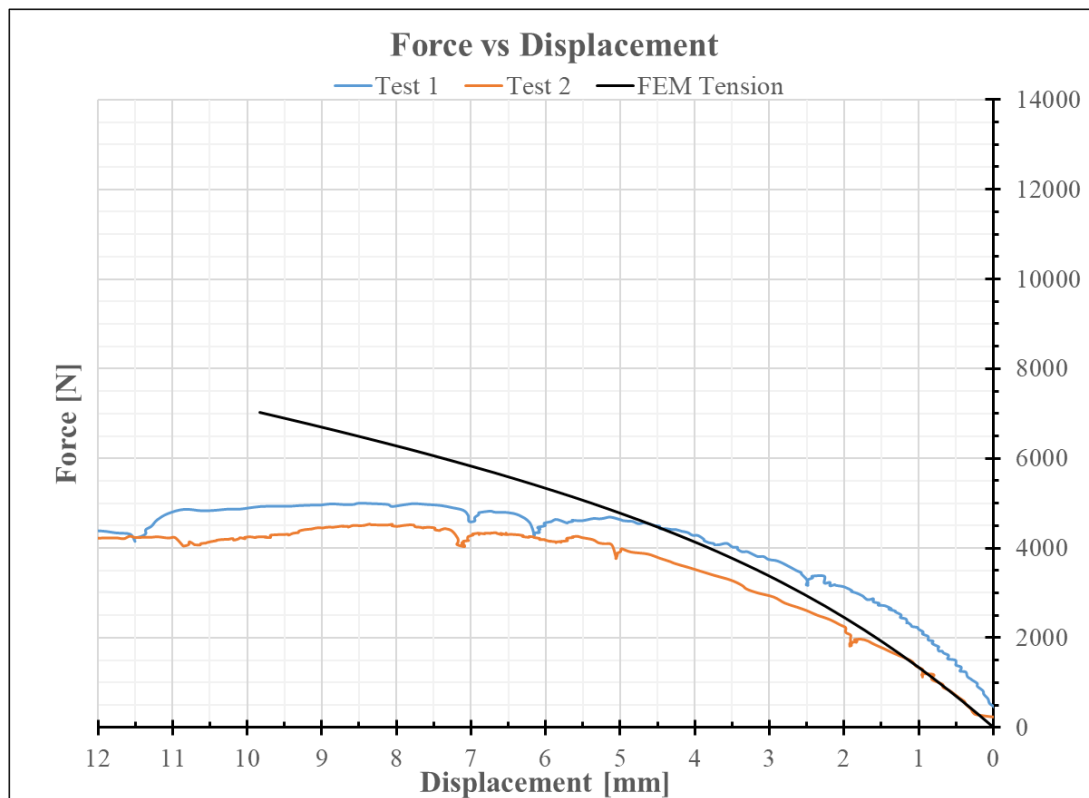


Figure 5.20 Silicone. Tension. Force vs. Displacement.

A similar match between curves is observed in **Figure 5.20**, where the tensile tests and the numerical model are compared in relation to their Load vs. Displacement behaviour. In this case, the model and the tests curves are similar until reaching 5 mm of displacement with an applied force of around 4.500 N. after this displacement the calculated value shows a stiffer behaviour when compared with the test results

By comparing these results with the stated by Silvestrau V., et all. [78] it is possible to observe that this time there is not an identical agreement between the silicone modelled in this research (184x25x8 mm) and the silicone from the paper (100x20x12mm), where the silicone modelled shows a slightly stiffer behaviour; this is caused by the difference in the dimensions of the elements. However, the behaviour of both curvatures follow the path of the tested samples until 5 mm of displacement is reached. is caused. Both results can be observed in table 5.22.

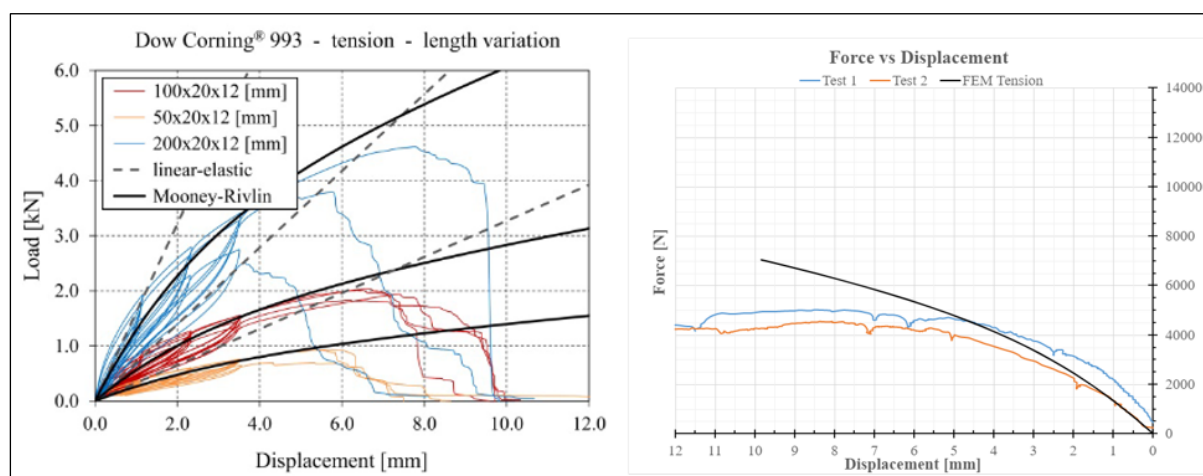


Figure 5.21 Load vs. Displacement Tension. Left: Silvestrau V., et all results [78]. Right: research result

5.1.6 Potential causes of discrepancy

In general, it is observed that the behaviour of the connections modelled and tested is similar. However, it is also possible to see that some FEMs overestimate the stiffness capacity of the connections. The potential causes for the increased stiffness in the numerical model can be boundary conditions, load application, cross-section location respect to each other, and model limitations.

The first two conditions may be solved with the implementation of a 3D model; however, it is important to understand why a 2D model may be affected by the boundary conditions and load application. It was noticed during the analysis that a change in the boundary conditions of the model could affect drastically the stiffness of the connection, increasing or decreasing the capacity of the connection to resist forces. When assigning restraint conditions to a 2D model, it is assumed by the software that the whole depth of the element is restrained with the same conditions, but this could be not the case in the real test. An example of this can be observed in the transom out-of-plane cases, where the top part of the transom loaded is restrained vertically, assuming for the model a full vertical restraint along the depth of the cross-section; on the other hand, during the testing sequence the restraint was applied only at the two borders of the frame elements, similar to a simple supported beam, see Figure 5.5.12.

For the case of the 3D models elaborated to replicate the behaviour of the brackets, it was observed again that the boundary conditions had a significant role in the final results. It was observed that unexpected rotations occurred in the bolted connections which could be caused by the bolts themselves or by accommodations of displacements occurring in the channel that connected the testing apparatus with the bracket. To counter these effects, it is important to model the bolts as rotational springs capable of resist a certain amount of force with initial rotation.

The load application can be another reason for the stiffness difference. During the elaboration of the model, the position of the imposed displacement was estimated based on photographs taken during the test and applied evenly along defined edges. However, it can be noticed that the load application in the test does not fully corresponds to the one used in the model. Therefore, unexpected rotations and deflections, could be the cause of the difference between the displacements reported.

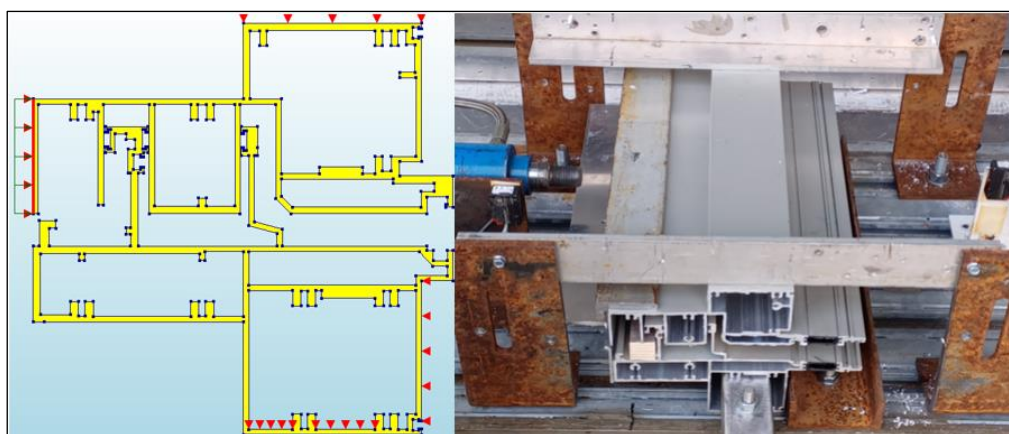


Figure 5.22 Transom-starter sill. Boundary conditions model vs. real

It was also observed during the analysis that the location of the two cross sections respect to each other played a key role in the model. During the discussion of the out-of-plane behaviour of the frame-frame connections it was explained that the stiffness of a connection can increase or decrease depending on the relative distance between elements. This can be simply explained with the deflection formula of a cantilever beam, see Equation 5.1. From the formula it can be observed that the point of application of the load influences the deformation in a factor of L^3 . Moreover, this consideration was used in the numerical model of the transom-starter sill connection, resulting in values closer to the ones observed during the tests.

Moreover, a second fact that could be affecting the model results is the model limitations. During this research, the models were elaborated with suggested values implemented in the contact analysis such as the increased abort criterion; however, in this report, the influence of the increased abort criterion in the model was not studied. Moreover, examples about contact analysis could not be found for DIANA software in the literature. For this reason, it was not possible to select a previously used and/or standardized procedure to evaluate the performance of the connections. In general, it can be assumed that the procedure adopted, and the values implemented are a good starting point for future and more "refined" connection models.

6

Conclusions and Recommendations

6.1 Conclusions

The present research project was carried out mainly to contribute to the literature with additional information and with a general guide of the seismic performance of curtain walls and the use of commercial tools such as DIANA FEA, specifically to analyse the numerical results of the models that were obtained through the tests carried out in collaboration with Permasteelisa. That is why this research had as its first focus the evaluation of the performance of the connections that contribute to the seismic response of a glass curtain wall by considering finite element models and experimental results

To evaluate the achievement of the main goal the next conclusions are made:

As an initial criterion, to select the connections that influence the seismic performance of a glazed curtain wall, the use of the literature gives an adequate insight of the damage mechanisms than could be formed when a CW is submitted to a seismic event. Therefore, based on the literature, it is concluded that the connections influencing the seismic performance of a glazed CW are the: frame to frame connections, anchorage system, and glazing system. The anchorage system must be able to resist the inertial forces originated by the seismic action and must have the capacity to accommodate movements to prevent collateral damage to the other CW elements. The frame-to-frame open connections are susceptible to damage when two CW units meet each other during a seismic event, causing a deformation of the elements that can compromise the serviceability of the CW unit. Moreover, the glazing system adopted influences the capacity of a CW unit to accommodate the relative displacement between the glass infill and the frame.

To establish a finite element model capable of simulate the in- and out-of-plane behaviour of the connections within a CW, an evaluation of the contact between two frame elements with DIANA FEA can be carried out in two manners: using contact elements or using interface elements. It is identified that the best option to analyse the in-plane behaviour of two frame connections is by implementing structural interface elements because it provides more flexibility in terms of model definition and analysis procedures when no large slips are expected. Moreover, to evaluate the out-of-plane behaviour of a frame-to-frame connection the best option is to use contact elements because large slips are expected during the contact of both elements and these elements give a higher tolerance for slips along the target elements. For the analysis of the brackets, the use of a fully fixed connection representing the bolts

behaviour is considered acceptable for the in-plane vertical analysis. However, for the horizontal analysis this consideration can lead to a difference in the Load vs. Displacement behaviour, caused mainly by the rotation of the element because bolts shall not be considered as fully fixed.

In this research, to provide more flexibility in terms of model definition and analysis procedures, structural interface elements shall be selected for contact simulation in models where large slips were not expected; for example, the in-plane interaction of between the transom-stater sill or mullion-mullion connections. In terms of model definition, the use of structural interface elements makes it possible to adapt the interface stiffness to help the convergence process; in terms of analysis, it gives the possibility of using Line Search tools, reducing the computational work of the iteration process.

One of the objectives of this thesis was to elaborate a FEM capable of represent the behaviour of different structural silicones and gaskets. In the attempt to achieve results, the Mooney-Rivlin hyper-elasticity theory was selected for the elaboration of the numerical model in DIANA. Once the results for shear and tension behaviour were obtained, it was noticed that the experimental and the numerical results were similar. As a conclusion of the outcome, it was noticed that the silicone behaviour modelled with the hyper-elasticity theory developed by Mooney-Rivlin is an accurate approach to capture the shear and tensile behaviour of the silicone. It was proven that the FEM of a Dow Corning 993 silicone specimen based on Mooney-Rivlin approach gives a better fit for shear analysis rather than for tensile analysis.

To determine special boundary conditions (e.g., rotational springs instead fully fixed bolted connections), it is necessary to compare numerical results with experimental results. In this research, the so-called special boundary conditions were localized in the bracket modelling, where the bolted connection has to account rotations and accommodation of displacements originated in the halfen channel that connect the bracket to the supporting beam. To understand and where the localize special boundary conditions, it was necessary to compare the numerical and experimental results in terms of Force vs. Displacement diagrams. It is important to highlight that after an extensive comparison, it was observed that for the analysis of the in-plane behaviour of the brackets, special boundary conditions were needed to achieve the same behaviour observed during the tests. The assumption used for the bracket models is that the bolted connections is fully fixed, but it has to be modelled as a rotational spring to capture the behaviour observed in the tests.

To determine special boundary conditions that shall be adopted to simulate accurately the behaviour of connections, it is necessary to compare numerical results with experimental results. In this `case, the tool used to localize these special boundary conditions was the comparison of the numerical and experimental results in terms of Force vs. Displacement diagrams. It is important to highlight that after an extensive comparison, it was observed that for the analysis of the in-plane behaviour of the brackets, special boundary conditions were needed to account rotations and accommodation of displacements originated in the halfen channel that connect the bracket to the supporting beam. The assumption used for the bracket models is that the bolted connections are fully fixed, but it has to be modelled as a rotational spring to capture the behaviour observed in the tests.

A full-size CW façade model (global model) was not executed in this research projects due to time and complexity limitations. Nevertheless, the best approach to translate the behaviour of the connections modelled into a spring model to be used in a global FEM of a CW is to use the Load vs. Displacement diagrams for each connection and in all the directions where the connection modelled has influence.

As an answer to the main research question elaborated “How to evaluate the performance of the connections that contribute to the seismic response of a glazed curtain wall by considering finite element models and experimental results?” It is possible to conclude that the evaluation of the performance of the connections that contribute to the seismic response of a CW can be carried out with the methodology described in this research because the modelling procedure was validated with experimental tests with relatively optimal results. Nonetheless, there are still limitations in the development of this topic that will be described in the recommendations.

6.2 Recommendations

The next recommendations are given for future work:

For future projects it would be ideal to determine the influence of the connections when applying them in a global model of a CW façade because in this study the selection of the possible connections that influence the behaviour of a CW façade was only based on the literature. With a proper analysis in a numerical model it could be possible to determine which connections may not have enough relevance to affect the overall behaviour of a facade.

It would be interesting to carry out new analyses following the same directions used in this thesis to have more reference values in terms of the accuracy of the numerical models following the approach presented in this thesis. With more samples, it would be easier to determine the percentage of error expected with this approach to validated in a more accurate manner this approach.

In addition, it would be important to focus more on the design of each group of connections (e.g., frame-frame or brackets) because during this study the considerable number of connections analysed did not provide much opening for a more detailed calibration of the models. For this reason, some detailed about the boundary conditions could have been neglected in this project.

Besides, for an exact evaluation of the connections, it would be recommended to check the stresses, displacements, strains, and/or forces that act on each of the connections with the use of a full-size mock-up seismic test of a curtain wall because there is a significant difference when analysing the connections in a real size mock up test compared to individual analysis of all connections. For example, the behaviour of the top bracket would vary because it would have more resistance to lateral displacement, since it would be loaded with the weight of the curtain wall.

For a more accurate evaluation of the connections, the local evaluation of the components within a curtain wall should be included in a real-size mock-up test to capture the real behaviour

of each component. In this way, a proper evaluation to determine which connections influence the seismic response of a curtain wall can be found.

It is recommended to investigate all the essential variables to be considered before starting the project. One of them is the selection of the computational tools based on availability of information. During this research it was noticed that DIANA offers a good number of tutorials related with the analysis of structural elements, but information, tutorials, and guidance regarding the modelling of contact between elements is not available. During this research, a considerable part of information used was not found on the internet, and initially most of the work carried out was the result of several trial-and-error operations. It was noticed that with a proper selection of the software, a smoother solution can be achieved. However, it would be interesting to compare the approach used with DIANA with a different using a software used in the design of CW.

References

- [1] C. Lomnitz and B. Wisner, “Earthquakes,” in *the routledge handbook of hazards and disaster risk reduction*, 2012, pp. 310–321.
- [2] S. Baxter, *Earthquakes basics*, vol. 23. University of Delaware, 2000.
- [3] L. Wald, “The science of earthquakes,” *USGS*, 2013. [Online]. Available: <https://www.usgs.gov/programs/earthquake-hazards/science-earthquakes>. [Accessed: 21-Sep-2022].
- [4] Y. Zhang, C. Zhang, W. Drake, and R. Olshansky, “Planning and recovery following the Great 1976 Tangshan earthquake,” *J. Plan. Hist.*, vol. 14, no. 3, pp. 224–243, 2015.
- [5] D. Todd, N. Carino, and R. Chung, *1994 Northridge Earthquake Performance of Structures, Lifelines, and Fire Protection Systems*. U.S. Government Printing Office, 1995.
- [6] P. Esper and E. Tachibana, *Lessons from the Kobe earthquake*. BGS Special Publications, 1998.
- [7] United Nations Human Settlements Programme, *Financing Urban Shelter*. UN-HABITAT, 2005.
- [8] Demographia, *Demographia World Urban Areas (Built Up Urban Areas or World Agglomerations)*, Edition 18th. Demographia, 2022.
- [9] V. Giuncu and F. Mazzolani, *Earthquake Engineering for Structural Design*. New York, NY: Spon Press, 2011.
- [10] N. Purnachandra, *Earthquakes*. Acharya Nagarjuna University Campus: National Geophysical Research Institute, 2016.
- [11] N. Yoan, Ed., *Earthquakes and Tsunamis*. Japan Meteorological Agency: Miss Press, 2011.
- [12] C. Murty, R. Goswami, and V. M. A. Vijayanarayanan, *Earthquake Behaviour of Buildings*. Government of Gujarat: Gujarat State Disaster Management Authority.
- [13] D. Perrone, P. M. Calvi, R. Nascimbene, E. C. Fischer, and G. Magliulo, “Seismic performance of non-structural elements during the 2016 Central Italy earthquake,” *Bull. Earthquake Eng.*, vol. 17, no. 10, pp. 5655–5677, 2019.

- [14] U. Galli, "Seismic behaviour of curtain wall facades. A comparison between experimental mock up test and finite element method analysis," Politecnico di Milano, Milano, 2011.
- [15] D. Basulto, "Terremoto en Chile," *ArchDaily en español*, 28-Feb-2010. [Online]. Available: <https://www.archdaily.cl/cl/02-37979/terremoto-en-chile>. [Accessed: 22-Sep-2022].
- [16] A. Filiatrault and T. Sullivan, "Performance-based seismic design of nonstructural building components: The next frontier of earthquake engineering," *Earth. Eng. Eng. Vib.*, vol. 13, no. S1, pp. 17–46, 2014.
- [17] E. Miranda, G. Mosqueda, R. Retamales, and G. Pekcan, "Performance of Nonstructural Components during the 27 February 2010 Chile Earthquake," *Earthq. Spectra*, vol. 28, no. 1_suppl1, pp. 453–471, 2012.
- [18] G. J. O'Reilly, D. Perrone, M. Fox, R. Monteiro, and A. Filiatrault, "Seismic assessment and loss estimation of existing school buildings in Italy," *Eng. Struct.*, vol. 168, pp. 142–162, 2018.
- [19] B. Chalarca, A. Filiatrault, and D. Perrone, "Seismic demand on acceleration-sensitive nonstructural components in viscously damped braced frames," *J. Struct. Eng. (N. Y.)*, vol. 146, no. 9, pp. 340–360, 2020.
- [20] K. Boswell, *Exterior Building Enclosures. Design Process and Composition for Innovative Facades*. Hoboken, New Jersey: John Wiley & Sons, Inc., 2013.
- [21] D. D. Mijovic, D. Milanovic, and S. Jelena, "CURTAIN WALLS: HISTORY AND A CONTINUING CHALLENGE," Sofia, 2018, p. 7.
- [22] Permasteelisa Group, "Architectural envelopes". [Online]. Available: <https://www.permasteelisagroup.com/your-place-with-us>. [Accessed: 22-Sep-2022].
- [23] Permasteelisa Group, "Headquarters," www.permasteelisagroup.com. [Online]. Available: <https://www.permasteelisagroup.com/project-detail?project=2560>. [Accessed: 23-Sep-2022].
- [24] B. Huang, S. Chen, W. Lu, and K. M. Mosalam, "Seismic demand and experimental evaluation of the nonstructural building curtain wall: A review," *Soil Dyn. Earthq. Eng.*, vol. 100, pp. 16–33, 2017.
- [25] N. Caterino, M. D. Zoppo, G. Maddaloni, A. Bonati, G. Cavanna, and A. Occhiuzzi, "Seismic assessment and finite element modelling of glazed curtain walls," *Struct. Eng. Mech.*, vol. 61, no. 1, pp. 77–90, 2017.
- [26] M. Bârnaure and M. Voiculescu, "The seismic behaviour of curtain walls: An analysis based on numerical modelling," *Math. Model. Civ. Eng.*, vol. 9, no. 4, pp. 1–8, 2013.
- [27] P. Lalas, "Curtainwalls' resistance of building movements, including seismic effects," *Current Trends in Civil & Structural Engineering*, pp. 1–6, 2022.

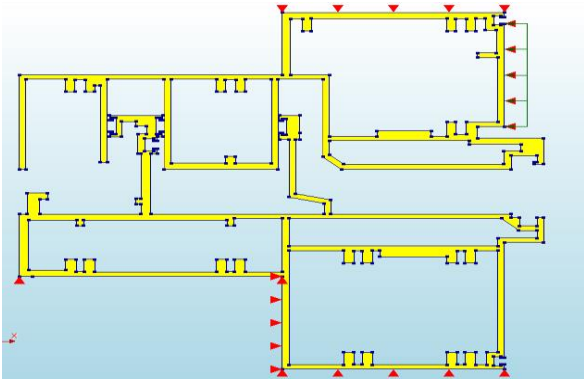
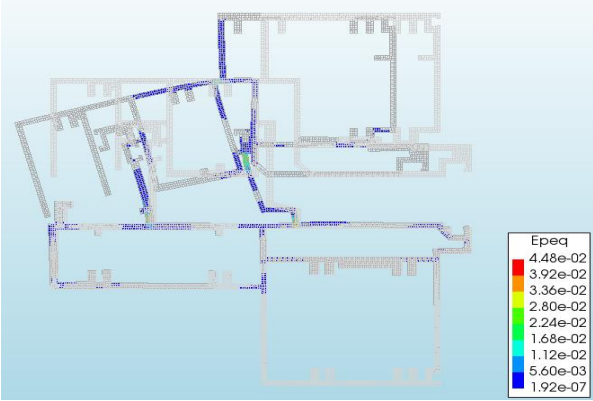
- [28] D. Djuric-Mijovic, J. Savic, D. Milanovic, and A. Cilic, "Seismic damage mitigation of the glazed building façade," *Facta univ. - ser. Archit. Civ. Eng.*, vol. 16, no. 3, pp. 343–353, 2018.
- [29] P. Lalas, "Curtainwalls; Seismic experience, design and assessment," *Australian Earthquake Engineering Society 2018 Conference*, pp. 1–9, 2018.
- [30] S. Toyao, T. Nagae, J. Chen, K. Kajiwara, Y. Kanzaki, and Y.-L. Chung, "Assessment of a curtain wall system used in high-rise buildings and development of a monitoring method," *International Conference in Commemoration of 20th Anniversary of the 1999 Chi-Chi Earthquake*, pp. 1–8, 2019.
- [31] K. P. Allana, "Curtain wall issues, problems, and solutions," *Building Envelope Technology Symposium*, pp. 1–15, 2012.
- [32] Kawneer, "Principles of Curtain Walling," *Kawneer White Paper 1999*, Alcoa Company, pp. 2–16, 1999.
- [33] Crown, "Introduction to Glass Curtain Wall Systems," *Physical Security. Guidance introducing Glass Curtain Wall Systems*, pp. 1–7, 2019.
- [34] M. J. Crosbie, *Curtain walls: Recent developments by Cesar Pelli & associates*. Basel, Switzerland: Birkhauser Verlag AG, 2005.
- [35] American Architectural Manufacturers Association, "AAMA-TIR-A: Maximum Allowable Deflection of Framing Systems for Building Cladding Components at Design Winds Loads", Vol.2, 2004.
- [36] C. Regan, *Structural use of glass in buildings*, 2nd Edition. London: The institution of structural engineers, 2015.
- [37] Shenzhen Sun Global Glass, 11.14mm heat strengthened laminated glass, 2022. [Online]. Available:<https://www.sggglassmanufacturer.com/products/11.14mm-heat-strengthened-laminated-glass-5-1.14-5-clear-HS-toughened-laminated-glass.html>. Accessed: 29-Sep-2022].
- [38] European Committee for Standardization, "NEN-EN 13119 Curtain Walling - Terminology," *Nederlandse norm NEN EN 13119*, pp. 1–26, Brussels, 2016.
- [39] European Committee for Standardization, "NVN-CEN/TS 19100-1 Design of glass structures- Part 1: Basis of design and materials," *NEN TECHNICAL SPECIFICATION*, pp. 1–44, Brussels, 2021.
- [40] Canada Mortgage and Housing Corporation, "Glass and metal curtain walls," *Best practice guide building technology*, pp. 5–257, 2004.
- [41] C. Silveira and M. Pereira Costa, "Quality control of glass facades. Curtain wall and point-fixed systems," *Instituto Superior Técnico, Universidad de Lisboa*, Portugal, pp. 1–12, 2018.

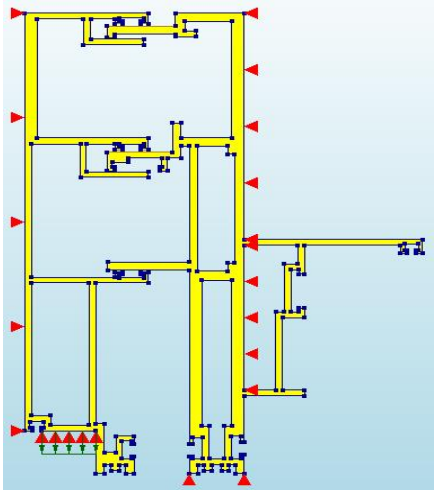
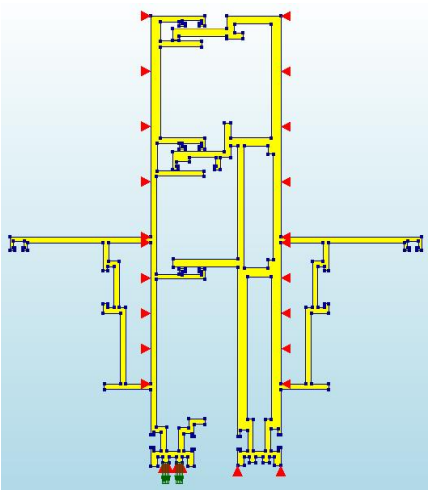
- [42] D. McFarquhar, “3. MATERIALS AND CONFIGURATIONS,” in *Curtain Wall Systems*, Virginia: American Society of Civil Engineers, 2013, pp. 8–32.
- [43] F. A. Morris, “2. DEFINITION AND TYPES OF CURTAINS WALLS,” in *Curtain Wall Systems*, Virginia: American Society of Civil Engineers, 2013, pp. 3–7.
- [44] Maeda USA, mc285-2 curtain wall installation, 2022. [Online]. Available: <https://www.maedausa.com/mini-crane/mc285-2-curtain-wall-installation-13433570753- o/>. [Accessed: 02-Oct-2022].
- [45] K. Kazmierczak, “Review of curtain walls, focusing on design problems and solutions,” *Morrison Hershfield Corporation*, pp. 1–20, 2010.
- [46] M. M. Ali, R. Behr, and P. Kremer, “Seismic Behaviour of Curtain Walls Containing Insulating Glass Units,” *Univ. La Sapienza di Roma*, pp. 1–16, 2020.
- [47] A. M. Memari, “8. DESIGN OF CURTAIN WALLS FOR EARTHQUAKE-INDUCED LOADS AND DRIFTS,” in *Curtain Wall Systems*, Virginia: American Society of Civil Engineers, 2013, pp. 105–128.
-
- [48] Bouwkamp JG and Meehan JF. Drift limitations imposed by glass, In: *Proceedings of the 2nd world conference on earthquake engineering*, volume III, Tokyo and Kyoto, Japan, 1960. p. 1763–78.
- [49] JH. Sucuoglu and C. V. Girija Vallabhan, “Behaviour of window glass panels during earthquakes,” *Department of civil engineering Middle East Technical University*, vol.19, pp. 1–10, 1997.
- [50] C. Clift and N. Bonnheim, “7. DESIGN OF CURTAIN WALLS FOR WIND LOAD,” in *Curtain Wall Systems*, Virginia: American Society of Civil Engineers, 2018, pp. 87-104.
- [51] A. M. Memari and T. A. Schwartz, “Glazing and curtain wall systems to resist earthquakes,” in *Architectural Glass to Resist Seismic and Extreme Climatic Events*, R. A. Behr, Ed. Elsevier, 2009, pp. 28–63.
- [52] G. Hayes and D. Wald, “The 03/11/2011 Mw9.0 Tohoku, Japan Earthquake,” *U.S. Geological Survey, National Earthquake Information Center*, pp. 1–36, 2011.
- [53] European Committee for Standardization, Eurocode 8 - *Design of structures for earthquake resistance - Part 1-1: General rules and seismic action*. Brussels, 2004.
- [54] European Committee for Standardization, *Nederlandse norm NEN-EN 13830+A1 Curtain walling - Product standard*. Brussels, 2020.
- [55] European Committee for Standardization, *RECOMMENDED PROVISIONS FOR SEISMIC REGULATIONS FOR NEW BUILDINGS AND OTHER STRUCTURES (FEMA 450) Part 2: Commentary*. Brussels, 2003.

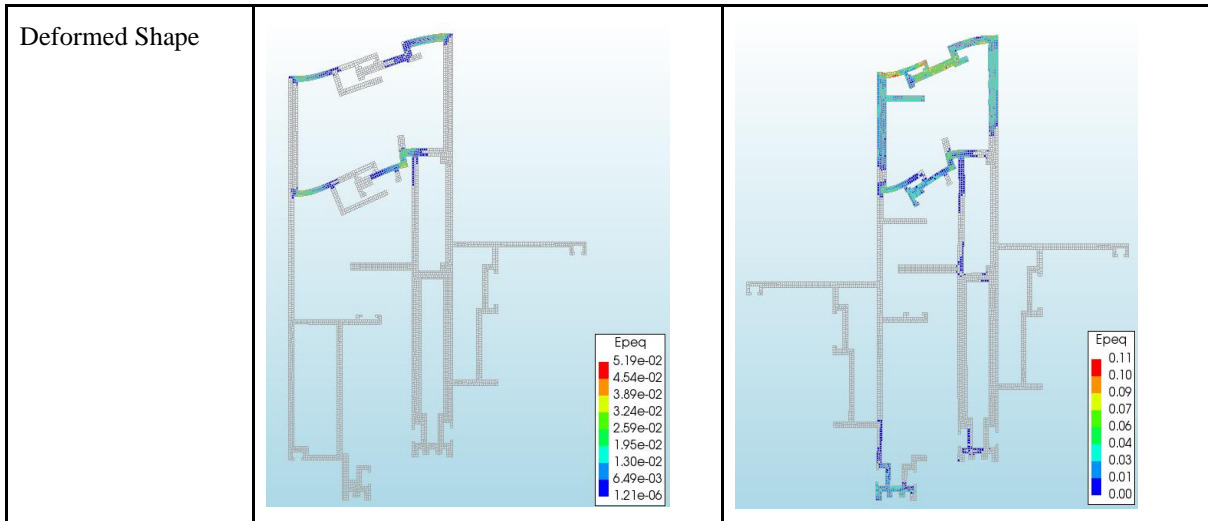
- [56] A. M. Memari, R. A. Behr, and P. A. Kremer, "Seismic Behavior of Curtain Walls Containing Insulating Glass Units," *Test methods for performance of glazing systems and exterior walls during earthquakes and extreme climatic events*, pp. 232–251, 2003.
- [57] V. Nardini and F. Doebbel, "Performance-Based Concept for Design of Structural Silicone Joints in Façades Exposed to Earthquake," *Challenging Glass 5 – Conference on Architectural and Structural Applications of Glass*, pp. 1–12, 2016.
- [58] Building Seismic Safety Council, "NEHRP RECOMMENDED PROVISIONS FOR SEISMIC REGULATIONS FOR NEW BUILDINGS AND OTHER STRUCTURES FEMA 450) Part 1: Provisions," *National Institute of Building Sciences*, 2003, pp. 200–353.
- [59] Architectural Institute of Japan, *Building Construction Standard Specifications and Commentary JASS14 Car Ten-wall construction*. Japan, 2012.
- [60] BRANZ, "Curtain wall cladding," Branz Build, 01-Aug-2019. [Online]. Available: <https://www.buildmagazine.org.nz/index.php/articles/show/curtain-wall-cladding>. [Accessed: 10-Oct-2022].
- [61] BuildCorp, *Laminated glass*, 2020. [Online]. Available: <https://build.com.au/laminated-glass>. [Accessed: 10-Oct-2022]. W. Aya, Y. Abdelhady, A. Atef, and D. Faggal, "Conventional and advanced glazing technologies for enhancing thermal and lighting performance," *Engineering Research Journal*, pp. 1–15, 2021.
- [62] W. Aya, Y. Abdelhady, A. Atef, and D. Faggal, "Conventional and advanced glazing technologies for enhancing thermal and lighting performance," *Engineering Research Journal*, pp. 1–15, 2021.
- [63] H. Ali, B. McCabe, A. Shahi, D. Berardis, and R. Lyall, "Window wall and curtain wall: An objective review," *Building Tall Research Centre, Department of Civil Engineering, University of Toronto*, pp. 1–11, 2017.
- [64] A. Watts, "Modern Constructions Envelopes," *Modern construction series*, vol. 2. Ambra, London, pp. 13–177, 2011.
- [65] E. Gil, "COMPUTATIONAL MODELING OF GLASS CURTAIN WALL SYSTEMS TO SUPPORT FRAGILITY CURVE DEVELOPMENT," Virginia Tech, Virginia, 2019.
- [66] European Committee for Standardization, "EUROCODE 3 - Design of steel structures – Part 1-5: Plated structural elements", in Eurocode 3, Brussels, 2006.
- [67] O' Brien W., and A. Memari, "Fragility Curves for architectural glass in stick built glazing systems," vol. 28, *Earthquake Spectra*, 2012, pp. 639–665.
- [68] R. A. Behr, A. Belarbi, and A. T. Brown, "Seismic performance of architectural glass in a storefront wall system," *Earthq. Spectra*, vol. 11, no. 3, pp. 367–391, 1995.
- [68] S. Bianchi, "TESTING PROTOCOL - SAFE FACE RESEARCH PROJECT," 2020.

- [69] European Committee for Standardization, Nederlandse norm NEN-EN 12152 (en). Curtain walling - Air permeability - Performance requirements and classification. Brussels, 2020.
- [70] European Committee for Standardization, Nederlandse norm NEN-EN 13051 (en). Curtain Walling - Watertightness - Site test. Brussels, 2020.
- [71] European Committee for Standardization. The European standard EN 12155:2000 has the status of a British standard. Curtain walling - Watertightness - Laboratory test under static pressure. Brussels, 2000.
- [72] European Committee for Standardization, Nederlandse norm NEN-EN 13116 (en). Curtain walling - Resistance to wind load - Performance requirements. Brussels, 2001.
- [73] European Committee for Standardization, NEN-EN 12179 (en). Curtain walling Structural-Wind resistance - Test method. Brussels, 2000.
- [74] DIANA FEA, "User's Manual 10.5," 24 January 2022. [Online]. Available: <https://manuals.dianafea.com/d105/Diana.html>. [Accessed February 2022].
- [75] Autodesk Inc, "Architecture, Engineering & Construction", 30-Sep-2022. [Online]. Available: <https://www.autodesk.com/>. [Accessed: 13-Nov-2022].
- [76] European Committee for Standardization, "Design of aluminium structures - Part 1-1: General structural rules," in Eurocode 9, Brussels, 2009, pp. 3–210.
- [77] V. A. Silvestru, O. Englhardt, and J. Schneider, "Investigations on linear silicone joints for glass-metal elements with composite structural behaviour," 2018.

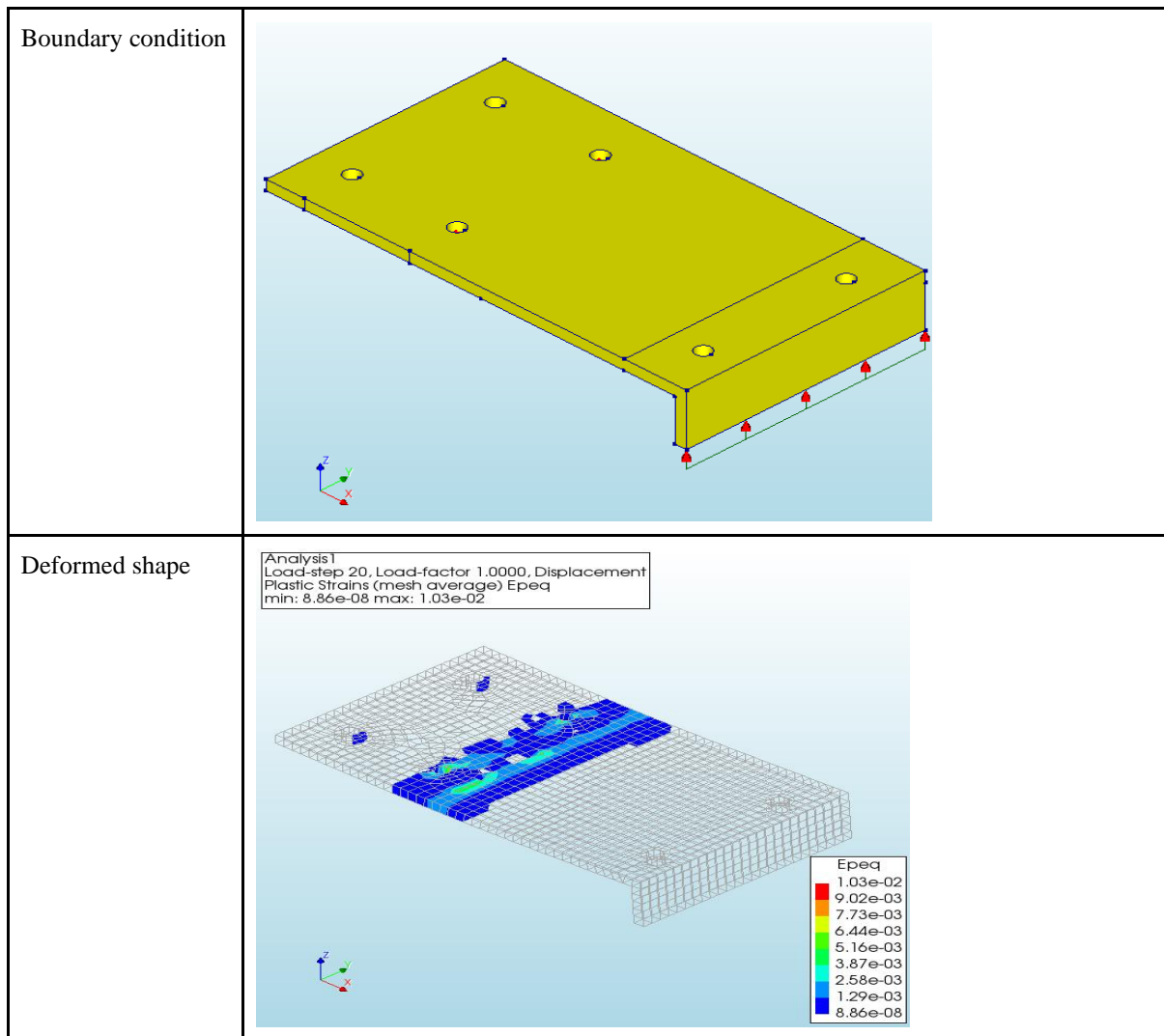
Annex A: Boundary conditions Case Study 2

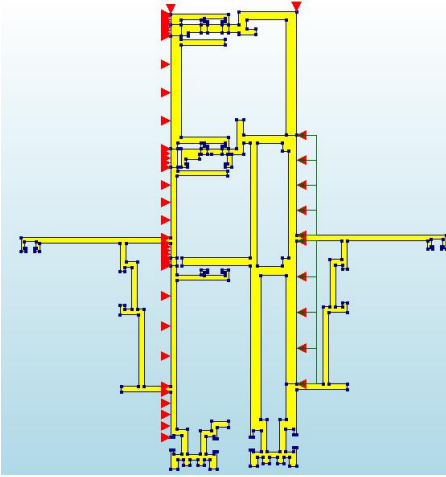
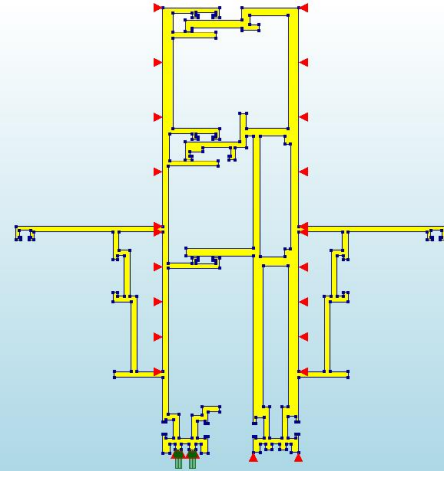
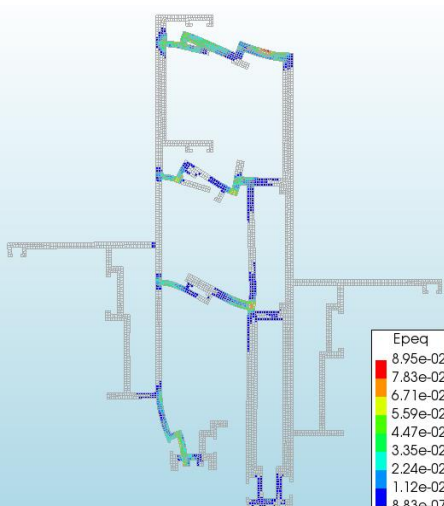
Connection	Transom	
Direction	Inward	
Boundary condition		
Deformed Shape		

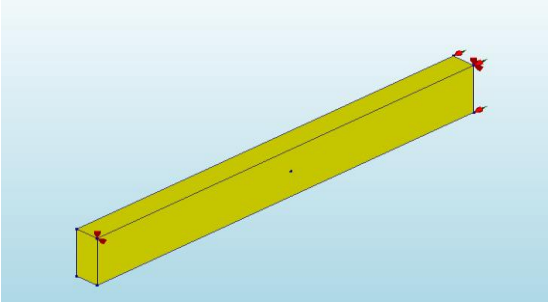
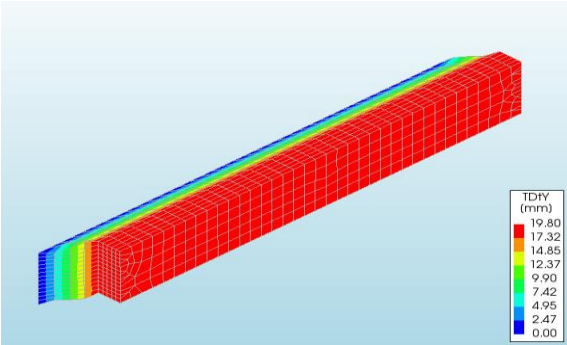
Connection	Mullion-Mullion	
Direction	Large-small out of plane inwards	Small-Small inward
Boundary condition		

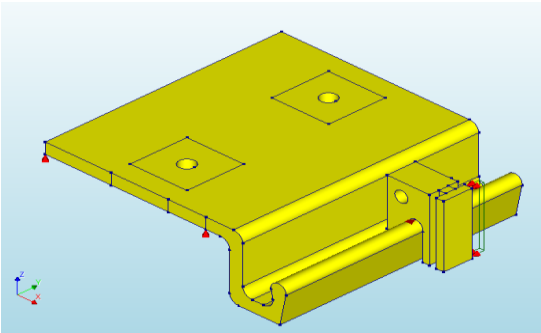


Connection	Bottom Bracket	
Direction	In Plane Horizontal	In Plane Vertical Down
Boundary condition		
Deformed Shape	<p>Analysis1 Load-step 20, Load-factor 1.0000, Displ Plastic Strains Epeq min: 1.19e-07 max: 5.64e-02</p>	<p>Analysis1 Load-step 20, Load-factor 1.0000, Displacement Displacements TDZ min: -2.00mm max: 0.04mm</p>
Direction	In plane vertical up	

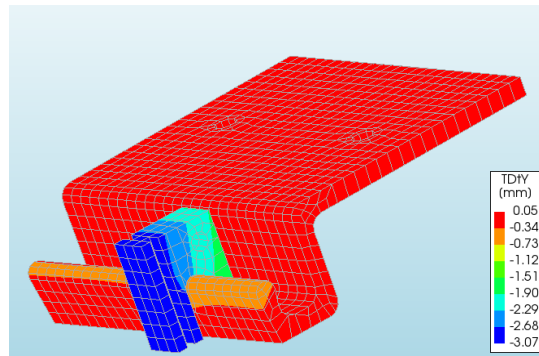


Connection	Mullion-Mullion	
Direction	In-plane small-small inwards	Out of plane mullion-mullion outwards
Boundary condition		
Deformed Shape		

Connection	Silicone
Direction	Silicone shear in plane horizontal
Boundary condition	
Deformed Shape	

Connection	Aluminium bracket
Direction	Aluminium bracket in plane horizontal load on hook
Boundary condition	

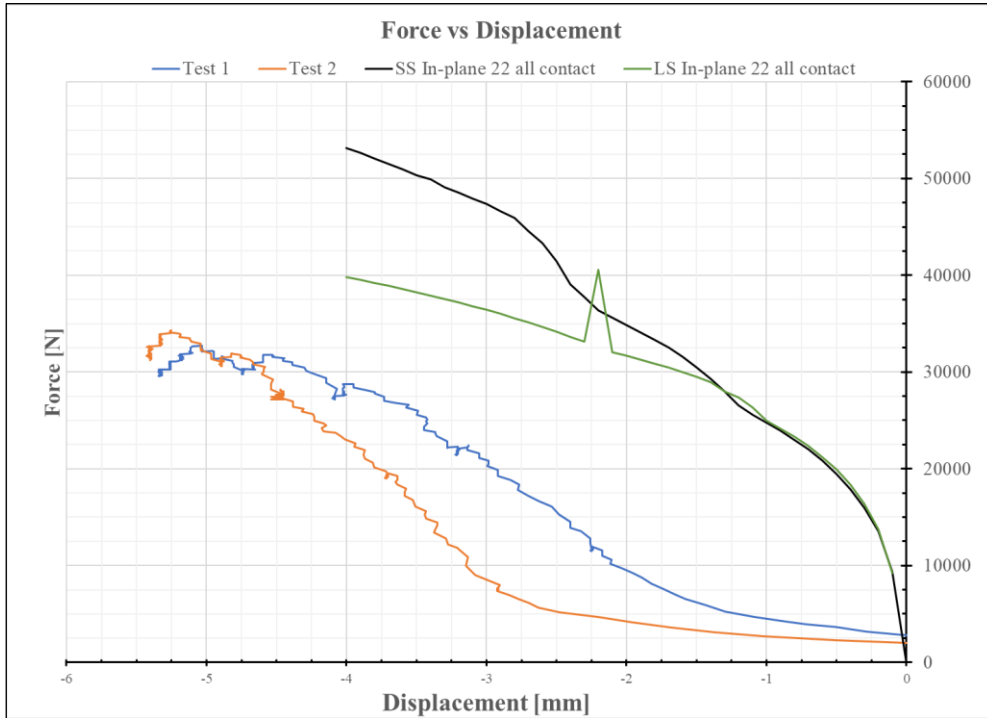
Deformed Shape



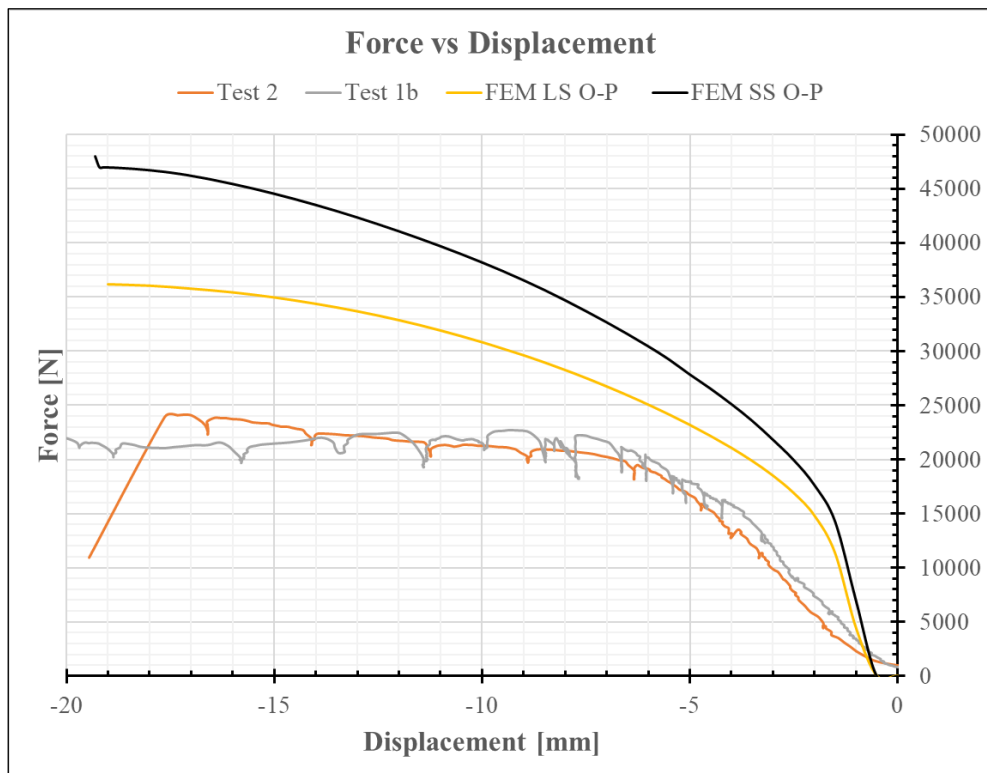
Annex B: Results Case Study 2

Mullion-Mullion

In-plane:

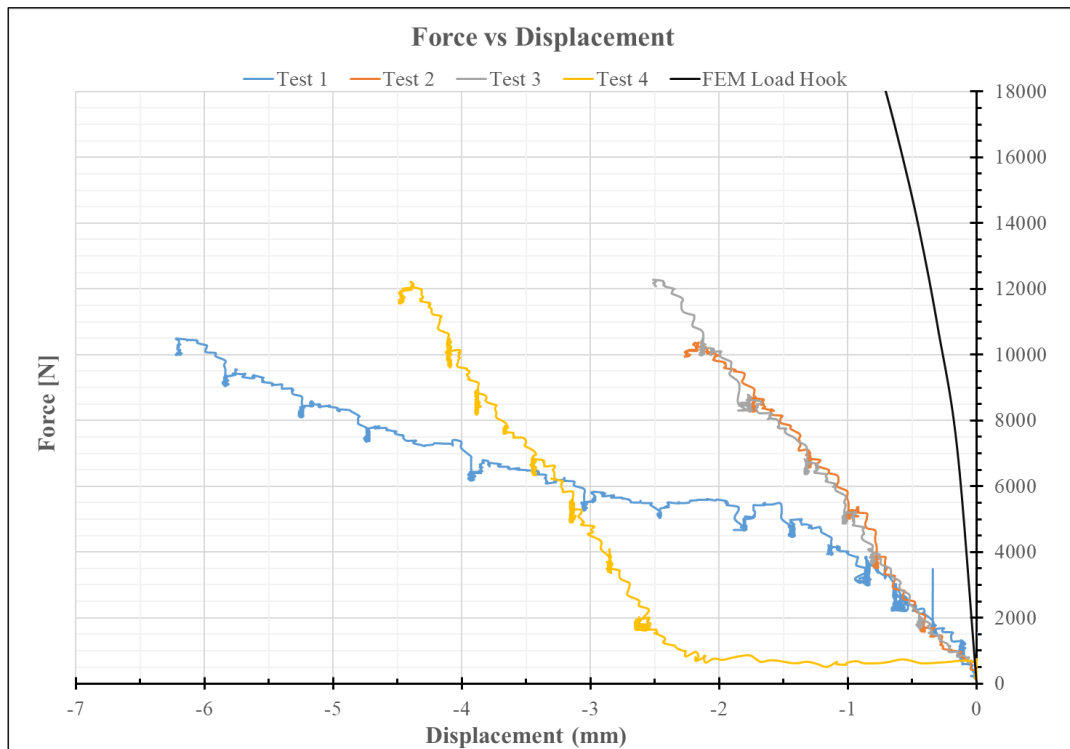


Out of plane Outwards:



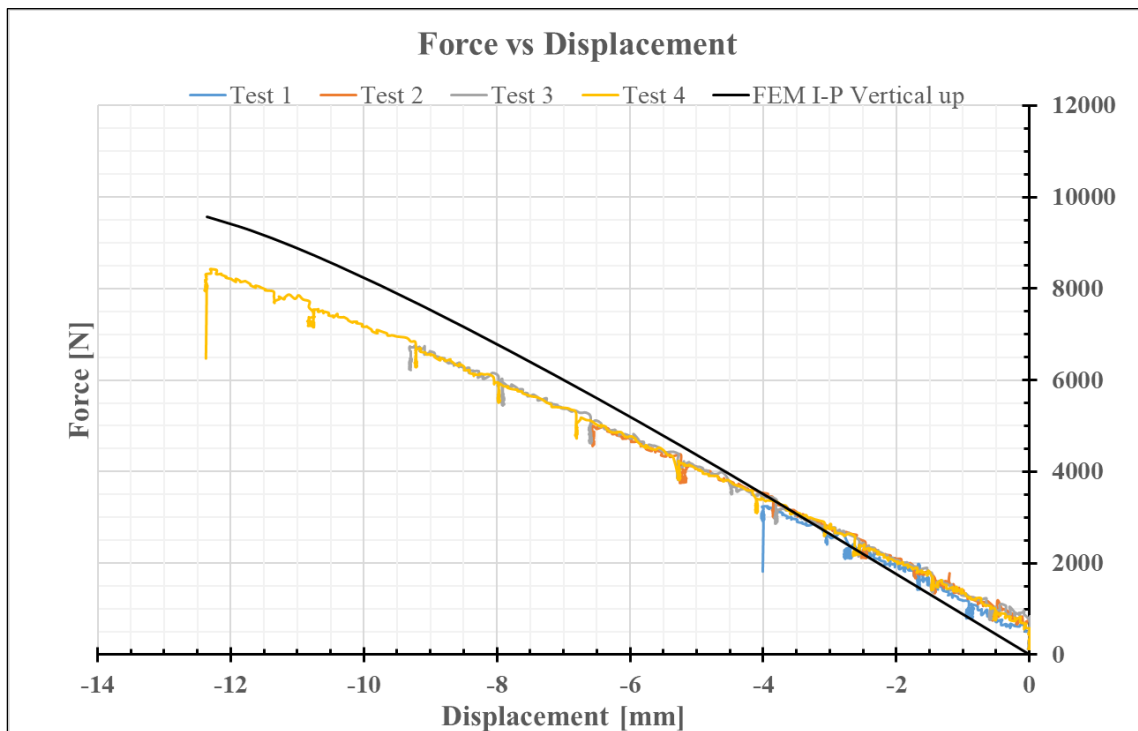
Top bracket and hook

In-plane horizontal (load on hook):



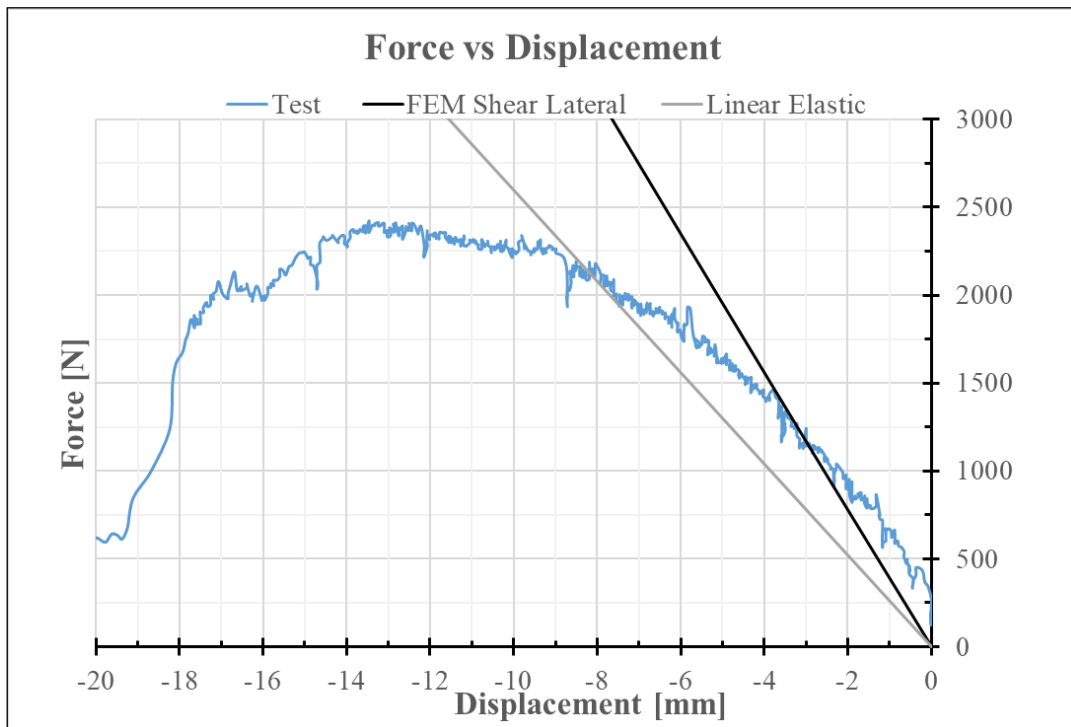
Bottom bracket

In-plane vertical up:

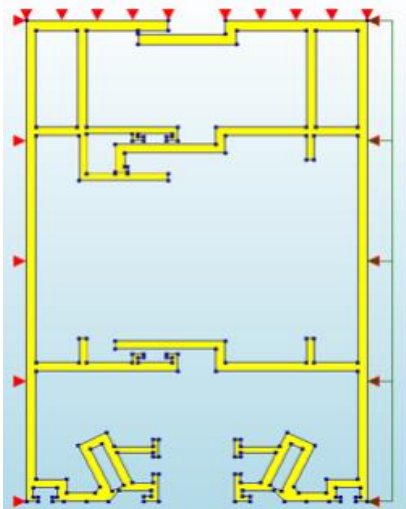
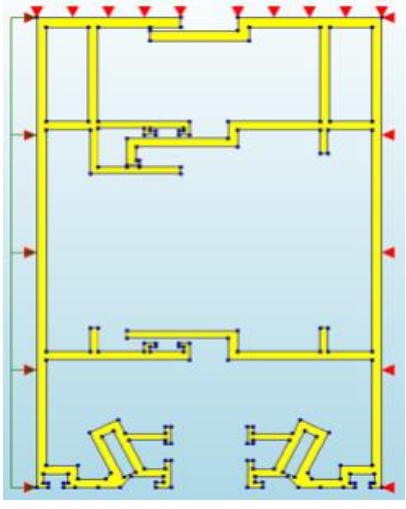
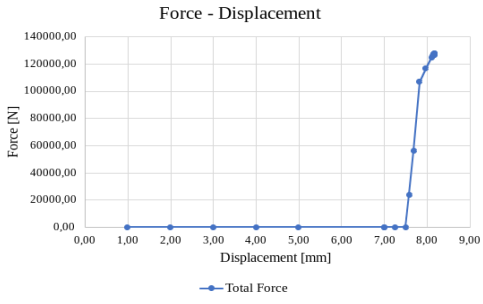
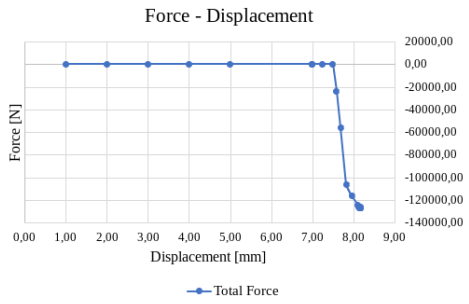


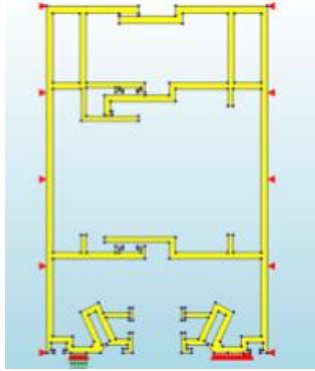
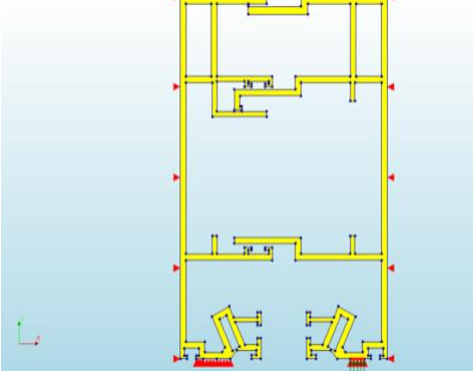
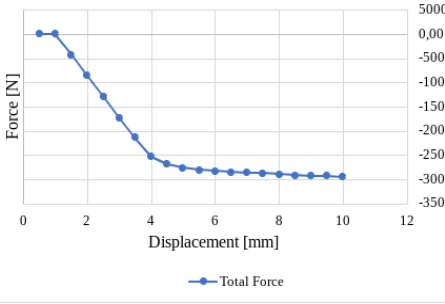
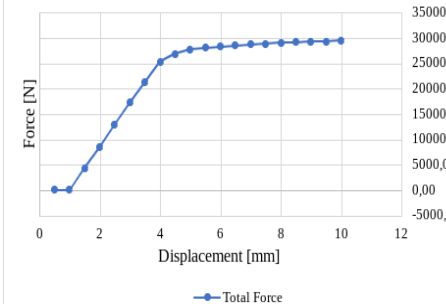
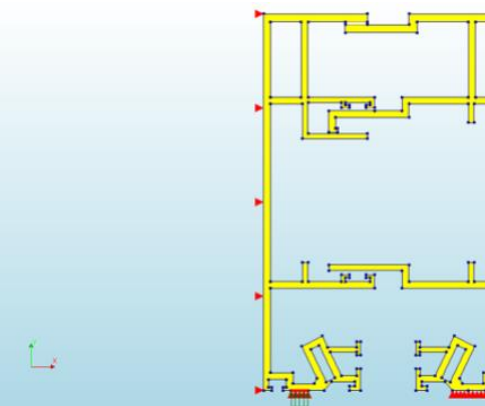
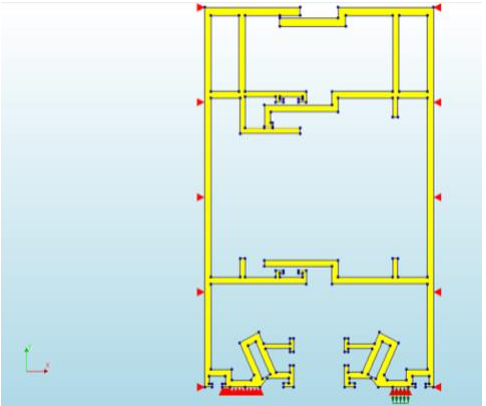
Silicone

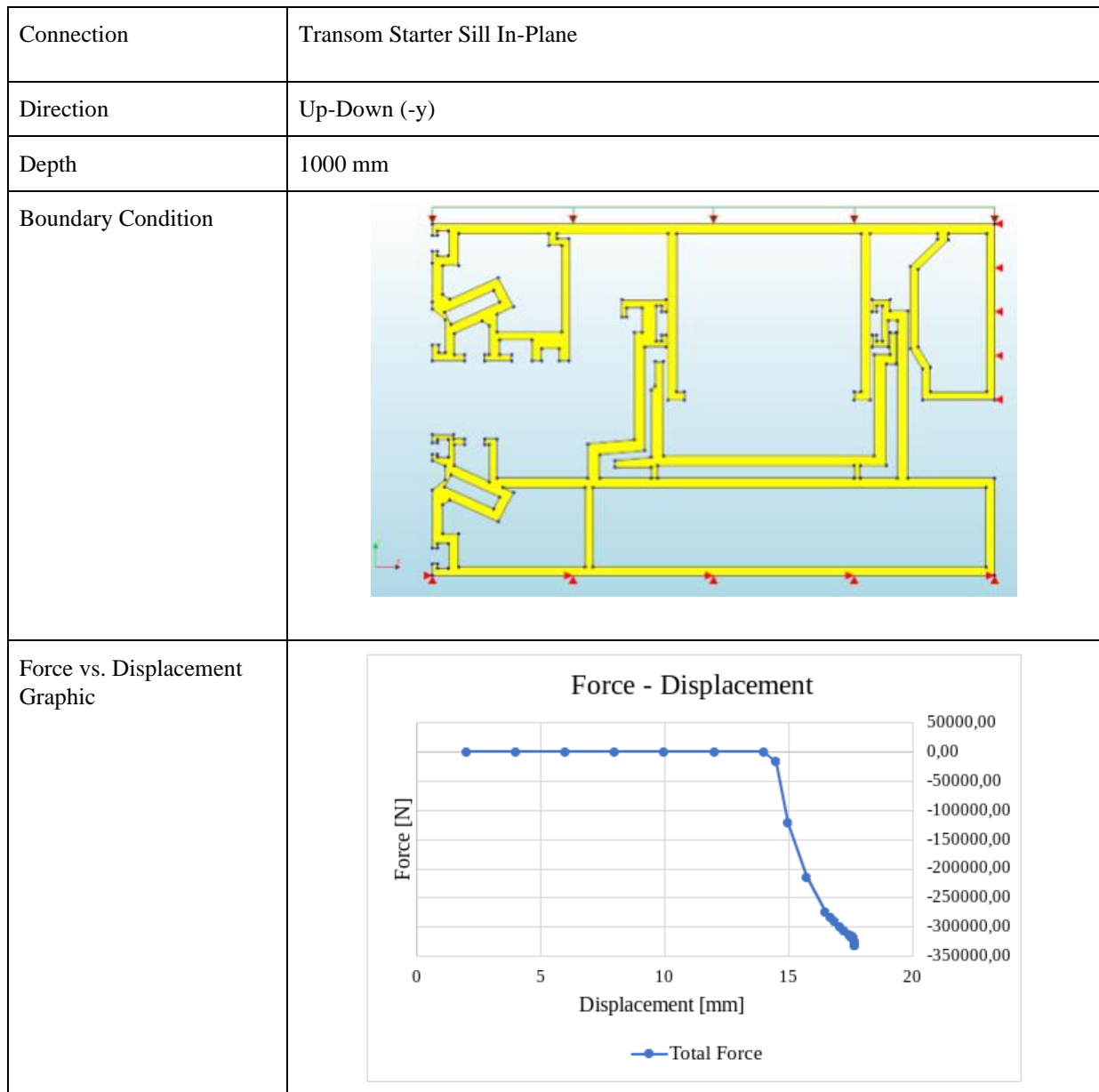
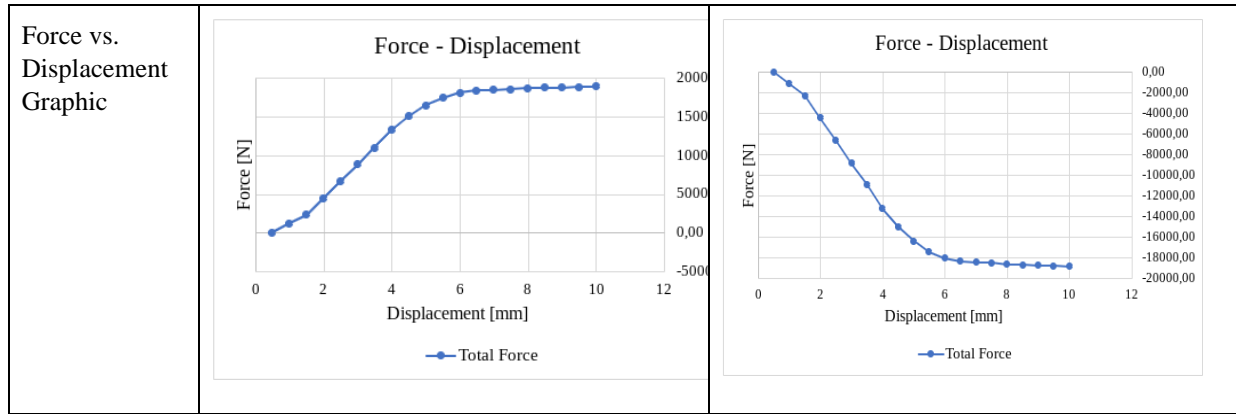
Shear lateral:

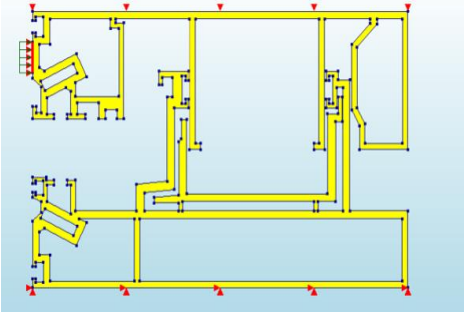
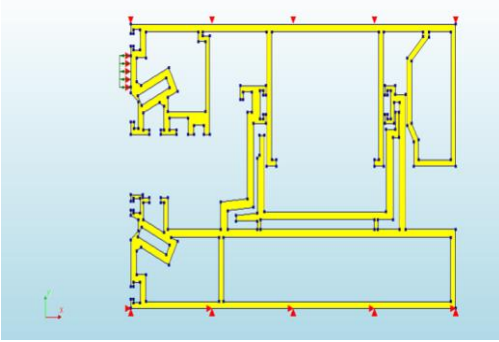
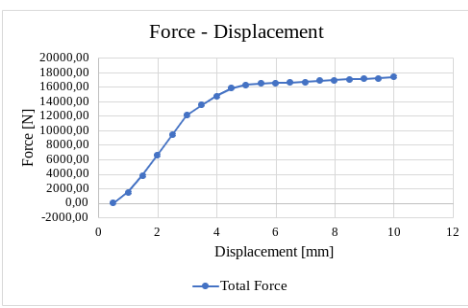
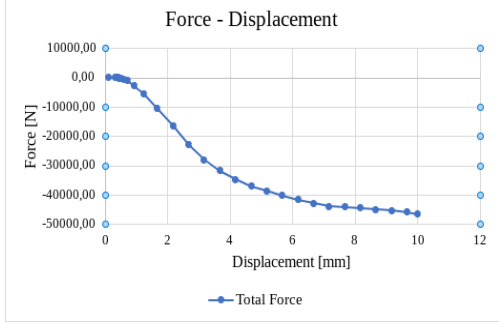


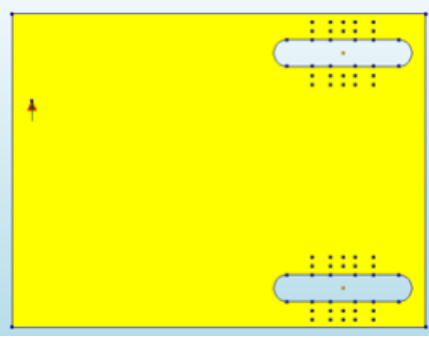
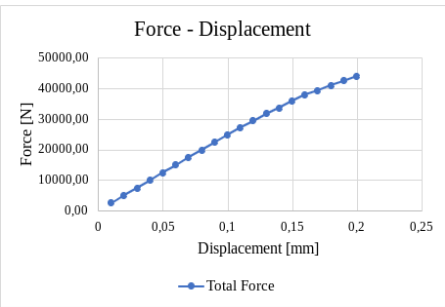
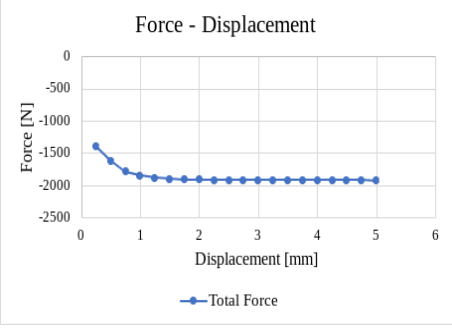
Annex C: Connections Case Study 1

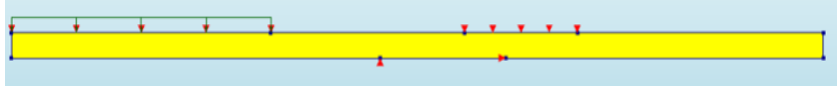
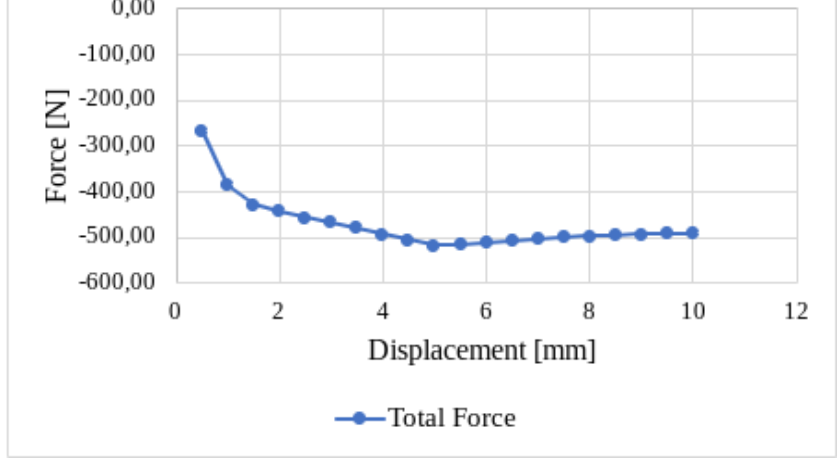
Connection	Mullion-Mullion In-Plane	
Direction	Right-Left (-X)	Left-Right (+X)
Depth	1000 mm	1000 mm
Boundary Conditions		
Force vs. Displacement Graphic	<p style="text-align: center;">Force - Displacement</p> 	<p style="text-align: center;">Force - Displacement</p> 

Connection	Mullion-Mullion out of plane	
Direction	Left - outside (-Y)	Right inside (+Y)
Depth	1000 mm	1000 mm
Boundary Condition		
Force vs. Displacement Graphic	<p style="text-align: center;">Force - Displacement</p> 	<p style="text-align: center;">Force - Displacement</p> 
Direction	Left inside (+Y)	Right outside (-Y)
depth	1000 mm	1000 mm
Boundary Conditions		



<p>Connection</p>	<p>Transom Starter Sill Out of Plane</p>																																																	
<p>Direction</p>	<p>Movement inside (X)</p>	<p>Movement outside (-X)</p>																																																
<p>Depth</p>	<p>1000 mm</p>	<p>1000 mm</p>																																																
<p>Boundary Condition</p>																																																		
<p>Force vs. Displacement Graph</p>	 <table border="1"> <caption>Approximate data for Force vs. Displacement (Inward Movement)</caption> <thead> <tr> <th>Displacement [mm]</th> <th>Total Force [N]</th> </tr> </thead> <tbody> <tr><td>0</td><td>0</td></tr> <tr><td>1</td><td>2000</td></tr> <tr><td>2</td><td>6000</td></tr> <tr><td>3</td><td>10000</td></tr> <tr><td>4</td><td>13000</td></tr> <tr><td>5</td><td>15000</td></tr> <tr><td>6</td><td>16000</td></tr> <tr><td>7</td><td>16500</td></tr> <tr><td>8</td><td>16800</td></tr> <tr><td>9</td><td>17000</td></tr> <tr><td>10</td><td>17000</td></tr> </tbody> </table>	Displacement [mm]	Total Force [N]	0	0	1	2000	2	6000	3	10000	4	13000	5	15000	6	16000	7	16500	8	16800	9	17000	10	17000	 <table border="1"> <caption>Approximate data for Force vs. Displacement (Outward Movement)</caption> <thead> <tr> <th>Displacement [mm]</th> <th>Total Force [N]</th> </tr> </thead> <tbody> <tr><td>0</td><td>0</td></tr> <tr><td>1</td><td>-5000</td></tr> <tr><td>2</td><td>-15000</td></tr> <tr><td>3</td><td>-25000</td></tr> <tr><td>4</td><td>-35000</td></tr> <tr><td>5</td><td>-40000</td></tr> <tr><td>6</td><td>-43000</td></tr> <tr><td>7</td><td>-44500</td></tr> <tr><td>8</td><td>-45000</td></tr> <tr><td>9</td><td>-45000</td></tr> <tr><td>10</td><td>-45000</td></tr> </tbody> </table>	Displacement [mm]	Total Force [N]	0	0	1	-5000	2	-15000	3	-25000	4	-35000	5	-40000	6	-43000	7	-44500	8	-45000	9	-45000	10	-45000
Displacement [mm]	Total Force [N]																																																	
0	0																																																	
1	2000																																																	
2	6000																																																	
3	10000																																																	
4	13000																																																	
5	15000																																																	
6	16000																																																	
7	16500																																																	
8	16800																																																	
9	17000																																																	
10	17000																																																	
Displacement [mm]	Total Force [N]																																																	
0	0																																																	
1	-5000																																																	
2	-15000																																																	
3	-25000																																																	
4	-35000																																																	
5	-40000																																																	
6	-43000																																																	
7	-44500																																																	
8	-45000																																																	
9	-45000																																																	
10	-45000																																																	

<p>Connection</p>	<p>Top Bracket Steel</p>																																			
<p>Direction</p>	<p>In Plane Horizontal Up (+Y)</p>	<p>In Plane Vertical Down (-Y)</p>																																		
<p>Depth</p>	<p>14 mm</p>	<p>1 mm</p>																																		
<p>Boundary Condition</p>																																				
<p>Force vs. Displacement Graph</p>	 <table border="1"> <caption>Force vs. Displacement (+Y)</caption> <thead> <tr> <th>Displacement [mm]</th> <th>Force [N]</th> </tr> </thead> <tbody> <tr><td>0.00</td><td>0.00</td></tr> <tr><td>0.05</td><td>10000.00</td></tr> <tr><td>0.10</td><td>20000.00</td></tr> <tr><td>0.15</td><td>30000.00</td></tr> <tr><td>0.20</td><td>40000.00</td></tr> <tr><td>0.25</td><td>50000.00</td></tr> </tbody> </table>	Displacement [mm]	Force [N]	0.00	0.00	0.05	10000.00	0.10	20000.00	0.15	30000.00	0.20	40000.00	0.25	50000.00	 <table border="1"> <caption>Force vs. Displacement (-Y)</caption> <thead> <tr> <th>Displacement [mm]</th> <th>Force [N]</th> </tr> </thead> <tbody> <tr><td>0.0</td><td>-1500</td></tr> <tr><td>0.5</td><td>-1800</td></tr> <tr><td>1.0</td><td>-1900</td></tr> <tr><td>1.5</td><td>-1950</td></tr> <tr><td>2.0</td><td>-1980</td></tr> <tr><td>3.0</td><td>-2000</td></tr> <tr><td>4.0</td><td>-2000</td></tr> <tr><td>5.0</td><td>-2000</td></tr> <tr><td>6.0</td><td>-2000</td></tr> </tbody> </table>	Displacement [mm]	Force [N]	0.0	-1500	0.5	-1800	1.0	-1900	1.5	-1950	2.0	-1980	3.0	-2000	4.0	-2000	5.0	-2000	6.0	-2000
Displacement [mm]	Force [N]																																			
0.00	0.00																																			
0.05	10000.00																																			
0.10	20000.00																																			
0.15	30000.00																																			
0.20	40000.00																																			
0.25	50000.00																																			
Displacement [mm]	Force [N]																																			
0.0	-1500																																			
0.5	-1800																																			
1.0	-1900																																			
1.5	-1950																																			
2.0	-1980																																			
3.0	-2000																																			
4.0	-2000																																			
5.0	-2000																																			
6.0	-2000																																			

Connection	Starter Sill																																										
Direction	In plane vertical down (-Y)																																										
Depth	1 mm																																										
Boundary Condition																																											
Force vs. Displacement Graph	<p style="text-align: center;">Force - Displacement</p>  <table border="1"> <caption>Data points for Force - Displacement Graph</caption> <thead> <tr> <th>Displacement [mm]</th> <th>Force [N]</th> </tr> </thead> <tbody> <tr><td>0.5</td><td>-270.00</td></tr> <tr><td>1.0</td><td>-380.00</td></tr> <tr><td>1.5</td><td>-430.00</td></tr> <tr><td>2.0</td><td>-450.00</td></tr> <tr><td>2.5</td><td>-460.00</td></tr> <tr><td>3.0</td><td>-470.00</td></tr> <tr><td>3.5</td><td>-480.00</td></tr> <tr><td>4.0</td><td>-490.00</td></tr> <tr><td>4.5</td><td>-500.00</td></tr> <tr><td>5.0</td><td>-510.00</td></tr> <tr><td>5.5</td><td>-515.00</td></tr> <tr><td>6.0</td><td>-515.00</td></tr> <tr><td>6.5</td><td>-515.00</td></tr> <tr><td>7.0</td><td>-515.00</td></tr> <tr><td>7.5</td><td>-515.00</td></tr> <tr><td>8.0</td><td>-515.00</td></tr> <tr><td>8.5</td><td>-515.00</td></tr> <tr><td>9.0</td><td>-515.00</td></tr> <tr><td>9.5</td><td>-515.00</td></tr> <tr><td>10.0</td><td>-515.00</td></tr> </tbody> </table>	Displacement [mm]	Force [N]	0.5	-270.00	1.0	-380.00	1.5	-430.00	2.0	-450.00	2.5	-460.00	3.0	-470.00	3.5	-480.00	4.0	-490.00	4.5	-500.00	5.0	-510.00	5.5	-515.00	6.0	-515.00	6.5	-515.00	7.0	-515.00	7.5	-515.00	8.0	-515.00	8.5	-515.00	9.0	-515.00	9.5	-515.00	10.0	-515.00
Displacement [mm]	Force [N]																																										
0.5	-270.00																																										
1.0	-380.00																																										
1.5	-430.00																																										
2.0	-450.00																																										
2.5	-460.00																																										
3.0	-470.00																																										
3.5	-480.00																																										
4.0	-490.00																																										
4.5	-500.00																																										
5.0	-510.00																																										
5.5	-515.00																																										
6.0	-515.00																																										
6.5	-515.00																																										
7.0	-515.00																																										
7.5	-515.00																																										
8.0	-515.00																																										
8.5	-515.00																																										
9.0	-515.00																																										
9.5	-515.00																																										
10.0	-515.00																																										

Annex D: Connection tests photographs

Transom-Transom test photographs

In-plane:



Out-of-plane inward:





Out-of-plane outward

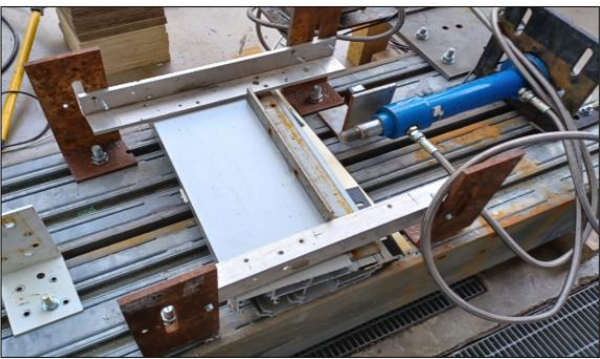


Mullion-Mullion test photographs

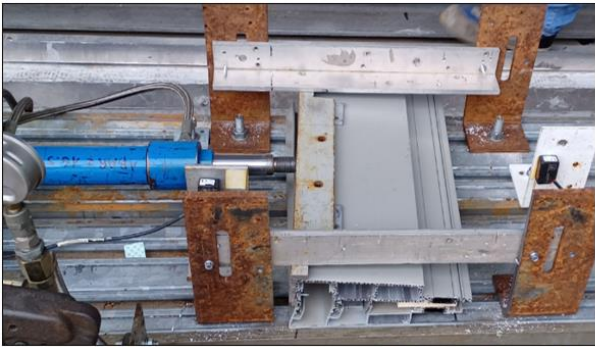
In -plane



Out-of-plane inward



Out-of-plane outward

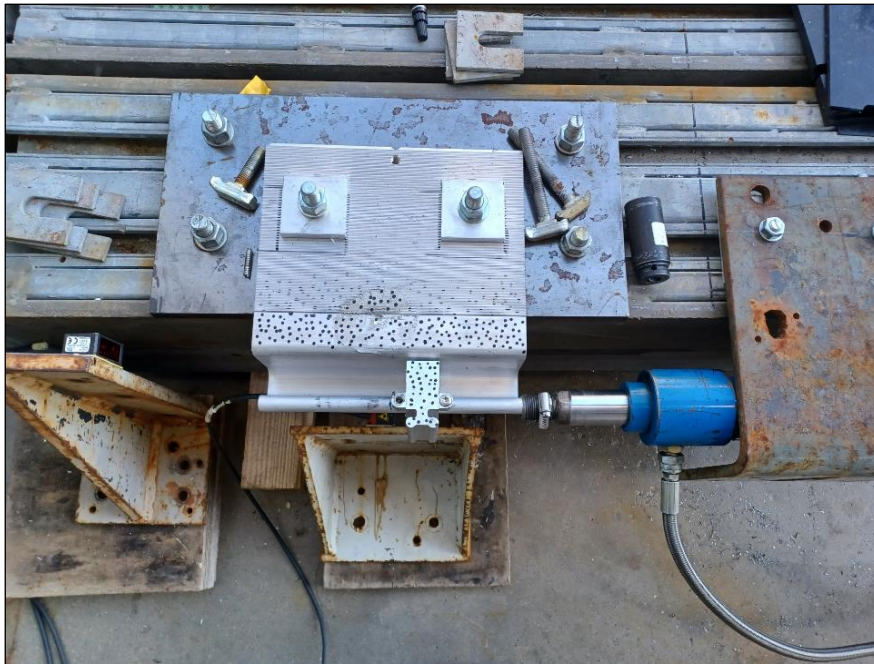


Top aluminium bracket and hook test photographs

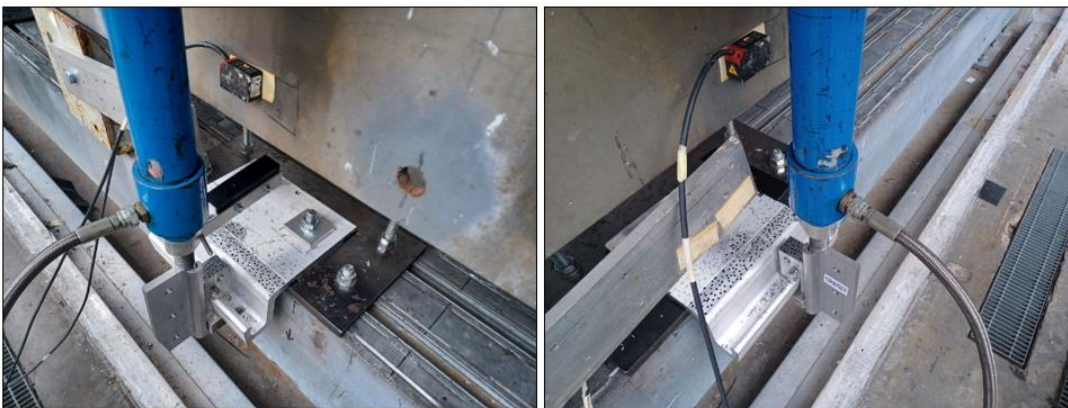
Aluminium bracket horizontal. Load on hook



Aluminium bracket horizontal. Load on bracket



Aluminium bracket vertical





Bottom steel bracket test photographs

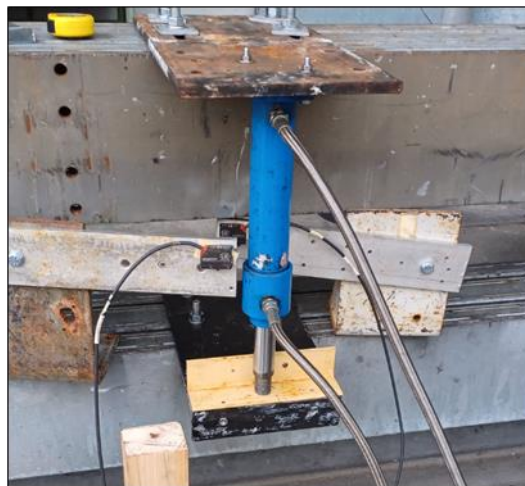
In-plane horizontal



In-plane vertical up

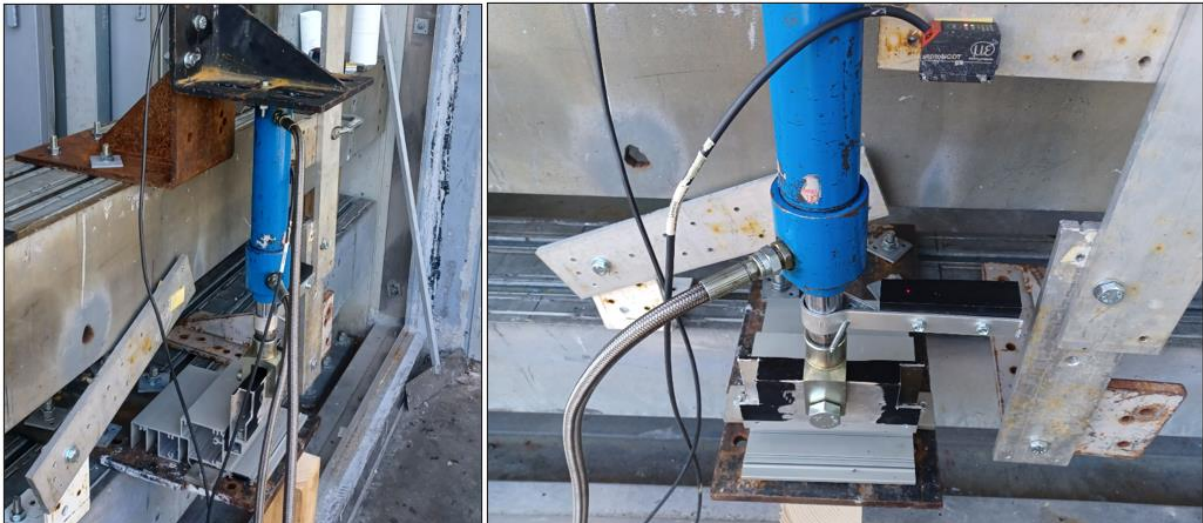


In-plane vertical down



Silicone test photographs

Shear vertical



Shear horizontal



Tension

